

The forgotten channels: charged Higgs boson decays to a W^\pm and a non-SM-like Higgs boson

Henning Bahl^{*1}, Tim Stefaniak^{†1}, and Jonas Wittbrodt^{‡2}

¹*Deutsches Elektronen-Synchrotron DESY, Notkestraße 85, D-22607 Hamburg, Germany*

²*Department of Astronomy and Theoretical Physics, Lund University, Sölvegatan 14A, 223 62 Lund, Sweden*

The presence of charged Higgs bosons is a generic prediction of multiplet extensions of the Standard Model (SM) Higgs sector. Focusing on the Two-Higgs-Doublet-Model (2HDM) with type I and lepton-specific Yukawa sectors, we discuss the charged Higgs boson collider phenomenology in the theoretically and experimentally viable parameter space. While almost all existing experimental searches at the LHC target the fermionic decays of charged Higgs bosons, we point out that the bosonic decay channels — especially the decay into a non-SM-like Higgs boson and a W boson — often dominate over the fermionic channels. Moreover, we revisit two genuine BSM effects on the properties of the discovered Higgs boson — the charged Higgs contribution to the diphoton rate and the Higgs decay to two light Higgs bosons — and their implication for the charged Higgs boson phenomenology. As main result of the present paper, we propose five two-dimensional benchmark scenarios with distinct phenomenological features in order to facilitate the design of dedicated LHC searches for charged Higgs bosons decaying into a W boson and a light, non-SM-like Higgs boson.

*henning.bahl@desy.de

†tim.stefaniak@desy.de

‡jonas.wittbrodt@thep.lu.se

Contents

1. Introduction	3
2. Charged Higgs boson phenomenology in doublet extensions of the SM	5
2.1. Charged Higgs couplings to bosons in N -Higgs-Doublet models	5
2.2. The Two Higgs Doublet Model	7
2.3. Phenomenological scan of the Two Higgs Doublet Model	9
3. Genuine BSM effects on the h_{125} properties	12
3.1. Charged Higgs boson contribution to $h_{125} \rightarrow \gamma\gamma$	12
3.2. The $h_{125} \rightarrow h_{\text{BSM}}h_{\text{BSM}}$ and $h_{125} \rightarrow AA$ decay modes	14
4. Searching for charged Higgs bosons at the LHC	15
4.1. Charged Higgs boson production at the LHC	16
4.1.1. $pp \rightarrow H^\pm tb$ production	16
4.1.2. $pp \rightarrow H^\pm h_i, H^\pm A$ production	17
4.1.3. $pp \rightarrow H^\pm W^\mp$ production	19
4.2. Charged Higgs boson decay modes	21
4.3. Current LHC searches for a charged Higgs boson	23
5. Unexplored LHC signatures and benchmark models	25
5.1. $\text{cH}(Wh_{\text{BSM}})$ scenario with large $\text{BR}(H^\pm \rightarrow W^\pm h_{\text{BSM}})$	30
5.2. $\text{cH}(WA)$ scenario with large $\text{BR}(H^\pm \rightarrow W^\pm A)$	32
5.3. $\text{cH}(Wh_{\text{BSM}}^{\text{fphob}})$ scenario with fermiophobic h_{BSM}	35
5.4. $\text{cH}(Wh_{\text{BSM}}^{\text{light}})$ scenario with light h_{BSM}	37
5.5. $\text{cH}(Wh_{\text{BSM}}^{\text{phil}})$ scenario with light leptophilic h_{BSM}	39
6. Conclusions	41
A. Benchmark scenarios: di-photon rate of h_{125}	43
B. Realizing the fermiophobic limit	44
C. Suppressing $h_{125} \rightarrow h_{\text{BSM}}h_{\text{BSM}}$ in the $\text{cH}(Wh_{\text{BSM}}^{\text{light}})$ scenario	45

1. Introduction

The discovery of a Higgs boson at the LHC in 2012 [1, 2] has initiated the survey of the scalar sector and the concomitant mechanism of spontaneous electroweak (EW) symmetry breaking. The Higgs boson — predicted in the Standard Model (SM) to be a fundamental scalar boson h originating from a complex scalar $SU(2)_L$ doublet field with hypercharge $Y = +\frac{1}{2}$ and vacuum expectation value (vev) $v \approx 246$ GeV — is the first of its kind, and the thorough investigation of its properties is of paramount importance for the understanding of particle physics. To this end, the LHC collaborations perform detailed measurements of the signal rates of the discovered Higgs boson in various production and decay modes, from which (under certain model assumptions) the strengths of the Higgs-boson couplings to the W and Z -bosons and to the third generation fermions can be inferred.¹ By the end of Run-2 of the LHC, with ~ 140 fb⁻¹ of data each collected by the ATLAS and CMS experiment, the Higgs-boson rate measurements agree remarkably well with the predictions in the Standard Model (SM). Yet, with the currently achieved precision of $\gtrsim \mathcal{O}(10\%)$ in the coupling determination [4–7], it is far from certain that the scalar sector as predicted in the SM is realized in nature.

Indeed, there are many reasons to anticipate effects from beyond the SM (BSM) physics in the scalar sector. The Higgs field may interact with the dark matter (DM) sector through so-called Higgs portal interactions, or DM itself may be composed of a stable scalar particle that originates from an extension of the SM Higgs sector (see Ref. [8] for a recent review). Furthermore, a BSM scalar sector may lead to a strong first-order EW phase transition and feature new sources of \mathcal{CP} -violation — these may enable the successful generation of the baryon asymmetry observed in the Universe (see e.g. [9–14] for recent works). BSM theories addressing the hierarchy problem, e.g. Supersymmetry (SUSY) [15–18], often modify or extend the scalar sector. Lastly, one may wonder why the scalar sector should be *minimal*, while we clearly have a *non-minimal* matter sector with three generations of fermions.

In many BSM extensions of the scalar sector, the discovered Higgs state h_{125} can acquire tree-level couplings to fermions and gauge bosons identical to those predicted in the SM in the so-called *alignment limit* [19–22]. In this limit the physical Higgs state h_{125} is *aligned* in field space with the direction of the vacuum expectation value v . The current LHC Higgs signal rate measurements imply that this alignment limit is at least approximately realized. However, the *origin* of this alignment — whether it is dynamical, by symmetry, or accidental — is unknown, and is obviously model-dependent.² Given the experimental observations in the Higgs signal rates, any phenomenologically viable BSM model therefore has to contain a Higgs boson with a mass around 125 GeV that is approximately “SM-like” in its coupling properties, as achieved near the alignment limit.

Extending the scalar sector also introduces additional scalar particles that could be

¹The precise determination of the Higgs boson trilinear and quartic self-couplings as well as the much weaker couplings to first and second generation fermions is challenging at the LHC [3].

²For instance, in supersymmetric models, alignment is automatically realized if the second Higgs doublet is decoupled, i.e. if all other Higgs bosons of the model are very heavy [19]. However, SUSY scenarios of accidental alignment *without* decoupling exist as well, see Refs. [23–30].

either neutral or carry electromagnetic charge. Detecting these new states complements the precision studies of the discovered Higgs state in the quest of unraveling the details of the electroweak symmetry breaking mechanism. To this end, the ATLAS and CMS collaborations have performed searches for the direct production and decay of additional (electrically neutral and charged) Higgs bosons. The targeted collider signatures are often guided by popular BSM theories, e.g. the Minimal Supersymmetric Standard Model (MSSM), and predicted to be experimentally accessible with current detector capabilities and the current amount of accumulated data. Other experimental BSM searches look for decays of known particles (e.g. the discovered Higgs boson h_{125}) into BSM particles. A prominent example are searches for an invisibly decaying Higgs boson (see e.g. Ref. [31] and references therein).

However, all these searches have not found any convincing hints for the existence of new particles yet, and have thus only produced upper limits on their possible signal cross section. Both experimental results — the Higgs-boson signal rate and mass³ measurements and the upper limits from searches for additional Higgs bosons — give rise to important constraints on the parameters of BSM models. At the same time, they challenge the theoretical community to provide reasonable explanations for the absence of hints for BSM physics at the LHC, and to give guidance for future strategies to remedy this situation. Given the prospect of an LHC upgrade to the high-luminosity (HL) phase, with an anticipated 3 ab^{-1} of data per experiment, as well as recent and upcoming advances in data analysis techniques (see e.g. Refs. [33–39]), so-far disregarded collider signatures of additional Higgs bosons (re)gain attention (see e.g. Refs. [27, 40–49] for recent proposals).

In this work we focus on collider signatures that arise from the production of a charged Higgs boson H^\pm and its successive decay to a lighter neutral Higgs boson and a W boson. While this decay mode has been investigated in several phenomenological works [25, 27, 50–60], up to now the signatures arising from this process have not been actively searched for by the LHC experiments⁴— with the notable exception of Ref. [65].⁵ Confirming earlier works we shall show in the present paper that these decays occur at sizable rates quite naturally already in minimal models that contain a charged Higgs boson, namely Two-Higgs-Doublet Models (2HDM), and, therefore, need to be explored experimentally. The purpose of this work is to motivate and initiate dedicated experimental searches by exploring the possible signal rates and providing suitable benchmark models for these studies based on the 2HDM of type-I and the lepton-specific 2HDM. We base our benchmark model definitions on the latest experimental constraints and state-of-the-art

³The Higgs boson mass has been determined to $125.09 \pm 0.21(\text{stat}) \pm 0.11(\text{syst})\text{GeV}$ in the combined ATLAS and CMS analysis of LHC Run-1 data [32].

⁴A possible explanation for this omission is that LHC searches for charged Higgs bosons were ever-so-often guided and motivated by the expectations within the MSSM Higgs sector. While MSSM parameter regions exist where the charged Higgs boson dominantly decays to a neutral Higgs and a W boson — e.g. the $H^\pm \rightarrow W^\pm h$ decays in the M_H^{125} scenario of Ref. [27] — these decays are absent in most of the parameter space due to an approximate mass degeneracy of the BSM Higgs bosons [19, 61–64].

⁵The CMS collaboration has searched for the process $pp \rightarrow H^\pm tb$, $H^\pm \rightarrow W^\pm A$, with the light pseudoscalar boson A decaying to $\mu^+\mu^-$, using 35.9 fb^{-1} of Run-2 data [65].

model predictions.

This paper is organized as follows. We first review the coupling properties of charged Higgs bosons in multi-Higgs-doublet models in Section 2, and then discuss the charged Higgs boson phenomenology in the Two-Higgs-Doublet-Model (2HDM) in light of current experimental and theoretical constraints. In Section 3 we revisit two important BSM effects on the discovered Higgs boson h_{125} that subsist even in case of exact alignment — the charged Higgs contribution to the Higgs-to-diphoton rate and the neutral Higgs (h_{125}) decay to two lighter neutral Higgs bosons — and their implications on the charged Higgs boson phenomenology. We discuss the most relevant charged Higgs boson production and decay modes, as well as the current LHC searches in Section 4. We then elaborate on the experimentally unexplored charged Higgs boson signatures in Section 5 and present several benchmark scenarios for future searches for these signatures. We conclude in Section 6.

2. Charged Higgs boson phenomenology in doublet extensions of the SM

In this section we will first review the coupling structure of charged Higgs bosons in the general N -Higgs-Doublet model.⁶ Afterwards, we will focus on the 2HDM.

2.1. Charged Higgs couplings to bosons in N -Higgs-Doublet models

A genuine prediction of Lorentz- and gauge-invariant BSM theories with additional scalar $SU(2)_L$ doublet fields is the existence of one pair of electrically charged Higgs bosons per doublet added to the SM.

The couplings of the charged scalars to vector bosons are

$$H_i^\pm H_j^\mp \gamma : \quad g(H_i^\pm H_j^\mp \gamma)(p_{H_i^\pm}^\mu - p_{H_j^\mp}^\mu) = \frac{1}{2} \delta_{ij} e (p_{H_i^\pm}^\mu - p_{H_j^\mp}^\mu), \quad (1)$$

$$H_i^\pm H_j^\mp Z : \quad g(H_i^\pm H_j^\mp Z)(p_{H_i^\pm}^\mu - p_{H_j^\mp}^\mu) = \frac{\delta_{ij}}{2} (g c_W - g' s_W) (p_{H_i^\pm}^\mu - p_{H_j^\mp}^\mu), \quad (2)$$

$$H_i^\pm W^\mp Z, H_i^\pm W^\mp \gamma : \quad 0. \quad (3)$$

Here, H_i^\pm denotes the charged Higgs boson mass eigenstates, g and g' are the $SU(2)_L$ and $U(1)_Y$ gauge coupling, respectively, and e is the electric charge. We use the short-hand notation $c_W \equiv \cos \theta_W$ and $s_W \equiv \sin \theta_W$, with the weak mixing angle θ_W . All momenta p^μ are considered as incoming.

The couplings of the neutral Higgs boson h_i to gauge bosons are defined by

$$h_i Z Z : \quad g(h_i Z Z) g_{\mu\nu}, \quad (4)$$

$$h_i W W : \quad g(h_i W W) g_{\mu\nu}, \quad (5)$$

⁶Charged Higgs bosons can also appear in higher-multiplet extensions of the SM-Higgs sector. We will not discuss those models (see Ref. [66] for a review).

and fulfill the sum rules (see e.g. [67])

$$\sum_i g(h_i ZZ)^2 = g(h_{\text{SM}} ZZ)^2 = \frac{g^2}{c_W^2} M_Z^2, \quad (6)$$

$$\sum_i g(h_i WW)^2 = g(h_{\text{SM}} WW)^2 = g^2 M_W^2, \quad (7)$$

where the sum runs over all neutral Higgs bosons and h_{SM} is a state with exactly SM-like couplings.⁷ Furthermore, gauge invariance requires

$$\frac{g(h_i ZZ)}{g(h_{\text{SM}} ZZ)} = \frac{g(h_i WW)}{g(h_{\text{SM}} WW)} \equiv c(h_i VV) \quad (8)$$

such that

$$\sum_i c(h_i VV)^2 = 1, \quad (9)$$

where $V = W, Z$.

We define the charged Higgs boson couplings to a neutral \mathcal{CP} -even or \mathcal{CP} -odd Higgs boson — h_j and a_j , respectively — and the W boson via

$$H_i^\pm W^\mp h_j : \quad g(H_i^\pm W^\mp h_j)(p_{h_i}^\mu - p_{H^\pm}^\mu), \quad (10)$$

$$H_i^\pm W^\mp a_j : \quad g(H_i^\pm W^\mp a_j)(p_{a_i}^\mu - p_{H^\pm}^\mu). \quad (11)$$

They obey sum rules for any j [67],⁸

$$\sum_i |g(H_i^\pm W^\mp h_j)|^2 = \frac{g^2}{4} (1 - c(h_j VV)^2), \quad (12)$$

$$\sum_i |g(H_i^\pm W^\mp a_j)|^2 = \frac{g^2}{4}, \quad (13)$$

where the sum runs over all charged Higgs bosons (excluding the charged Goldstone boson).

This sum-rule structure leads to important correlations between constraints on the couplings $c(h_j VV)$ and the couplings $g(H_i^\pm W^\mp h_j)$. In particular, in the alignment limit where one of the neutral \mathcal{CP} -even Higgs bosons is SM-like, $h_j = h_{\text{SM}}$, these correlations imply $\sum_i g(H_i^\pm W^\mp h_j) = 0$. In turn, the remaining neutral Higgs bosons h_i ($i \neq j$) will have rather large couplings to the charged Higgs bosons and the W boson. In the special case of the \mathcal{CP} -conserving Two-Higgs-Doublet Model (2HDM), which contains only two \mathcal{CP} -even neutral Higgs bosons and a single pair of charged Higgs bosons, this implies that the coupling between the charged Higgs boson, the non-SM-like \mathcal{CP} -even

⁷If the SM-Higgs sector is extended only by $SU(2)_L$ doublets and singlets, it is always possible to construct such a SM-like state. In general, this state is, however, not a mass eigenstate (see e.g. Ref. [67]).

⁸In the presence of \mathcal{CP} violation, the sum rule holds separately for the real and imaginary components of the \mathcal{CP} -admixed neutral Higgs bosons.

Higgs boson and the W boson is maximal in the alignment limit. We will discuss this case in more detail in Section 2.2.

Phenomenologically, these correlations have very important implications for collider searches for charged and neutral Higgs bosons. In particular, if there is a sizable difference between a charged Higgs boson mass, $m_{H_i^\pm}$, and the mass of a neutral, non-SM-like Higgs bosons, m_{h_j} , the decay modes

$$H_i^\pm \rightarrow W^\pm h_j \quad \text{if} \quad m_{H_i^\pm} > m_{h_j} \quad (14)$$

and

$$h_i \rightarrow H_j^\pm W^\mp \quad \text{if} \quad m_{h_i} > m_{H_j^\pm} \quad (15)$$

can have sizable rates that potentially dominate and, in turn, suppress the Higgs decay modes to SM fermions and gauge bosons. We shall focus on the first case, Eq. (14), in this work.

2.2. The Two Higgs Doublet Model

The two Higgs doublet model (2HDM) (see Refs. [61, 68] for reviews) is the simplest extension of the SM containing a charged Higgs state H^\pm , as it adds one additional Higgs doublet to the SM. In the present work, we focus on the most commonly studied version: the \mathcal{CP} -conserving 2HDM with a softly broken \mathbb{Z}_2 symmetry. Its scalar potential is given by

$$\begin{aligned} V_{2\text{HDM}}(\Phi_1, \Phi_2) = & m_{11}^2 \Phi_1^\dagger \Phi_1 + m_{22}^2 \Phi_2^\dagger \Phi_2 - m_{12}^2 \left(\Phi_1^\dagger \Phi_2 + \Phi_2^\dagger \Phi_1 \right) \\ & + \frac{1}{2} \lambda_1 (\Phi_1^\dagger \Phi_1)^2 + \frac{1}{2} \lambda_2 (\Phi_2^\dagger \Phi_2)^2 + \lambda_3 (\Phi_1^\dagger \Phi_1) (\Phi_2^\dagger \Phi_2) \\ & + \lambda_4 (\Phi_1^\dagger \Phi_2) (\Phi_2^\dagger \Phi_1) + \frac{1}{2} \lambda_5 \left((\Phi_1^\dagger \Phi_2)^2 + (\Phi_2^\dagger \Phi_1)^2 \right) \end{aligned} \quad (16)$$

with the scalar doublets

$$\Phi_{1,2} = \begin{pmatrix} \phi_i^+ \\ \frac{1}{\sqrt{2}}(v_i + \phi_i + i\chi_i) \end{pmatrix}. \quad (17)$$

It is useful to rotate to the Higgs basis (see e.g. [19]),

$$\begin{pmatrix} H_1 \\ H_2 \end{pmatrix} = \begin{pmatrix} c_\beta & s_\beta \\ -s_\beta & c_\beta \end{pmatrix} \begin{pmatrix} \Phi_1 \\ \Phi_2 \end{pmatrix}. \quad (18)$$

where we introduced the abbreviations $s_\gamma \equiv \sin \gamma$ and $c_\gamma \equiv \cos \gamma$ for a generic angle γ . The angle β is defined via the ratio of the vacuum expectation values (vevs), $t_\beta \equiv \tan \beta = v_2/v_1$. In this basis, only H_1 receives a vev.

In the Higgs basis the charged Higgs field H^\pm and the \mathcal{CP} -odd scalar field A are automatically mass eigenstates. To obtain the mass eigenstates h_1 and h_2 of the \mathcal{CP} -even scalars — whose masses fulfill, by definition, $m_{h_1} \leq m_{h_2}$ — a further rotation is

necessary,

$$\begin{pmatrix} h_1 \\ h_2 \end{pmatrix} = R \begin{pmatrix} h_1^{\text{HB}} \\ h_2^{\text{HB}} \end{pmatrix} = \begin{pmatrix} s_{\beta-\alpha} & c_{\beta-\alpha} \\ c_{\beta-\alpha} & -s_{\beta-\alpha} \end{pmatrix} \begin{pmatrix} h_1^{\text{HB}} \\ h_2^{\text{HB}} \end{pmatrix}, \quad (19)$$

where $h_{1,2}^{\text{HB}}$ are the \mathcal{CP} -even scalars in the Higgs basis and α is the rotation angle relating the fields ϕ_i of Eq. (17) to the mass eigenstates (see e.g. Ref. [19] for explicit formulas relating α to the potential parameters in Eq. (16)). In the following, we will denote the SM-like Higgs boson among $h_{1,2}$ by h_{125} and the non-SM-like Higgs boson by h_{BSM} .

The unitary matrix R is crucial for the phenomenology of the 2HDM. For instance, the couplings of the \mathcal{CP} -even scalars to gauge bosons $V \in \{W^\pm, Z\}$ are given by

$$c(h_i VV) = R_{i1}, \quad (20)$$

where R_{i1} is the $(i1)$ -entry of the mixing matrix R .

In the alignment limit, where $s_{\beta-\alpha} \simeq 1$ if $h_1 \rightarrow h_{\text{SM}}$ and $c_{\beta-\alpha} \simeq 1$ if $h_2 \rightarrow h_{\text{SM}}$, these couplings are maximized for the SM-like Higgs boson, i.e. it acquires SM-like couplings to gauge bosons. At the same time, orthogonality of the mixing matrix, Eq. (19), or equivalently Eq. (9), implies that the couplings of the other \mathcal{CP} -even neutral Higgs boson to gauge bosons have to vanish.

As already discussed in Section 2.1, this has important consequences for the charged Higgs boson H^\pm . Its coupling to a neutral Higgs boson h_i and a W^\pm is given by

$$g(H^\pm W^\mp h_i) = -\frac{g}{2} R_{i2} (p_{h_i}^\mu - p_{H^\pm}^\mu). \quad (21)$$

In the alignment limit this coupling vanishes for h_{125} and is maximized for h_{BSM} since R is a 2×2 orthogonal matrix. The coupling of the charged Higgs boson to the A boson and a W^\pm boson,

$$g(H^\pm W^\mp A) = -\frac{g}{2}, \quad (22)$$

is not affected by the alignment of the SM-like Higgs boson.

The Yukawa sector of the 2HDM is determined by its symmetry structure. In order to avoid tree-level flavor changing neutral currents, the \mathbb{Z}_2 symmetry can be extended to the fermion sector resulting in four distinct types of Yukawa sectors (see Table 1): type I, type II, flipped, and lepton specific. In this work we will focus on type-I and lepton-specific models since in type II (and flipped) 2HDMs measurements of flavor observables constrain the charged Higgs boson to be very heavy [69, 70]. In type-I Yukawa sectors, the SM-normalized couplings of each Higgs boson to all fermion types are equal.

Via this Yukawa interaction, also the charged Higgs boson interacts with fermions,

$$\mathcal{L}_{\text{Yuk}} \supset - \sum_i H^+ \left(\frac{\sqrt{2} V_{u_i d_j}^{\text{CKM}}}{v} \bar{u}_i (m_{u_i} \lambda_{uu} P_L + m_{d_j} \lambda_{dd} P_R) d_j + \frac{\sqrt{2}}{v} m_{l_j} \lambda_{ll} \bar{\nu}_{iL} l_{jR} \right), \quad (23)$$

where V^{CKM} is the Cabibbo-Kobayashi-Maskawa matrix, and $P_{L,R}$ are the left- and right-handed chirality projection operators.

Type	u_R	d_R	l_R	λ_{uu}	λ_{dd}	λ_{ll}
I	+	+	+	$\cot \beta$	$\cot \beta$	$\cot \beta$
II	+	-	-	$\cot \beta$	$-\tan \beta$	$-\tan \beta$
Flipped	+	-	+	$\cot \beta$	$-\tan \beta$	$\cot \beta$
Lepton-specific	+	+	-	$\cot \beta$	$\cot \beta$	$-\tan \beta$

Table 1.: Assignment of the \mathbb{Z}_2 charges to the right-handed fermions for the different types of 2HDMs. The resulting coefficients of the charged Higgs–fermion interaction are also shown.

As a consequence of the coupling dependence on the quark masses (m_{u_i} and m_{d_i}) and the lepton masses (m_{l_j}), the most important charged Higgs decay modes to fermions are $H^+ \rightarrow c\bar{b}$ and $H^+ \rightarrow \tau^+\nu$ for low masses below the top quark mass, and $H^+ \rightarrow t\bar{b}$ for heavier masses.

For the rest of the paper we will work in the 2HDM framework introduced above. In many extended models, the charged Higgs boson phenomenology is very similar. Often, only the overall rates of the $H_i^\pm \rightarrow W^\pm h_j$ decays are expected to be lower due to the corresponding sum rules (see Eqs. (12) and (13)).

2.3. Phenomenological scan of the Two Higgs Doublet Model

We base our phenomenological study on a large parameter scan of the 2HDM type-I parameter space using the code `ScannerS` [71–75]. We require all parameter points to fulfill current theoretical and experimental constraints. These include

- tree-level perturbative unitarity and boundedness from below (BfB) [68],
- absolute stability⁹ of the tree-level vacuum [76],
- electroweak precision constraints through the oblique parameters S , T and U using the prediction of Refs. [77, 78] and the fit result of Ref. [79],
- flavor constraints using the results of Ref. [79],
- bounds from searches for additional scalars using `HiggsBounds-5.9.0` [80–85],
- and agreement with the Higgs signal measurements using `HiggsSignals-2.6.0` [86–89], which incorporates the combined LHC Run-1 results [4] as well as the latest Run-2 Higgs measurements by the ATLAS [90–98] and CMS [99–110] collaborations.

⁹A sufficiently long-lived metastable EW vacuum would be acceptable as well. In the 2HDM, most parameter regions that could feature a metastable EW vacuum are, however, excluded by LHC measurements [76]. We, therefore, do not expect any different collider phenomenology by allowing metastable vacua, and exclude them for simplicity.

	$m_{h_{\text{BSM}}} [\text{GeV}]$	$m_A [\text{GeV}]$	$m_{H^\pm} [\text{GeV}]$	$\tan \beta$	$c(h_{\text{BSM}}VV)$	$m_{12}^2 [\text{GeV}^2]$
min	30	30	50	0.8	-0.5	0
max	1000	1000	1000	25.0	0.5	10^6

Table 2.: Input parameter ranges for the parameter scan in the type I 2HDM.

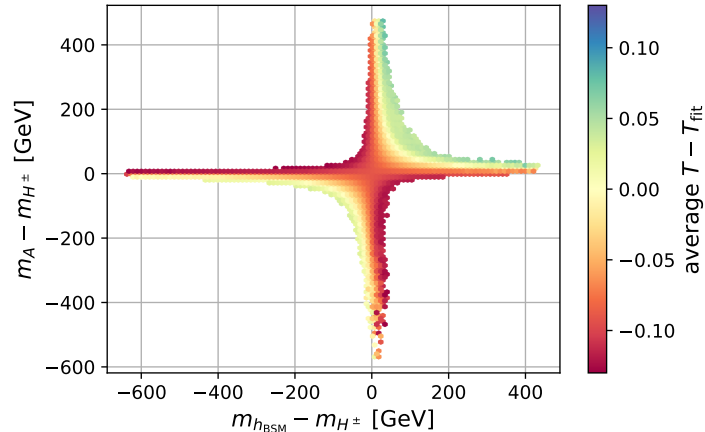


Figure 1.: Possible mass separations between the charged Higgs boson and the non- h_{125} neutral Higgs bosons. The color code indicates the (per-bin averaged) deviation of the T parameter from the central value of the fit from Ref. [79].

The required branching ratios of the scalars are calculated using HDECAY [111–113] and the neutral scalar production cross sections using SusHi [114, 115].¹⁰ See Ref. [75] for details on the scanning procedure.

We fix the mass of the h_{125} boson to its observed value from the ATLAS and CMS LHC Run-1 combined analysis, $m_{h_{125}} = 125.09 \text{ GeV}$ [32], and uniformly sample the remaining model parameters within the ranges given in Table 2. For convenience, we choose the coupling $c(h_{\text{BSM}}VV)$ as input parameter in order to cover the two possible cases $h_1 \simeq h_{\text{SM}}$ and $h_2 \simeq h_{\text{SM}}$ together in one scan (see Ref. [75] for details). Valid parameter points with $\tan \beta$ larger than the chosen upper limit are possible. However, since we are interested in scenarios where both the fermionic channels — suppressed by large $\tan \beta$ — and the bosonic channels — mostly independent of $\tan \beta$ — are potentially observable at the LHC, we focus on the low and medium $\tan \beta$ region and use the arbitrary upper limit of $\tan \beta < 25$. In the following, we show results for a sample of 10^6 parameter points that fulfill all of the above constraints (at the 2σ level, where applicable).

As a first scan result, we investigate the well-known and important impact of the electroweak precision constraints on the Higgs mass spectrum (see e.g. Ref. [116]). Especially the constraint on the T parameter forces m_{H^\pm} to be always close to one of the neutral Higgs masses. This is illustrated in Fig. 1 showing the deviation of the T

¹⁰The used cross-section calculations for charged Higgs boson production are described in detail in Section 4.1.

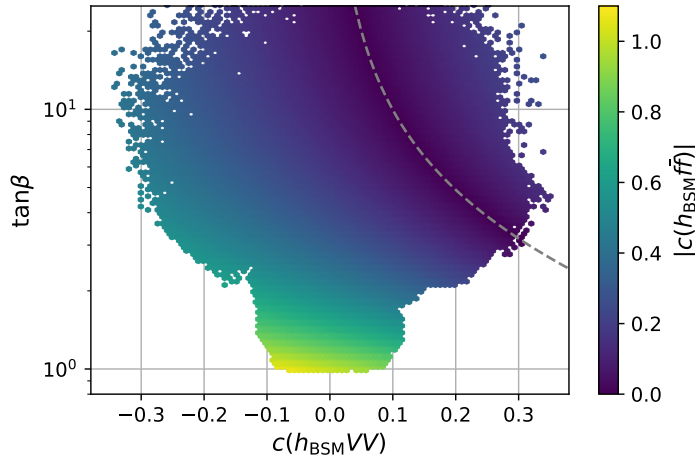


Figure 2.: The allowed parameter region for the effective gauge coupling $c(h_{\text{BSM}}VV)$ of the non- h_{125} \mathcal{CP} -even scalar h_{BSM} and $\tan\beta$. The exact alignment limit for h_{125} is realized when $c(h_{\text{BSM}}VV) = 0$. The color code represents the SM-normalized fermion coupling of h_{BSM} , which vanishes in the fermiophobic limit indicated by the dashed line. Parameter points where both $m_{h_{1,2}} \in [120, 130]$ GeV are not shown to allow a clear distinction between h_{BSM} and h_{125} .

parameter from the central value of the fit in Ref. [79] in the $(m_{h_{\text{BSM}}} - m_{H^\pm}, m_A - m_{H^\pm})$ plane. As mentioned above, only parameter points with a deviation less than 2σ are shown. It is clearly visible that either $m_{h_{\text{BSM}}} \sim m_{H^\pm}$ or $m_A \sim m_{H^\pm}$ needs to be fulfilled. In the context of the charged Higgs boson decay into a W boson and a lighter Higgs boson, as discussed in Sections 2.1 and 2.2, this constraint implies that either h_{BSM} or A — but not both — can be significantly lighter than the charged Higgs boson. As a consequence, at least one of the channels $H^\pm \rightarrow h_{\text{BSM}}W^\pm$ or $H^\pm \rightarrow AW^\pm$ can be kinematically accessible in large parts of the parameter space.

Fig. 2 shows the scan results in the plane of the two important coupling parameters $c(h_{\text{BSM}}VV)$ and $\tan\beta$. The Higgs signal rate measurements constrain

$$|c(h_{\text{BSM}}VV)| \lesssim 0.3 \quad (24)$$

for almost all allowed parameter points in this scan, thus the alignment limit for h_{125} — which would mean $c(h_{\text{BSM}}VV) = 0$ — is always approximately realized. With Eq. (12) this in turn means that the $H^\pm W^\mp h_{\text{BSM}}$ coupling reaches always at least $\sqrt{1 - 0.3^2} \approx 95\%$ of its maximum possible value. The color map in Fig. 2 shows the SM-normalized coupling of h_{BSM} to fermions,

$$c(h_{\text{BSM}}f\bar{f}) \equiv \frac{g(h_{\text{BSM}}f\bar{f})}{g(h_{\text{SM}}f\bar{f})} = \begin{cases} \frac{c_\alpha}{s_\beta} & \text{if } h_1 \equiv h_{\text{BSM}}, \\ \frac{s_\alpha}{s_\beta} & \text{if } h_2 \equiv h_{\text{BSM}}, \end{cases} \quad (25)$$

which is identical for all fermions if the Yukawa sector is of type I.¹¹ It can clearly be seen that $c(h_{\text{BSM}}f\bar{f})$ becomes small for large $\tan\beta$. Furthermore, in the 2HDM there exists a so-called *fermiophobic* limit for each of the \mathcal{CP} -even neutral scalars (no corresponding limit exists for the A boson), where the couplings of this particle to SM-fermions vanish. This limit is indicated for h_{BSM} by the dashed line in Fig. 2 and is reached for

$$\tan\beta = \frac{\sqrt{1 - c(h_{\text{BSM}}VV)^2}}{c(h_{\text{BSM}}VV)}. \quad (26)$$

It is clear from the equation and also visible in Fig. 2 that this limit is only reachable if the h_{125} alignment is not exact. Trying to satisfy Eq. (26) in the case of exact alignment would require $\tan\beta \rightarrow \infty$.

The fermiophobic limit is phenomenologically interesting in our study because most of the direct LHC searches for h_{BSM} rely on production and decay modes governed by its coupling to fermions, e.g. gluon fusion, which vanish in the fermiophobic limit. Only the gauge-boson mediated production channels — such as vector boson fusion (VBF) and W/Z -associated production — are non-zero, but are suppressed by the small $c(h_{\text{BSM}}VV)$. Similarly, the h_{BSM} decay modes to fermions are suppressed (or even vanish in the exact fermiophobic limit). In such a scenario, production of H^\pm followed by $H^\pm \rightarrow h_{\text{BSM}}W^\pm$ could well be the most promising discovery channel for both H^\pm and h_{BSM} . We come back to the discussion of the fermiophobic Higgs limit in Section 5, where we introduce a dedicated benchmark scenario that features a fermiophobic non-SM-like Higgs boson.

3. Genuine BSM effects on the h_{125} properties

As outlined in Section 2.2, the role of the observed Higgs boson h_{125} can be played by either the lighter or the heavier \mathcal{CP} -even neutral Higgs state, h_1 or h_2 . Its tree-level couplings to fermions and gauge bosons become identical to the predictions of the SM in the alignment limit. However, through the interplay with the remaining Higgs states of the model, deviations from the SM Higgs properties can still occur in the exact alignment limit. These can either be loop-induced (effective) coupling modifications, or additional decay modes to BSM Higgs bosons. In this section we will first discuss the charged Higgs boson contribution to the $h_{125} \rightarrow \gamma\gamma$ decay, and then elaborate on the possibility of the decays $h_{125} \rightarrow h_{\text{BSM}}h_{\text{BSM}}$ and $h_{125} \rightarrow AA$ in case of very light h_{BSM} and A bosons.

3.1. Charged Higgs boson contribution to $h_{125} \rightarrow \gamma\gamma$

The $h_{125} \rightarrow \gamma\gamma$ decay channel is currently measured with an accuracy at the level of $\sim 10\%$ [6, 117], which is expected to improve to $\lesssim 3\%$ at the HL-LHC [3]. The charged Higgs boson induces deviations from the SM prediction at the leading order, as depicted in Fig. 3. These corrections do not vanish in the alignment limit in which all tree-level couplings of h_{125} are exactly equal to the respective SM values. Interestingly, these

¹¹For the lepton-specific 2HDM, the coupling of h_{BSM} to leptons is $-s_\alpha/c_\beta$ if $h_1 \equiv h_{\text{BSM}}$ and c_α/c_β if $h_2 \equiv h_{\text{BSM}}$. The couplings to quarks are identical to those in the 2HDM type I.

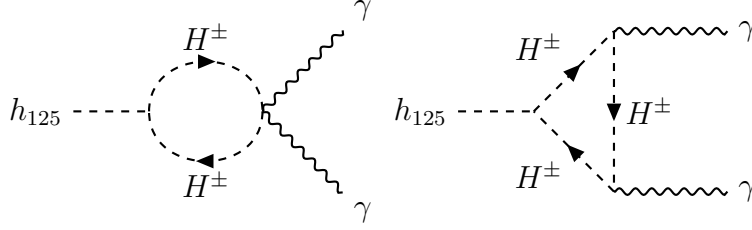


Figure 3.: Charged Higgs contribution to $h_{125} \rightarrow \gamma\gamma$ at the one-loop level.

corrections also do not necessarily vanish if the charged Higgs boson is much heavier than the electroweak scale. This non-decoupling effect (described in detail in Refs. [21, 22, 118–122]) opens the possibility to indirectly probe the charged Higgs boson via precision $h_{125} \rightarrow \gamma\gamma$ measurement.

The relevant couplings of the \mathcal{CP} -even Higgs bosons h_i ($i = 1, 2$) to a pair of charged Higgs boson are given by

$$g_{h_i H^+ H^-} = -\frac{1}{v} \left\{ [m_{h_1}^2 + 2(m_{H^\pm}^2 - \bar{m}^2)] R_{i1} + 2(m_{h_1}^2 - \bar{m}^2) \frac{R_{i2}}{t_{2\beta}} \right\}, \quad (27)$$

where $\bar{m}^2 = m_{12}^2/(s_\beta c_\beta)$ and R is the unitary mixing matrix defined in Eq. (19). In the alignment limit, in which one of the h_i becomes SM-like (implying that $R_{i1} \rightarrow 1$), we obtain

$$g_{h_{125} H^+ H^-} \rightarrow -\frac{1}{v} [m_{h_{125}}^2 + 2(m_{H^\pm}^2 - \bar{m}^2)], \quad (28)$$

In the $m_{H^\pm} \gg v$ limit, the terms involving $m_{H^\pm}^2$ can compensate the suppression arising through the loop integrals which scale proportional to v^2/m_{H^\pm} . Consequently, the charged Higgs boson contribution to the di-photon decay rate can reach a constant value even if $m_{H^\pm} \gg v$.

While the $h_1 = h_{125}$ and $h_2 = h_{125}$ cases appear to be very similar, they actually have a distinct phenomenology. This is illustrated in Fig. 4 showing the di-photon signal strength of h_{125} as a function of m_{H^\pm} for the parameter scan described in Section 2.3. For the blue points, the lighter \mathcal{CP} -even Higgs boson is SM-like ($h_1 = h_{125}$); for the orange points, the heavier \mathcal{CP} -even Higgs boson is SM-like ($h_2 = h_{125}$). Scan points for which $m_{h_1}, m_{h_2} \in [120, 130]$ GeV are not shown in order to allow for a clear distinction of these cases.

In case of $h_1 = h_{125}$, the di-photon rate can deviate from the SM value by up to $\pm 17\%$ for $m_{H^\pm} \lesssim 200$ GeV. For $m_{H^\pm} \gtrsim 300$ GeV, positive deviations from the SM of up to $\sim 5\%$ and negative deviations of up to $\sim 15\%$ are possible. If the di-photon rate is close to the SM value, the term proportional to \bar{m}^2 compensates the remaining terms in Eq. (28). This is exactly what happens in the decoupling limit of the 2HDM [19], where $m_H^2 \approx m_A^2 \approx m_{H^\pm}^2 \approx m_{12}^2 \gg v^2$ and this contribution vanishes as expected.

This is not possible in the case of $h_2 = h_{125}$. If $m_{h_1}, m_{h_2} \ll m_{H^\pm}$, constraints arising from perturbative unitarity (and perturbativity) force $\bar{m}^2 \sim \mathcal{O}(v^2)$ and the term proportional to $m_{H^\pm}^2 \gg \mathcal{O}(v^2)$ in Eq. (28) can not be compensated (see Ref. [22] for more details). Therefore, the charged Higgs boson contribution to the di-photon rate reaches

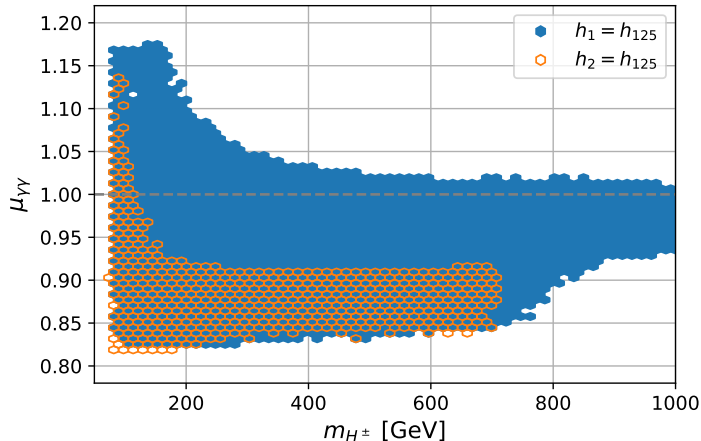


Figure 4.: Scatter plot of the signal strength $\mu_{\gamma\gamma}$ of h_{125} as a function of the charged Higgs mass. The dashed line indicates the SM value of $\mu_{\gamma\gamma} = 1$. For the blue (orange) points the light (heavy) \mathcal{CP} -even Higgs boson is h_{125} . To allow a clear distinction of these cases, parameter points where both $m_{h_1}, m_{h_2} \in [120, 130]$ GeV are not shown.

an approximately constant value for $m_{H^\pm} \gtrsim 200$ GeV with a negative deviation from the SM by $\sim 9 - 15\%$. Perturbative unitarity also implies that m_{H^\pm} can not reach values above ~ 700 GeV if $h_2 = h_{125}$. Given these observations, we may optimistically argue that the $h_2 = h_{125}$ scenario in the 2HDM can completely be covered experimentally at the HL-LHC, using two complementary probes: in the heavy H^\pm regime, $m_{H^\pm} \gtrsim 200$ GeV, the deviations from the SM in the $h_{125} \rightarrow \gamma\gamma$ rate will be probed with corresponding precision measurements. In contrast, the light H^\pm regime, $m_{H^\pm} < 200$ GeV, may be probed experimentally with direct H^\pm searches due rather large production cross sections. In this endeavor, though, all possible H^\pm collider signatures have to be searched for, including, in particular, the signatures arising from the $H^\pm \rightarrow W^\pm h_{\text{BSM}}$ decay, as proposed in this work.

The charged Higgs contribution to the h_{125} di-photon rate also affects the selection of the benchmark scenarios to be discussed in Section 5 (see also the discussion in Appendix A).

3.2. The $h_{125} \rightarrow h_{\text{BSM}}h_{\text{BSM}}$ and $h_{125} \rightarrow AA$ decay modes

The parameter space with a very light non-SM-like neutral Higgs boson h_{BSM} or A , with a mass $\sim \mathcal{O}(\text{few } 10 \text{ GeV})$, is interesting for the charged Higgs boson phenomenology for two reasons: First, it kinematically enables the decay $H^\pm \rightarrow W^\pm h_{\text{BSM}}$ or $H^\pm \rightarrow W^\pm A$, respectively, even in case that the charged Higgs boson is very light, e.g., below the top quark mass ($m_{H^\pm} \lesssim m_t$). This, in turn, can lead to a sizable charged Higgs boson production cross section. Second, very light BSM Higgs bosons in the final state can lead to distinct kinematics, e.g., boosted and collimated BSM Higgs decay products, warranting the design of specific analysis techniques in the experimental searches. However, scenar-

ios with a light non-SM-like neutral Higgs boson with mass below $m_{h_{125}}/2 \approx 62.5$ GeV have to obey stringent constraints, as the additional decay mode $h_{125} \rightarrow h_{\text{BSM}}h_{\text{BSM}}$ or $h_{125} \rightarrow AA$ is kinematically allowed. In the 2HDM, direct searches for such decays, e.g. Refs. [123–129], are currently weaker than the indirect constraints arising from the 125 GeV Higgs boson precision rate measurements (see e.g. Ref. [43]). In this section we therefore investigate these decays in detail and discuss under which circumstances the constraints can be evaded by suppressing the corresponding decay rate.

The triple scalar couplings governing these decay modes are given by

$$4v \cdot g_{h_1 h_1 h_2} = \frac{c_{\beta-\alpha}}{s_\beta c_\beta} [(3\bar{m}^2 - m_H^2 - 2m_h^2) s_{2\alpha} - \bar{m}^2 s_{2\beta}] , \quad (29)$$

$$-v \cdot g_{h_i AA} = (m_{h_i}^2 + 2m_A^2 - 2\bar{m}^2) R_{i1} + 2(m_{h_1}^2 - \bar{m}^2) R_{i2}/t_{2\beta} . \quad (30)$$

Even in the alignment limit $h_{125} \rightarrow h_{\text{SM}}$, the resulting couplings

$$g_{h_{125} h_{\text{BSM}} h_{\text{BSM}}} \rightarrow \frac{2\bar{m}^2 - m_{h_{125}}^2 - 2m_{h_{\text{BSM}}}^2}{2v} , \quad (31)$$

$$g_{h_{125} AA} \rightarrow \frac{2\bar{m}^2 - m_{h_{125}}^2 - 2m_A^2}{v} \quad (32)$$

can lead to decays of $h_{125} \rightarrow h_{\text{BSM}}h_{\text{BSM}}, AA$ if kinematically allowed. Even for BSM Higgs masses above $m_{h_{125}}/2$, the off-shell branching ratios into these final states can be substantial.

For the purpose of studying charged Higgs phenomenology for $m_{h_{\text{BSM}/A}} < 62.5$ GeV it is useful to define scenarios where the $h_{125} \rightarrow h_{\text{BSM}}h_{\text{BSM}}, AA$ decays are not the most sensitive observables (in order to not be experimentally excluded by these channels). This can be accomplished by choosing \bar{m}^2 and thus m_{12}^2 such that the respective triple scalar couplings are zero,

$$g_{h_1 h_1 h_2} = 0 : \quad m_{12}^2 = \frac{(m_{h_2}^2 + 2m_{h_1}^2)c_\alpha s_\alpha}{3\frac{c_\alpha s_\alpha}{c_\beta s_\beta} - 1} , \quad (33)$$

$$g_{h_i AA} = 0 : \quad m_{12}^2 = \frac{1}{2} ((2m_A^2 + m_{h_1}^2)R_{i1} + 2m_{h_1}^2 R_{i2}/t_{2\beta}) \frac{c_\beta s_\beta}{R_{i1} + R_{i2}/t_{2\beta}} . \quad (34)$$

For the benchmark scenarios to be discussed in Section 5, we only consider the case of a light \mathcal{CP} -even Higgs boson for simplicity (we expect the case of light A boson to be very similar phenomenologically). In this context, we find that $g_{h_1 h_1 h_2} = 0$ is not possible in the exact $h_2 = h_{125} \rightarrow h_{\text{SM}}$ alignment limit without violating theoretical constraints and therefore consider scenarios that deviate slightly from alignment (see also Appendix C).

4. Searching for charged Higgs bosons at the LHC

In this section we will discuss in detail the various LHC production and decay modes of the charged Higgs boson and give an overview of current LHC searches focusing on the 2HDM structure introduced in Section 2.2

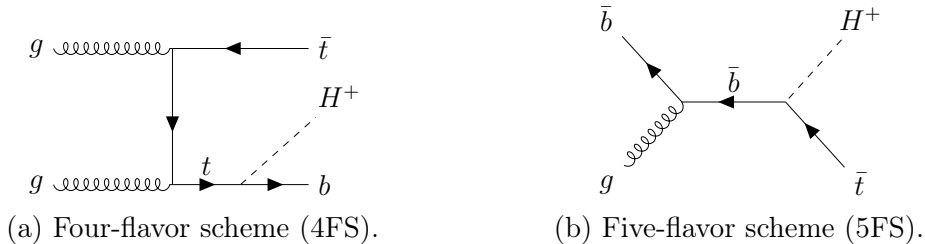


Figure 5.: Exemplary Feynman diagrams for $pp \rightarrow H^\pm tb$ production.

4.1. Charged Higgs boson production at the LHC

At the LHC there are three main channels for direct charged Higgs boson production (see e.g. Refs. [55, 63] for other comprehensive reviews): The charged Higgs boson can be produced in association with a top and a bottom quark, in association with a neutral Higgs boson, and in association with a W boson. These production modes will be discussed in more detail below. In addition to these channels, charged Higgs bosons can also be produced in pairs (see e.g. Ref. [63]), albeit at a very small rate, or in vector-boson fusion, if the charged Higgs boson originates from a $SU(2)$ Higgs triplet.

All used cross-section values (except of $pp \rightarrow H^\pm tb$ production) are available as data tables in the form of ancillary files accompanying the present paper. The cross section calculations in these channels use the MMHT2014 pdf set [130].

4.1.1. $pp \rightarrow H^\pm tb$ production

Charged Higgs boson production in association with a top and a bottom quark can be calculated either in the four-flavor scheme (4FS) as shown in Fig. 5a — corresponding to the process $gg \rightarrow \bar{t}bH^\pm$ — or in the five-flavor scheme (5FS) as shown in Fig. 5b — corresponding to the process $g\bar{b} \rightarrow \bar{t}H^\pm$. While the calculation in the 5FS is more precise in the collinear region of phase space in which the transverse momentum of the b quark is small, the 4FS yields more accurate results if the transverse momentum of the b quark is large. To obtain a prediction precise for all phase space regions, both calculations have been matched by identifying terms which would be double-counted if both calculations would be summed naively [131].

A related issue appears for low charged Higgs boson masses, m_{H^\pm} , well below the top-quark mass, m_t . In this regime a charged Higgs boson can be produced via the decay of a top quark. This process can be conveniently calculated in the narrow-width approximation. If the mass of the charged Higgs boson is, however, close to the top-quark mass, the narrow-width approximation becomes invalid and all contributions to the process $pp \rightarrow H^\pm tb$ have to be taken into account (see Refs. [131–133] for LO calculations).

NLO corrections for charged Higgs boson production in association with a top and a bottom quark in the regime of $m_{H^\pm} > m_t$ have been calculated in Refs. [134–142]. In the regime $m_{H^\pm} < m_t$, NLO corrections have been derived in Refs. [143–153]. The intermediate mass regime of $m_{H^\pm} \sim m_t$ has been addressed at the NLO level in Refs. [137,

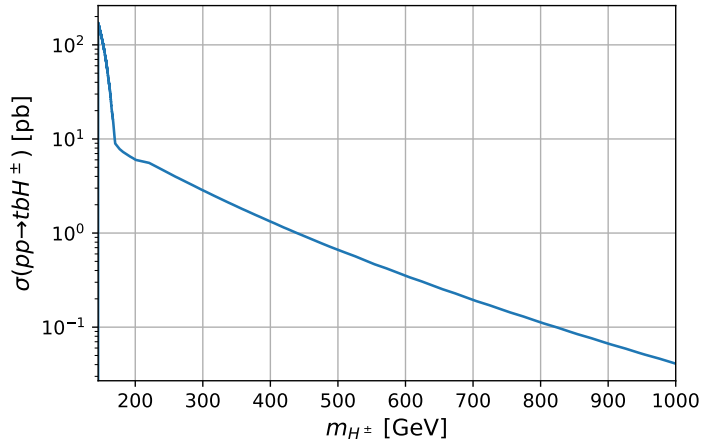


Figure 6.: Charged Higgs production cross section in the $pp \rightarrow H^\pm tb$ channel at the 13 TeV LHC for $\tan\beta = 1$ at NLO [142, 154].

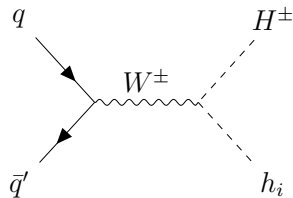


Figure 7.: Dominant leading-order s -channel Feynman diagram for $pp \rightarrow H^\pm h$ production.

141, 154].

For our present study, we use the tabulated NLO results of Refs. [142, 154] for $m_{H^\pm} > 145$ GeV. We refer to those references for details on the calculation, the 4FS/5FS matching procedure, and the input parameters. Figure 6 shows the corresponding numerical prediction for the 2HDM type-I (and the lepton-specific 2HDM) with $\tan\beta = 1$. The cross section for other $\tan\beta$ values can be obtained by dividing by $\tan^2\beta$. For lower charged Higgs masses, we multiply the 13 TeV LHC $\sigma(pp \rightarrow t\bar{t})$ cross section of ~ 803 pb [155] by the appropriate branching fraction

$$2 \text{BR}(t \rightarrow H^\pm b) (1 - \text{BR}(t \rightarrow H^\pm b)) \quad (35)$$

obtained from HDECAY [111, 113]. While $\sigma(pp \rightarrow H^\pm tb)$ can reach values of more than 100 pb for $m_{H^\pm} < m_t$, the cross section is substantially smaller above the t -threshold with values of 6 pb at $m_{H^\pm} = 200$ GeV decreasing to ~ 0.1 pb at 800 GeV.

4.1.2. $pp \rightarrow H^\pm h_i, H^\pm A$ production

Another important production channel is charged Higgs production in association with a neutral Higgs boson [156–161], see Fig. 7 for the dominant LO s -channel diagram. The contribution from this diagram is proportional to the $H^\pm W^\mp h_i$ coupling, which is

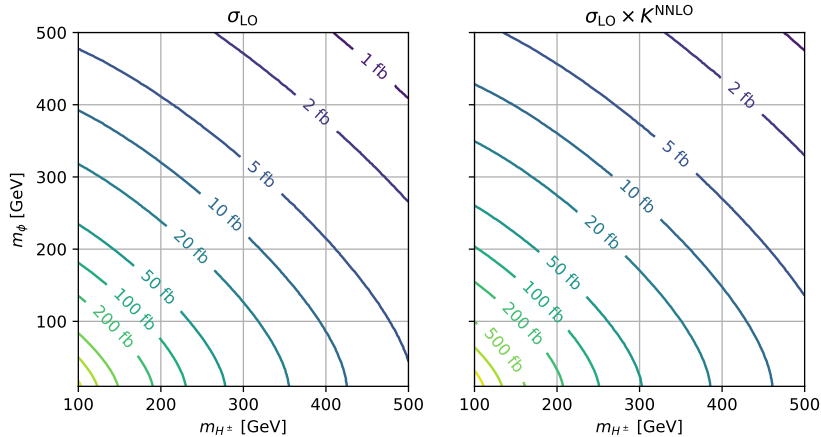


Figure 8.: *Left*: LO cross section for $pp \rightarrow H^\pm \phi$ production (with $\phi = h_{\text{BSM}}, A$) as a function of m_{H^\pm} and m_ϕ . *Right*: Same as left but the LO cross section multiplied with NNLO K -factor is shown. Both figures assume exact alignment.

maximized in the alignment limit for $h_i = h_{\text{BSM}}$, while it vanishes for $h_i = h_{125}$ (see Section 2). As the experimental data favors an approximate realization of the alignment limit (see discussion in Section 2.3), we only consider the case where the charged Higgs boson is produced in association with the non-SM-like \mathcal{CP} -even Higgs boson h_{BSM} or the \mathcal{CP} -odd Higgs boson A .

For the $pp \rightarrow H^\pm h_{\text{BSM}}$ process, no dedicated calculation beyond the LO exists. While NLO-QCD corrections could easily be derived using automated NLO tools, we estimate the impact of higher-order corrections to the $pp \rightarrow H^\pm h_{\text{BSM}}$ cross section by comparing it to the SM $pp \rightarrow W^+ h$ process. Since the only colored states in both processes are the incoming quarks, QCD corrections arise only as initial state radiation and as virtual corrections to the $W^\pm q\bar{q}$ vertex, which are identical in both processes. Since the different couplings in the second vertex cancel out in the K -factor, the only remaining difference between the two process is the different mass of the final state particles, and the resulting differences in phase space and scale. We use this analogy by employing the NNLO-QCD $pp \rightarrow W^+ h$ calculation implemented in the code `vh@nnlo-2.1` [162, 163] adjusted to account for the changed final state masses¹² in order to derive a mass-dependent K -factor, which is defined as the ratio of the NNLO cross section over the LO cross section. We then use this K -factor to rescale the LO $pp \rightarrow H^\pm h_{\text{BSM}}$ cross section obtained with `MadGraph5-2.8.0` [164]. Both calculations are performed in the 4FS, as is appropriate for an s -channel W^\pm -exchange process, where b -quark contributions are negligible.

The left panel of Fig. 8 shows the 13 TeV LHC LO cross section as a function of m_{H^\pm} and $m_{h_{\text{BSM}}}$, assuming exact alignment of h_{125} . The right panel displays the LO cross section multiplied with the NNLO K -factor. The K -factor only varies slightly within the considered mass plane with a range between 1.34 for low masses and 1.37 for high masses. Both plots show the cross section summed over both possible charges of H^\pm .

¹²We thank Stefan Liebler for discussions on this possibility and adjusting the code to our needs.

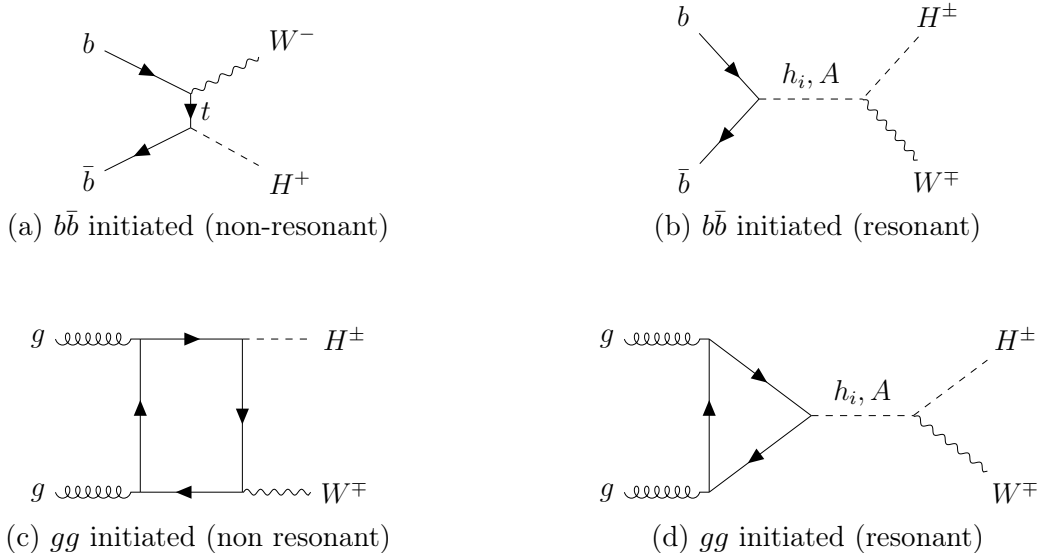


Figure 9.: Leading-order Feynman diagrams for $pp \rightarrow H^\pm W^\mp$ production.

Cross sections for $pp \rightarrow h_{\text{BSM}} H^\pm$ for different values of $c(h_{\text{BSM}} VV)$ can be obtained by rescaling with $c(h_{\text{BSM}} VV)^2$. The $pp \rightarrow A H^\pm$ cross sections are independent of all other model parameters.

Let us consider this production mode in conjunction with the subsequent decay of the charged Higgs boson into a W boson and the non-SM-like Higgs boson, $pp \rightarrow H^\pm h_{\text{BSM}} \rightarrow W^\pm h_{\text{BSM}} h_{\text{BSM}}$. This final state can also arise from double-Higgsstrahlung, or Higgsstrahlung followed by an $h_{\text{BSM}} \rightarrow h_{\text{BSM}} h_{\text{BSM}}$ splitting. These could contribute and may even interfere with our signal process. However, both of these processes involve the coupling $c(h_{\text{BSM}} VV)$ which is strongly suppressed in the alignment limit. Using MadGraph5-2.8.0 we have verified that the total cross sections for the exclusive subprocess $pp \rightarrow H^\pm h_{\text{BSM}} \rightarrow W^\pm h_{\text{BSM}} h_{\text{BSM}}$ and the inclusive $pp \rightarrow W^\pm h_{\text{BSM}} h_{\text{BSM}}$ process agree within less than 3% for all benchmark scenarios defined in Section 5. Thus, the alternative processes can be safely neglected.

In the used approximation, the cross section for the production of the charged Higgs boson in association with an A boson is identical to the $pp \rightarrow H^\pm h_{\text{BSM}}$ cross section.

4.1.3. $pp \rightarrow H^\pm W^\mp$ production

At the leading order, four different subprocesses contribute to the production of a charged Higgs boson in association with a W boson: the $b\bar{b}$ -initiated non-resonant channel (see Fig. 9a), the $b\bar{b}$ -initiated resonant channel (see Fig. 9b), the gg -initiated non-resonant channel (see Fig. 9c), and the gg -initiated resonant channel mediated by any of the three neutral Higgs bosons (see Fig. 9d).

The cross section for this process has been calculated at the leading order in Refs. [165–169]. Higher-order corrections have been derived in Refs. [170–173]. Studies focusing on the collider phenomenology of $H^\pm W^\mp$ production can be found in Refs. [174–179].

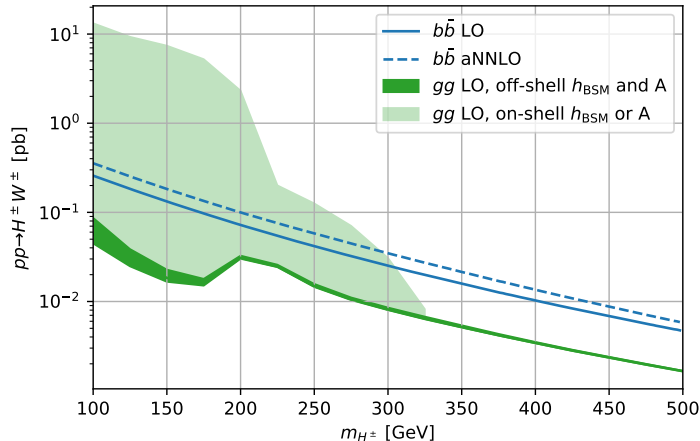


Figure 10.: Contributions of the different subprocesses to the overall $pp \rightarrow H^\pm W^\mp$ cross section as evaluated in the 2HDM type-I assuming exact alignment and $\tan \beta = 1$.

For our present study in the 2HDM type-I, we have derived the 13 TeV LHC cross section for charged Higgs production in association with a W boson using `MadGraph` assuming exact alignment limit and $\tan \beta = 1$. We work in the 5FS, as is appropriate for the dominant $b\bar{b}$ -initiated channel, for which we take into account approximate NNLO (aNNLO) corrections by multiplying with the given K -factors derived in Ref. [173]. The blue curves in Fig. 10 show the cross section of the $b\bar{b}$ -initiated channel at LO (solid curve) as well as at aNNLO (dashed curve).¹³ While the cross section of the $b\bar{b}$ -initiated channel only depends on m_{H^\pm} in the given approximation and scales with $\tan^{-2} \beta$, the cross section of the gg -initiated channels additionally depend on $m_{h_{\text{BSM}}}$ and m_A . We quantify this dependence by varying them in the interval 10 GeV to 500 GeV, which results in the green region for the gg -initiated contributions. As a simple criterion to differentiate the non-resonant and the resonant case, we regard points for which $m_A < m_{H^\pm} + m_W$ and $m_{h_{\text{BSM}}} < m_{H^\pm} + m_W$ as dominated by the non-resonant process — since neither h_{BSM} nor A can be on-shell¹⁴ — and color them dark-green. All other points are considered to be dominated by resonant production and are shown in light-green.

For $m_{H^\pm} \gtrsim 300$ GeV, the $b\bar{b} \rightarrow H^+ W^-$ subprocess dominates with a cross section that is ~ 3.5 larger than for the other shown channels. For lower charged Higgs boson masses the non-resonant gg -initiated contribution remains smaller than the $b\bar{b}$ initiated cross section by a factor between 3 and 9. In this region, the resonant gg -initiated channel can, however, yield a significant contribution to the total cross section potentially exceeding the contribution of the $b\bar{b}$ -initiated channel by a factor of ~ 40 for $m_{H^\pm} = 100$ GeV.

For our benchmark scenarios defined below, we will always assume that either $m_A =$

¹³We neglect the contribution from the resonant $b\bar{b}$ -initiated channel due to the smallness of the bottom Yukawa couplings in the 2HDM type-I.

¹⁴The contribution of the SM-like Higgs boson is negligible since its coupling to a charged Higgs boson and a W vanishes in the alignment limit.

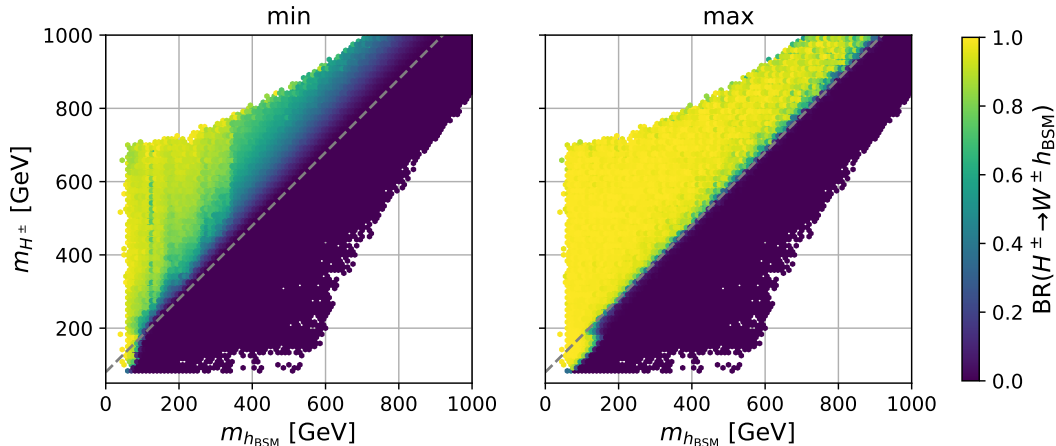


Figure 11.: Branching ratio of the charged Higgs H^\pm into $W^\pm h_{\text{BSM}}$ in the plane of the two Higgs masses, where h_{BSM} denotes the non- h_{125} \mathcal{CP} -even neutral Higgs boson. The left (right) plot shows the minimal (maximal) possible BR for each bin. The dashed line indicates where $m_{H^\pm} = m_{h_{\text{BSM}}} + m_W$.

m_{H^\pm} or $m_{h_{\text{BSM}}} = m_{H^\pm}$ in order to satisfy the constraints from electroweak precision observables (see discussion in Section 2.3). Additionally, the second non-SM-like neutral Higgs boson is assumed to be lighter in order to kinematically allow the $H^\pm \rightarrow h_{\text{BSM}}W^\pm$ or the $H^\pm \rightarrow AW^\pm$ decay processes. For this mass setting, the gg -initiated channel is always significantly smaller than the $b\bar{b}$ -initiated channel. Therefore, we approximate the total cross section for charged Higgs boson production in association with a W boson used in our numerical analysis by only taking into account the $b\bar{b}$ -initiated channel, which we rescale by a factor of $\tan^{-2}\beta$ if $\tan\beta \neq 1$.

4.2. Charged Higgs boson decay modes

The coupling structure of the charged Higgs boson (see Section 2.2) allows charged Higgs boson decays into SM fermions as well as into a W boson and a neutral Higgs boson. Among the fermionic decay channels, the $H^+ \rightarrow t\bar{b}$ as well as the $H^+ \rightarrow \tau^+\bar{\nu}_\tau$ decays are phenomenologically most important due to the comparatively large respective couplings, followed by the $H^+ \rightarrow c\bar{s}$ decay. In the 2HDM of type-I, the partial widths for the fermionic decays are proportional to $\cot^2\beta$, and thus become small for large $\tan\beta$.

In contrast, as discussed in Sections 2.1 and 2.2, the charged Higgs coupling to a W boson and a non-SM-like Higgs boson becomes maximal in the alignment limit. Therefore, if kinematically allowed, the decay $H^\pm \rightarrow W^\pm h_{\text{BSM}}$ can easily become the dominant decay mode. In order to assess this statement more quantitatively, we show in Fig. 11 the minimal (*left panel*) and maximal (*right panel*) value of the $H^\pm \rightarrow W^\pm h_{\text{BSM}}$ branching ratio in the $(m_{h_{\text{BSM}}}, m_{H^\pm})$ plane for all allowed scan points. Above the dashed line the decay happens on-shell, $m_{H^\pm} \geq m_W + m_{h_{\text{BSM}}}$, whereas the W^\pm is off-shell below the dashed line.

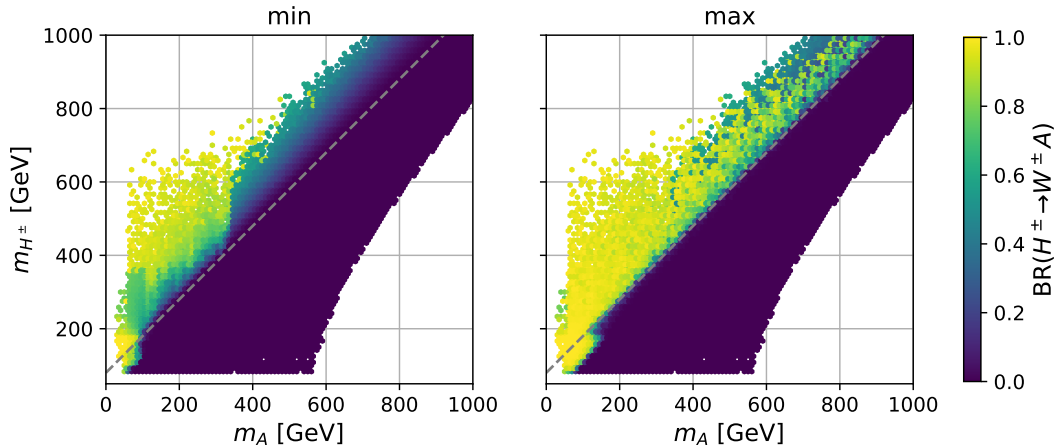


Figure 12.: Branching ratio of the charged Higgs H^\pm into $W^\pm A$ in the plane of the two Higgs masses. The left (right) plot shows the minimal (maximal) possible BR for each bin. The dashed line indicates where $m_{H^\pm} = m_A + m_W$.

In the kinematically allowed region for the on-shell decay, the *minimal* branching ratio often reaches values of above 60%. As expected, the branching ratio is especially large for low masses of the non-SM-like Higgs boson. The $H^\pm \rightarrow W^\pm h_{\text{BSM}}$ decay mode is, however, also important in the off-shell region if $m_{h_{\text{BSM}}}$ is below ~ 150 GeV and the $H^\pm \rightarrow tb$ decay is suppressed because $m_{H^\pm} < m_t$. The right panel of Fig. 11 shows that in almost the entire parameter region of these two kinematical regimes, i.e. in the on-shell region and in the off-shell region with $m_{h_{\text{BSM}}} \lesssim 150$ GeV, the $H^\pm \rightarrow W^\pm h_{\text{BSM}}$ decay can reach branching ratios very close to 100%. The right panel also shows that the BR can reach 100% in the off-shell region even for larger $m_{h_{\text{BSM}}}$, as long as $m_{H^\pm} < m_t$.

Besides the $H^\pm \rightarrow W^\pm h_{\text{BSM}}$ decay also the $H^\pm \rightarrow W^\pm A$ can be phenomenologically relevant. The minimal and maximal branching ratios for this decay are shown in the left and right panel of Fig. 12 in the (m_A, m_{H^\pm}) plane, respectively. While the overall behavior is quite similar to the previously discussed $H^\pm \rightarrow W^\pm h_{\text{BSM}}$ decay, the minimal $\text{BR}(H^\pm \rightarrow W^\pm A)$ tends to be smaller than $\text{BR}(H^\pm \rightarrow W^\pm h_{\text{BSM}})$.

In the parameter regions in which $\text{BR}(H^\pm \rightarrow W^\pm h_{\text{BSM}})$ and $\text{BR}(H^\pm \rightarrow W^\pm A)$ are both small, the charged Higgs boson decays predominantly into a top and bottom quark, if kinematically allowed. This is apparent in the left and right panels of Fig. 13 which display the minimal and maximal value, respectively, of $\text{BR}(H^\pm \rightarrow tb)$ in the $(\min(m_{h_{\text{BSM}}}, m_A), m_{H^\pm})$ plane. If the decays $H^\pm \rightarrow W^\pm h_{\text{BSM}}/A$ are kinematically suppressed (i.e., below the dashed line), the charged Higgs boson decays almost always to $\sim 100\%$ to a top and a bottom quark.¹⁵

We observe a steep rise of the maximal $\text{BR}(H^\pm \rightarrow tb)$ for $\min(m_{h_{\text{BSM}}}, m_A)$ greater than ~ 350 GeV, which corresponds to the decrease in the minimal value of $\text{BR}(H^\pm \rightarrow W^\pm h_{\text{BSM}})$ and $\text{BR}(H^\pm \rightarrow W^\pm A)$, seen in the left panels of Figs. 11 and 12, respectively.

¹⁵The clear exception is when $H^\pm \lesssim m_t$, where the dominant fermionic decay modes are $H^+ \rightarrow \tau^+ \bar{\nu}_\tau$ and $H^+ \rightarrow c\bar{s}$.

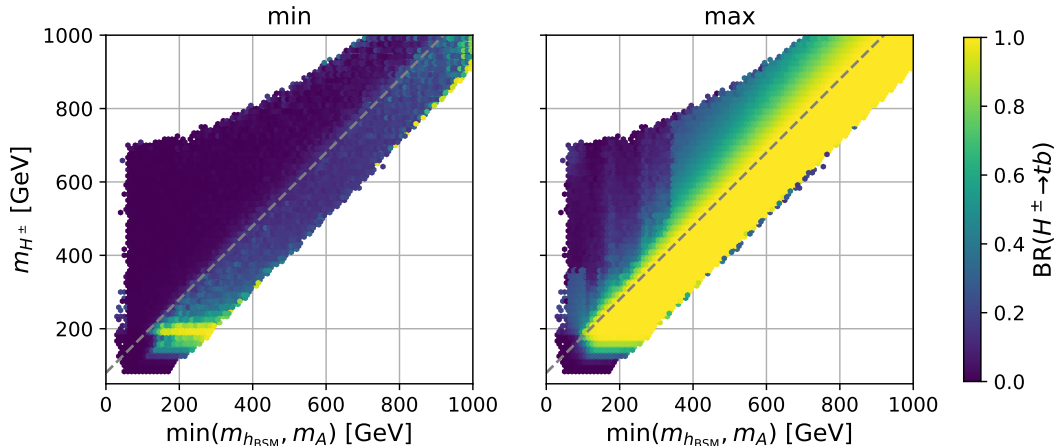


Figure 13.: Branching ratio of the charged Higgs H^\pm into tb in the plane of m_{H^\pm} and the smaller of the two non- h_{125} (\mathcal{CP} -even or \mathcal{CP} -odd) neutral Higgs masses. The left (right) plot shows the minimal (maximal) possible BR for each bin. For parameter points above the dashed line, at least one of the on-shell decay modes $H^\pm \rightarrow W^\pm h_{\text{BSM}}/A$ is allowed.

At this mass value — corresponding to $\sim 2m_t$ — the decays of the h_{BSM} and A bosons to a pair of top quarks become kinematically accessible suppressing the branching ratio of all other decays. Since the di-top final state is experimentally challenging, only rather weak bounds exist for scalars decaying dominantly to $t\bar{t}$. Consequently, lower values of $\tan\beta$ — and thereby higher values of $\text{BR}(H^\pm \rightarrow tb)$ — remain allowed by current direct searches.

It is interesting to note that $\text{BR}(H^\pm \rightarrow tb)$ can be small even if the decay channel is open and neither of the competing $H^\pm \rightarrow W^\pm h_{\text{BSM}}/A$ decays is kinematically allowed. This is visible in the left plot of Fig. 13 in which the minimal $\text{BR}(H^\pm \rightarrow tb)$ is only $\sim 30\%$ for most of region below the dashed line as long as $m_{H^\pm} \gtrsim 220$ GeV. For these points, the alignment limit is only approximately realized resulting in a non-zero $H^\pm W^\mp h_{125}$ coupling (see Section 2.2). In addition, $\tan\beta$ is comparably high and therefore $\text{BR}(H^\pm \rightarrow tb)$ is rather small. As a consequence, for these points the charged Higgs boson decays dominantly into a the SM-like Higgs boson and a W boson. This parameter region can therefore also be probed by searches for a bosonically decaying charged Higgs boson. The exception is the mass region $m_{H^\pm} \approx m_t + m_b$, where the $H^\pm \rightarrow tb$ decay is resonant and always dominates the decay width if the $H^\pm \rightarrow W^\pm A/h_{\text{BSM}}$ decay modes are not accessible. This is the origin of the yellow region in Fig. 13 (left).

4.3. Current LHC searches for a charged Higgs boson

Existing LHC searches for a charged Higgs boson (as listed in Table 3) have mainly focused on the charged Higgs boson decays into SM fermions. One exception are searches for a charged Higgs boson produced in a vector-boson-fusion process and decaying to a

Production process	Higgs decay processes	Final state particles	Exp. searches
$pp \rightarrow H^\pm tb$	$H^\pm \rightarrow \tau\nu_\tau$	$tb(\tau\nu_\tau)$	Refs. [180–184]
$pp \rightarrow H^\pm tb$	$H^\pm \rightarrow tb$	$tbtb$	Refs. [181, 185–187]
$pp \rightarrow tt, t \rightarrow H^\pm b$	$H^\pm \rightarrow cb$	$tbcb$	Ref. [188]
$pp \rightarrow tt, t \rightarrow H^\pm b$	$H^\pm \rightarrow cs$	$tbc s$	Refs. [189, 190]
$pp \rightarrow H^\pm qq'$ (VBF)	$H^\pm \rightarrow W^\pm Z$	$W^\pm Z qq'$	Refs. [191–193]
$pp \rightarrow tt, t \rightarrow H^\pm b$	$H^\pm \rightarrow W^\pm A$	$W^\pm \mu^+ \mu^-$	Ref. [65]

Table 3.: Experimentally covered LHC signatures for a (singly) charged Higgs boson, H^\pm .

W and a Z boson, but these production and decay channels are only possible in higher-multiplet extensions of the SM (e.g. Higgs triplet models). Another exception is the search for a light charged Higgs boson decaying to a W boson and an A boson, with the A boson decaying to a $\mu^+\mu^-$ pair [65]. While this search is the first experimental attempt to target the decay signatures discussed in this paper at the LHC, its results are only of very limited use, as the experimental limit has not been released for the two-dimensional mass plane (m_{H^\pm}, m_A) , but only for one-dimensional slices of the two-dimensional parameter space, assuming either $m_{H^\pm} = m_A + 85$ GeV or $m_{H^\pm} = 160$ GeV.

We illustrate the impact of the current LHC searches for a charged Higgs boson on our phenomenological 2HDM scan in Fig. 14. In the left panel we show the branching ratio $\text{BR}(H^\pm \rightarrow \tau\nu_\tau)$ normalized by t_β^2 as a function of m_{H^\pm} . This normalization is chosen as it allows us to show limits from the different LHC charged Higgs production modes that are relevant in this mass range on the same scale. The gray points are allowed by all constraints listed in Section 2.3. For charged Higgs boson masses below ~ 80 GeV, no points in our scan pass all constraints. The most important constraints in this region are set by combined LEP searches for charged Higgs pair production [194].¹⁶

Above the kinematic reach of the LEP searches, $m_{H^\pm} \gtrsim 90$ GeV, the LHC searches for a charged Higgs boson decaying into $\tau\nu$ and produced either from top quark decays, $t \rightarrow H^\pm b$, or through $pp \rightarrow tbH^\pm$ [183] become relevant (blue and orange curves in Fig. 14 (*left*)).¹⁷ They limit $\text{BR}(H^\pm \rightarrow \tau\nu_\tau)/t_\beta^2$ to be below $\sim 10^{-2}$. These searches lose sensitivity above the kinematic threshold for the $H^\pm \rightarrow tb$ decay at $m_{H^\pm} \sim m_t + m_b$, where $\text{BR}(H^\pm \rightarrow \tau\nu_\tau)$ becomes small due to the large partial width of the $H^\pm \rightarrow tb$ decay, as can be seen from the distribution of gray points in this mass range in the left panel of Fig. 14.

The impact of LHC searches for a charged Higgs boson decaying into a top and a bottom quark is shown in the right panel of Fig. 14, which displays the signal cross

¹⁶This LEP search limit cannot be shown explicitly in the left panel of Fig. 14 as it does not scale with $1/t_\beta^2$.

¹⁷Gray points located *above* the LHC search limits at around 90 GeV in Fig. 14 (*left*) are formally *not* excluded since `HiggsBounds` selects a different search — in this case the aforementioned combination of LEP searches [194] — to be the most sensitive channel for the given parameter point. This selection happens on the basis of the expected limit of the search, even if the corresponding observed limit has a different exclusion power (see Ref. [85] for a detailed discussion).

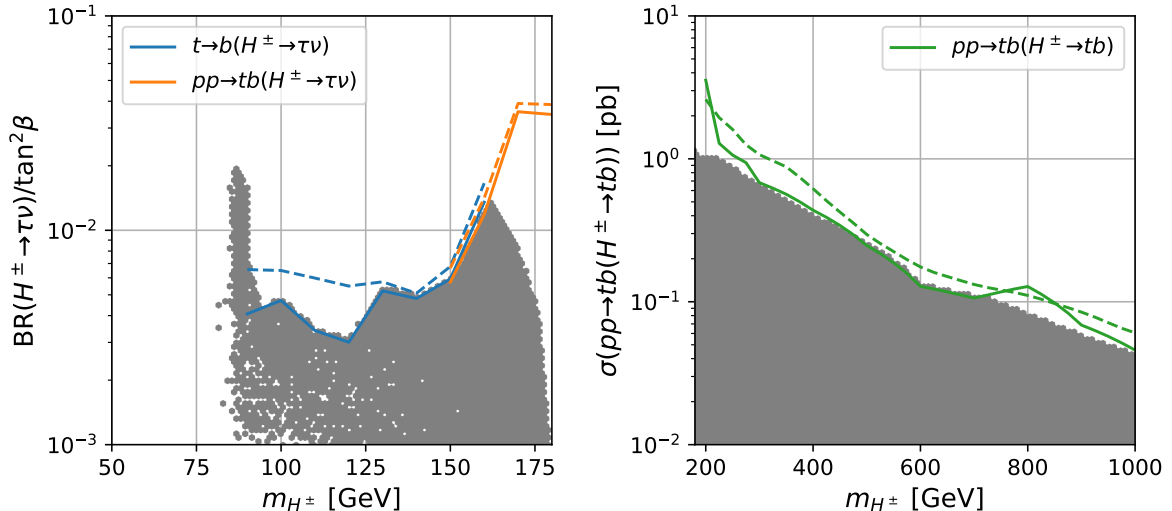


Figure 14.: Branching ratio of the charged Higgs boson into $\tau\nu_\tau$ (*left panel*, normalized by $\tan^2\beta$), and the 13 TeV LHC signal cross section in the $pp \rightarrow tbH^\pm, H^\pm \rightarrow tb$ channel (*right panel*) as a function of the charged Higgs boson mass, m_{H^\pm} . The *gray points* pass all relevant constraints. In the *left plot*, we include the observed (*solid line*) and expected (*dashed line*) limits from the most sensitive $t \rightarrow H^\pm b, H^\pm \rightarrow \tau\nu_\tau$ (*blue*) and $pp \rightarrow H^\pm tb, H^\pm \rightarrow \tau\nu_\tau$ (*orange*) searches [183]. In the *right panel*, the limit from the latest $pp \rightarrow H^\pm tb, H^\pm \rightarrow tb$ search [186] is shown (*green*).

section $pp \rightarrow tbH^\pm \rightarrow tbtb$ as a function of m_{H^\pm} . While this channel has a comparatively large cross section of up to ~ 1 pb, the tb final state is experimentally hard to disentangle from SM background processes. Therefore, the most recent experimental search [186] constrains the parameter space only slightly within the region $m_{H^\pm} \sim 500 - 700$ GeV.

From the discussion of the charged Higgs boson decay rates in Section 4.2 we know that many of our scan points in fact exhibit a large $H^\pm \rightarrow W^\pm h_{\text{BSM}}$ and/or $H^\pm \rightarrow W^\pm A$ decay rate, which in turn suppresses the decay modes with fermionic final states. This is also evident from the large swath of gray points in Fig. 14 that are far below the current limits from the discussed LHC searches. These observations strongly motivate experimental efforts to complement the existing searches by probing the $H^\pm \rightarrow W^\pm h_{\text{BSM}}$ and $H^\pm \rightarrow W^\pm A$ decay modes directly. In the upcoming section we focus on the collider signatures arising from these decays and present suitable benchmark scenarios for the design of such dedicated experimental searches.

5. Unexplored LHC signatures and benchmark models

As discussed above, vast parts of the phenomenologically viable parameter space of the 2HDM of type-I feature a charged Higgs boson that dominantly decays into a W boson and a non-SM like neutral Higgs boson (h_{BSM} or A). However, the collider signatures

Production process	Higgs decay processes	Final state particles
$pp \rightarrow H^\pm tb$	$H^\pm \rightarrow W^\pm \phi$ and $\phi \rightarrow$	$tbW^\pm + \begin{bmatrix} bb \\ \tau\tau \\ WW \\ ZZ \\ \gamma\gamma \end{bmatrix}$
$pp \rightarrow H^\pm \phi$	$H^\pm \rightarrow W^\pm \phi$ and $\phi \rightarrow$	$W^\pm + \begin{bmatrix} bb \\ \tau\tau \\ WW \\ ZZ \\ \gamma\gamma \end{bmatrix} \otimes \begin{bmatrix} bb \\ \tau\tau \\ WW \\ ZZ \\ \gamma\gamma \end{bmatrix}$
$pp \rightarrow H^\pm W^\mp$	$H^\pm \rightarrow W^\pm \phi$ and $\phi \rightarrow$	$W^\pm W^\mp + \begin{bmatrix} bb \\ \tau\tau \\ WW \\ ZZ \\ \gamma\gamma \end{bmatrix}$

Table 4.: LHC signatures arising from the charged Higgs boson decay $H^\pm \rightarrow W^\pm \phi$, with a neutral non-SM-like Higgs boson, $\phi = h_{\text{BSM}}, A$, for the most relevant production (*first column*) and decay (*second column*) processes. The resulting final state particles are given in the *third column* (further decays of the SM particles are not explicitly shown). The “ \otimes ” symbol in the center right cell indicates that any combination of the final states within the square brackets can occur due to the independent decays of the two neutral Higgs bosons.

arising from these decays are to a large extent not covered by LHC searches.

We summarize the most relevant LHC signatures in Table 4. These arise from charged Higgs production via one of the three main LHC production modes discussed in Section 4.1, and the successive decay of the charged Higgs boson into a W boson and a neutral Higgs boson ϕ , which can either be the h_{BSM} boson or the A boson. For the neutral Higgs boson decays we include the bb , $\tau\tau$, WW , ZZ and $\gamma\gamma$ final states, as these are typically the most frequent (bb , $\tau\tau$) or experimentally cleanest (WW , ZZ , $\gamma\gamma$) channels. The corresponding rates are model-dependent and will be discussed in more detail below in the context of benchmark scenarios. Besides the final states included in Table 4, the experimentally more challenging decays $\phi \rightarrow cc$ and $\phi \rightarrow gg$ may also become relevant in certain scenarios (see e.g. Refs. [195–197] for related searches and studies for the h_{125}). We shall therefore also include their rates in the following discussions if relevant.

While a detailed analysis of the LHC discovery potential of the various collider signatures must be postponed to future work, we briefly want to comment on a few features that may be exploited in collider searches, and the most important SM backgrounds. For

the $pp \rightarrow tbH^\pm$ production process — which is typically the dominant charged Higgs boson production mode, see Section 4.1 — inclusive SM processes with pairs of top quarks, $t\bar{t}(+X)$ and $t\bar{t}h_{125}$, are inevitably a major background, almost irrespective of how the neutral non-SM-like Higgs boson ϕ of the signal process decays (see also discussion in Ref. [58]). For the experimentally clean signature arising from the decay $\phi \rightarrow \gamma\gamma$, we expect that a good signal-background separation can be achieved by using similar techniques as in the $t\bar{t}h_{125}, h_{125} \rightarrow \gamma\gamma$ analyses [109, 198]. However, as the signal rate is typically very low — except for specific scenarios with a very light and/or fermiophobic ϕ (see below) — sensitivity may only be reached with a very large amount of data. Hence, we expect that for the more conventional 2HDM scenarios near the alignment limit the signal processes from $\phi \rightarrow bb$ and $\phi \rightarrow \tau\tau$ provide a more promising avenue (see also Refs. [52, 53]). Moreover, under the additional model-assumption on the relative size of $\text{BR}(\phi \rightarrow bb)$ and $\text{BR}(\phi \rightarrow \tau\tau)$ as predicted in the 2HDM, search results from the two signatures may be combined to maximize the sensitivity to the 2HDM parameter space.

For the $pp \rightarrow H^\pm\phi \rightarrow W^\pm\phi\phi$ process a multitude of signatures arises because the two ϕ bosons decay independently. As the production rate is already comparatively small, we also expect the typically more frequent decay modes $\phi \rightarrow bb$ and $\phi \rightarrow \tau\tau$ to exhibit the highest sensitivity in most of the 2HDM parameter space. In this case, a leptonically decaying W boson provides a triggerable isolated lepton. Moreover, dedicated signal regions for resolved, semi-boosted and fully-boosted $bb/\tau\tau$ pairs can be defined to enhance the sensitivity. Again, the main SM background to these signatures arises from (semi-leptonic) top quark pair production.

For the third process, $pp \rightarrow H^\pm W^\mp \rightarrow W^\pm W^\mp\phi$, we again expect the semi-leptonic analysis to be the most sensitive selection (see also Ref. [51]). SM backgrounds arise from inclusive electroweak boson production, $W^+W^- + X$ and top quark pair production. Note, however, that the signal cross section scales with $\cot^2\beta$, and is therefore typically smaller than the cross section of the previous processes. We therefore expect this production channel to be not as sensitive as the $pp \rightarrow tbH^\pm$ and $pp \rightarrow H^\pm\phi$ channels.

2HDM scenarios with large decay rates for $H^\pm \rightarrow W^\pm\phi$ typically feature a concomitant signature in the neutral Higgs sector — the $A \rightarrow Zh_{\text{BSM}}$ (if $\phi = h_{\text{BSM}}$) or $h_{\text{BSM}} \rightarrow ZA$ (if $\phi = A$) decay — with a sizable rate. This can be ascribed to the EW precision measurements discussed in Section 2.3 which constrain the mass of one of the neutral Higgs bosons to be close to the charged Higgs boson mass. Consequently, these scenarios are simultaneously probed by searches for $pp \rightarrow A \rightarrow Zh_{\text{BSM}}$ or $pp \rightarrow h_{\text{BSM}} \rightarrow ZA$, and current limits from these searches constrain parts of the relevant parameter space [199, 200] (see also discussion of benchmark scenarios below). Yet, direct charged Higgs boson searches for the $H^\pm \rightarrow W^\pm\phi$ decay signatures are highly warranted, as they are able to directly probe the charged Higgs sector independently of the (model-dependent) correlation between neutral and charged Higgs boson masses enforced by the EW precision constraints. In particular, in the optimistic case of a discovery in either of these channels, the model correlations would strongly suggest to look for a corresponding signal in the complementary channel as well.

Another related channel is of course the inverse decay $\phi \rightarrow H^\pm W^\pm$ if the mass hierarchy of H^\pm and ϕ is reversed. This decay is governed by the same coupling as the

$H^\pm \rightarrow W^\pm \phi$ decay, and is therefore also maximized in the alignment limit of h_{125} . However, through the mass correlation imposed by the EW precision measurements, this channel is even more strongly related to the $h_{\text{BSM}}/A \rightarrow ZA/h_{\text{BSM}}$ channels, since it also shares the initial production mode of the neutral scalar. We expect the $W^\pm H^\mp$ final state to be experimentally more challenging than the $Z\phi$ final state, regardless of the successive H^\pm and ϕ decay. As a result, the 2HDM parameter region where searches for $pp \rightarrow \phi \rightarrow H^\pm W^\mp$ are competitive with $pp \rightarrow A/h_{\text{BSM}} \rightarrow Zh_{\text{BSM}}/A$ searches is limited to the small mass region where the $Z\phi$ decay is kinematically suppressed, while the $H^\pm W^\mp$ decay is not. We stress that this decay channel is nevertheless very interesting to search for, since the mass correlations imposed by the EW precision constraints are model-dependent. We will further comment on this channel below, whenever our benchmark scenarios include parameter regions where it can appear.

In order to facilitate future searches for the $H^\pm \rightarrow W^\pm \phi$ signatures, we present in the following five benchmark scenarios, which are parametrized in the (m_{H^\pm}, m_ϕ) plane:

- $\text{cH}(Wh_{\text{BSM}})$ scenario with large $\text{BR}(H^\pm \rightarrow W^\pm h_{\text{BSM}})$: We choose $m_{H^\pm} = m_A$, and $m_H^\pm > m_{h_{\text{BSM}}}$ in most of the parameter plane. We assume the exact alignment limit and take a very small value $\tan \beta = 3$, which maximizes the $H^\pm \rightarrow W^\pm h_{\text{BSM}}$ decay rate and the $pp \rightarrow tbH^\pm$ production rate, respectively. The light non-SM-like Higgs boson h_{BSM} mainly decays to SM fermions ($bb, \tau\tau$) and gluons (gg);
- $\text{cH}(WA)$ scenario with large $\text{BR}(H^\pm \rightarrow W^\pm A)$: We choose $m_{H^\pm} = m_{h_{\text{BSM}}}$, and $m_H^\pm > m_A$ in most of the parameter plane. Analogous to the previous scenario, we assume the exact alignment limit and take a very small value $\tan \beta = 3$ to obtain a large $pp \rightarrow tbH^\pm$ production rate. The A boson predominantly decays to bb, gg and $\tau\tau$.
- $\text{cH}(Wh_{\text{BSM}}^{\text{fphob}})$ scenario with fermiophobic h_{BSM} : The charged Higgs boson and the A boson are chosen to be mass degenerate, $m_{H^\pm} = m_A$, and h_{BSM} is lighter in most of the parameter space. We depart slightly from the exact alignment limit, $c(h_{\text{BSM}}VV) = 0.2$, and chose $\tan \beta$ to fulfill the fermiophobic Higgs condition, Eq. (26), i.e. $\tan \beta \approx 4.9$. The fermiophobic Higgs boson h_{BSM} decays dominantly to di-photons (for $m_{h_{\text{BSM}}} < 90 \text{ GeV}$) or massive SM vector bosons (for $m_{h_{\text{BSM}}} \geq 90 \text{ GeV}$).
- $\text{cH}(Wh_{\text{BSM}}^{\text{light}})$ scenario with light h_{BSM} ($2m_{h_{\text{BSM}}} \leq m_{h_{125}}$): We choose $m_{H^\pm} = m_A$. In order to avoid constraints from LHC Higgs rate measurements we suppress the decay rate of $h_{125} \rightarrow h_{\text{BSM}}h_{\text{BSM}}$ by choosing m_{12}^2 according to Eq. (33). The light h_{BSM} boson decays predominantly to $bb, \tau\tau$ and $\gamma\gamma$. The dominant charged Higgs boson production mode is $pp \rightarrow H^\pm h_{\text{BSM}}$ with a 13 TeV LHC cross section $\sim \mathcal{O}(100 \text{ fb} - 1 \text{ pb})$.
- $\text{cH}(Wh_{\text{BSM}}^{\text{phil}})$ scenario with leptophilic h_{BSM} : Defined analogously to the $\text{cH}(Wh_{\text{BSM}}^{\text{light}})$ scenario but in the lepton-specific 2HDM (instead of the 2HDM type-I). Consequently, h_{BSM} decays almost exclusively to tau leptons.

	$m_{h_{125}}$ [GeV]	m_{H^\pm} [GeV]	$m_{h_{\text{BSM}}}$ [GeV]	m_A [GeV]	$c(h_{\text{BSM}}VV)$	$\tan\beta$	m_{12}^2 [GeV ²]
cH(Wh_{BSM})	125.09	150–300	65–200	m_{H^\pm}	0	3	500
cH(WA)			m_{H^\pm}	65–200			5000
cH($Wh_{\text{BSM}}^{\text{fphob}}$)	125.09	150–300	65–200	m_{H^\pm}	0.2	Eq. (26)	1200
cH($Wh_{\text{BSM}}^{\text{light}}$)		100–300	10–62.5	m_{H^\pm}	-0.062	16.6	Eq. (33)
cH($Wh_{\text{BSM}}^{\text{phil}}$)		same as cH($Wh_{\text{BSM}}^{\text{light}}$) but in the lepton-specific 2HDM					

Table 5.: Parameter choices in the five benchmark scenarios for the $H^\pm \rightarrow W^\pm\phi$ ($\phi = h_{\text{BSM}}, A$) decay the 2HDM. All scenarios except cH($Wh_{\text{BSM}}^{\text{phil}}$) are defined in the type I 2HDM.

Each of these scenarios features a distinct collider phenomenology and shows the importance of the $H^\pm \rightarrow W^\pm h_{\text{BSM}}$ or $W^\pm A$ decay mode. While the first two “standard” scenarios, cH(Wh_{BSM}) and cH(WA), aim to maximize the signal rate in the $pp \rightarrow tbH^\pm \rightarrow tbW^\pm\phi$ ($\phi = h_{\text{BSM}}, A$, respectively) channel, the latter three “specialized” scenarios highlight exceptional phenomena (fermiophobic, leptophilic, or very light h_{BSM}) that may occur for specific parameter choices, and lead to very different collider signatures. A significant part of the parameter planes evade all current constraints evaluated as specified in Section 2.3.

In order to evade constraints from electroweak precision observables (see Section 2.3), we set the mass of the other Higgs boson, A or h_{BSM} , respectively, equal to the charged Higgs boson mass, as described above. The other neutral \mathcal{CP} -even Higgs boson is considered to be the discovered Higgs boson h_{125} with a mass fixed to 125.09 GeV. The values for the remaining 2HDM input parameters are given in Table 5. Their choices are explained in the description of the respective benchmark scenarios. We provide the full data tables for all benchmark scenarios as ancillary files.

While we aimed to pick typical and illustrative scenarios, different choices of the fixed parameters could have led to different phenomenology and different parameter regions excluded by existing constraints. When designing experimental searches for these signatures, the search ranges should therefore never be constrained to the allowed region in the targeted benchmark scenario, but chosen as large as possible for the experimental analysis.

It is also possible to define similar scenarios in the type-II or flipped 2HDM. As discussed in Section 2.2, the light H^\pm region in these models is tightly constrained by flavor constraints. As a consequence, the charged Higgs boson mass would have to be significantly higher — $m_{H^\pm} \gtrsim 580$ GeV [69] — resulting in smaller signal cross sections for charged Higgs bosons decaying to a W and a non-SM like neutral Higgs boson.

5.1. $\text{cH}(Wh_{\text{BSM}})$ scenario with large $\text{BR}(H^\pm \rightarrow W^\pm h_{\text{BSM}})$

With our first benchmark scenario, the $\text{cH}(Wh_{\text{BSM}})$ scenario, we aim to provide a reference model that maximizes the rates of the $H^\pm \rightarrow W^\pm h_{\text{BSM}}$ decay and $pp \rightarrow tbH^\pm$ production mode. The h_{BSM} boson decays predominantly to bb , $\tau\tau$ and gg . This “standard” scenario exhibits a collider phenomenology that is found in large parts of the viable parameter space, without the need of tuning specific parameters.

We assume the exact alignment limit, $c(h_{\text{BSM}}VV) = 0$, and set $m_A = m_{H^\pm}$. The scenario is parametrized in the $(m_{H^\pm}, m_{h_{\text{BSM}}})$ plane, with $m_{h_{\text{BSM}}} < m_{H^\pm}$ in most of the parameter plane. As a consequence, the decay $H^\pm \rightarrow W^\pm h_{\text{BSM}}$ is one of the most important decay channels of the charged Higgs boson. The parameter $\tan\beta$ is chosen as low as possible without violating flavor constraints for light H^\pm , which maximizes the rates in the $pp \rightarrow tbH^\pm$ production mode. The charged Higgs boson phenomenology is not significantly affected by the choice of the parameter m_{12}^2 (see Table 5). With the m_{12}^2 value chosen here theoretical constraints are successfully evaded.

Similar scenarios in the exact alignment limit can easily be defined for larger values of $\tan\beta$. In that case all fermionic production and decay modes would be suppressed — since the fermionic couplings scale with $1/\tan\beta$ — while the $pp \rightarrow H^\pm h_{\text{BSM}}$ production cross section would be unaffected, and the $H^\pm \rightarrow W^\pm h_{\text{BSM}}$ branching ratio would be enhanced — due to the suppressed fermion decays. Therefore, this low $\tan\beta$ scenario is intentionally chosen as a *worst case* scenario for searches targeting $pp \rightarrow H^\pm h_{\text{BSM}} \rightarrow W^\pm h_{\text{BSM}} h_{\text{BSM}}$, while showing the complementarity with searches in fermionic channels.

The branching ratio $\text{BR}(H^\pm \rightarrow W^\pm h_{\text{BSM}})$ is shown in the upper left panel of Fig. 15 in the $(m_{H^\pm}, m_{h_{\text{BSM}}})$ parameter plane (colored contour lines). The colored regions are excluded by the following LHC searches: experimental searches for $pp \rightarrow A \rightarrow Zh_{\text{BSM}}$ [199–201] (orange region) exclude the upper left part of the parameter plane, $pp \rightarrow A/h_{\text{BSM}} \rightarrow \tau^+\tau^-$ searches [202] (green region) constrain the central right part of the parameter plane, and searches for $pp \rightarrow tbH^\pm, H^\pm \rightarrow \tau^\pm\nu_\tau$ [183] (blue region) exclude the lower right part of the parameter plane. In the remaining unconstrained parameter region, $\text{BR}(H^\pm \rightarrow W^\pm h_{\text{BSM}})$ can reach values above 99% (for $m_{H^\pm} \sim 170$ GeV and $m_{h_{\text{BSM}}} \sim 70$ GeV) rendering the $H^\pm \rightarrow W^\pm h_{\text{BSM}}$ decay a prime target for future searches in this part of the parameter space. The branching ratio decreases for increasing $m_{h_{\text{BSM}}}$ due to the decreasing phase space. All of the LHC searches that exclude parts of the scenario rely on fermionic production modes. Therefore, at larger $\tan\beta$ the existing experimental constraints would become significantly weaker.

The total signal cross sections for the three main charged Higgs production modes (as discussed in Section 4.1) with the subsequent H^\pm decay into a W boson and an h_{BSM} boson are shown in the remaining three panels of Fig. 15. In the unconstrained parameter region, the signal cross section can maximally reach about 13 pb for tb -associated charged Higgs production, 340 fb for h_{BSM} -associated charged Higgs boson production, and 20 fb for W -associated charged Higgs boson production. All of these maximal cross sections are reached for the lowest considered masses.

Figure 16 shows the branching ratios of h_{BSM} for the most important decay modes as a function of $m_{h_{\text{BSM}}}$. This completes the rate information required for designing experi-

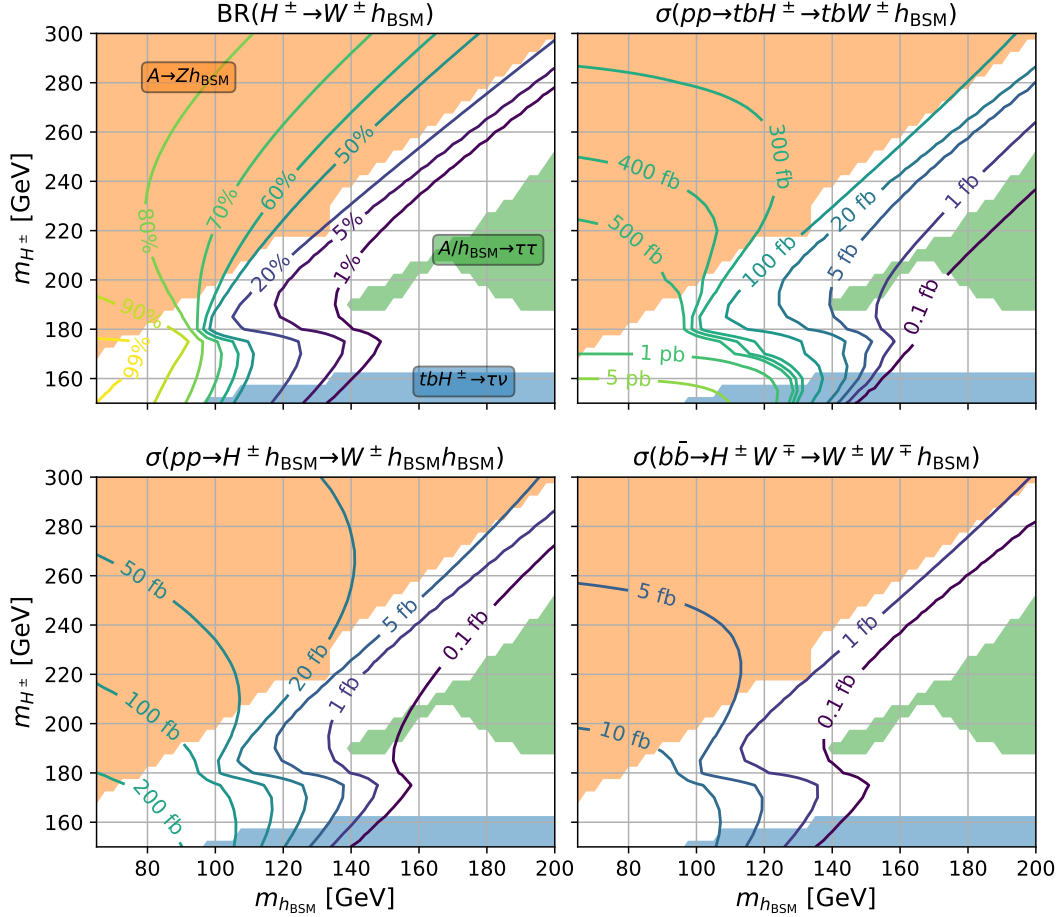


Figure 15.: Benchmark scenario $cH(W h_{\text{BSM}})$ in the $(m_{H^\pm}, m_{h_{\text{BSM}}})$ parameter plane. The *colored contour lines* indicate $\text{BR}(H^\pm \rightarrow W^\pm h_{\text{BSM}})$ in the *top-left* panel and the 13 TeV LHC signal cross sections in the $pp \rightarrow tbH^\pm \rightarrow tbW^\pm h_{\text{BSM}}$ (*top-right*), $pp \rightarrow H^\pm h_{\text{BSM}} \rightarrow W^\pm h_{\text{BSM}} h_{\text{BSM}}$ (*bottom-left*), and $pp \rightarrow W^\mp H^\pm \rightarrow W^\pm W^\mp h_{\text{BSM}}$ (*bottom-right*) channels in the remaining panels. The *colored regions* of parameter space are excluded by current constraints from searches in the $pp \rightarrow A \rightarrow Zh_{\text{BSM}}$ [199–201], $pp \rightarrow A/h_{\text{BSM}} \rightarrow \tau^+\tau^-$ [202] and $pp \rightarrow tbH^\pm, H^\pm \rightarrow \tau^\pm\nu_\tau$ [183] channels, as denoted by the labels.

mental searches to probe this benchmark scenario. Since the decay modes depend on the mass of H^\pm directly or indirectly through the total width, the ranges of BRs within the m_{H^\pm} range of the scenario are shown. The $cH(W h_{\text{BSM}})$ scenario is defined in the exact alignment limit, therefore h_{BSM} does not couple to massive vector bosons. Accordingly, h_{BSM} decays dominantly to two bottom quarks ($b\bar{b}$, blue curve) with branching ratios of up to 80% (70%) for low (high) masses. The decay into gluons (gg , green curve) becomes increasingly important for rising $m_{h_{\text{BSM}}}$, reaching decay rates of up to $\sim 25\%$. The branching ratios for h_{BSM} decays to a pair of tau leptons ($\tau^+\tau^-$, orange curve) and a pair of charm quarks ($c\bar{c}$, red curve) are approximately constant reaching values of

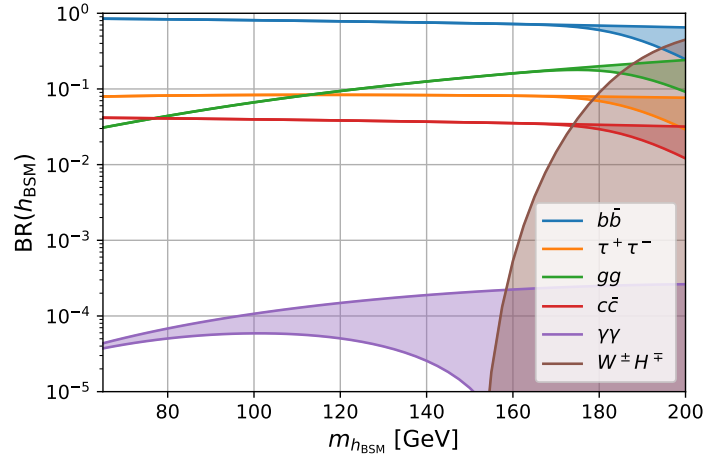


Figure 16.: Branching ratios of h_{BSM} in the $\text{cH}(Wh_{\text{BSM}})$ benchmark scenario as a function of $m_{h_{\text{BSM}}}$. The decays $h_{\text{BSM}} \rightarrow \gamma\gamma$ and $h_{\text{BSM}} \rightarrow W^\pm H^\mp$ additionally depend on m_{H^\pm} and induce a dependence in the remaining BRs through the total decay width. The bands for each BR indicate the impact of this dependence for $150 \text{ GeV} < m_{H^\pm} < 300 \text{ GeV}$.

$\sim 8\%$ and 4% , respectively. The partial width of h_{BSM} decaying into a pair of photons depends on the charged Higgs boson mass (see Section 3.1). The corresponding BR can reach values of up to 0.03% . For large $m_{h_{\text{BSM}}} \gtrsim 155 \text{ GeV}$ and low values of m_{H^\pm} , the (off-shell) decay $h_{\text{BSM}} \rightarrow W^\pm H^\mp$ becomes possible. The BR in this channel, shown as the brown filled region in Fig. 16, can reach values up to 45% at $m_{h_{\text{BSM}}} = 200 \text{ GeV}$ and very low m_{H^\pm} values. This decay rate is anti-correlated with all other decay rates, leading to the filled regions and declining slopes of the minimal decay rates for other decay modes. As discussed above, this illustrates that the $h_{\text{BSM}} \rightarrow W^\pm H^\mp$ decay can become equally large as the $H^\pm \rightarrow W^\pm h_{\text{BSM}}$ decay.

Finally, the charged Higgs boson contribution to the di-photon decay mode (see Section 3.1) also induces deviations in the h_{125} di-photon rate of up to 13% from the SM (see Appendix A for more details).

5.2. $\text{cH}(WA)$ scenario with large $\text{BR}(H^\pm \rightarrow W^\pm A)$

Our second benchmark model, the $\text{cH}(WA)$ scenario, is designed to feature a maximal rate for the $H^\pm \rightarrow W^\pm A$ decay and a dominant production through the $pp \rightarrow tbH^\pm$ process. In analogy with the previous scenario, we choose $m_{h_{\text{BSM}}} = m_{H^\pm}$, and m_A is allowed to vary. A small value of $\tan\beta = 3$ is chosen to obtain a large $pp \rightarrow tbH^\pm$ production cross section. The choice of m_{12}^2 (see Table 5) has no significant impact on the charged Higgs boson phenomenology but is chosen differently from the $\text{cH}(Wh_{\text{BSM}})$ scenario in order to satisfy theoretical constraints that depend differently on the \mathcal{CP} -even and \mathcal{CP} -odd Higgs masses. As in the $\text{cH}(Wh_{\text{BSM}})$ scenario, the low value for $\tan\beta$ is an intentionally chosen *worst case* scenario for the bosonic production and decay channels

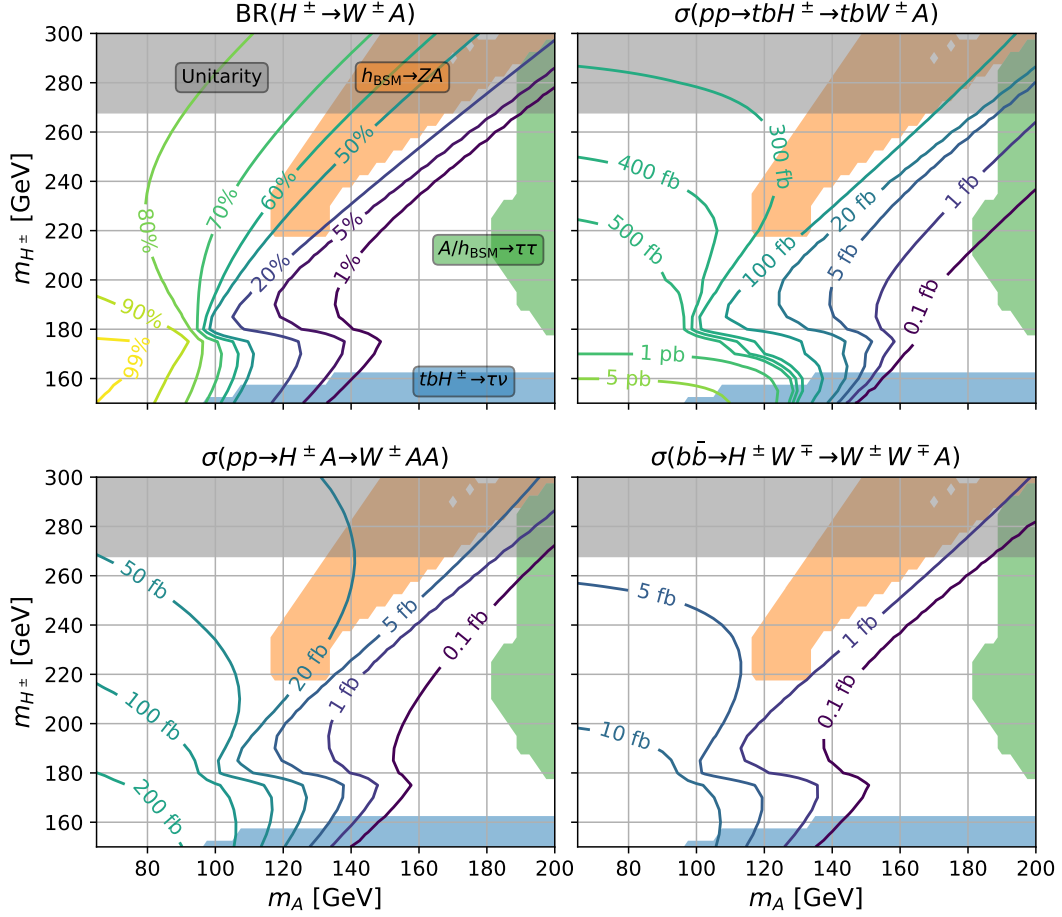


Figure 17.: Benchmark scenario $cH(WA)$ in the (m_{H^\pm}, m_A) parameter plane. The *colored contour lines* indicate $\text{BR}(H^\pm \rightarrow W^\pm A)$ in the *top-left* panel and the 13 TeV LHC signal cross sections in the $pp \rightarrow tbH^\pm \rightarrow tbW^\pm A$ (*top-right*), $pp \rightarrow H^\pm A \rightarrow W^\pm AA$ (*bottom-left*), and $pp \rightarrow W^\pm \rightarrow H^\mp \rightarrow W^\pm W^\mp A$ (*bottom-right*) channels in the remaining panels. The *colored regions* of parameter space are excluded by current constraints from searches in the $pp \rightarrow h_{\text{BSM}} \rightarrow ZA$ [199–201], $pp \rightarrow A/h_{\text{BSM}} \rightarrow \tau^+\tau^-$ [202] and $pp \rightarrow tbH^\pm, H^\pm \rightarrow \tau^\pm\nu_\tau$ [183] channel. Theoretical constraints from perturbative unitarity (*gray region*) also impact $cH(WA)$.

of H^\pm compared to the fermionic channels.

We display the branching ratio of the $H^\pm \rightarrow W^\pm A$ decay in the upper left plot of Fig. 17. The BR values are identical to those found in the $cH(Wh_{\text{BSM}})$ scenario (shown in the upper left plot of Fig. 15) under the exchange $A \leftrightarrow h_{\text{BSM}}$. The $pp \rightarrow h_{\text{BSM}} \rightarrow ZA$ searches [199–201] (orange region) cover a significantly smaller parameter region than the $pp \rightarrow A \rightarrow Zh_{\text{BSM}}$ searches in the $cH(Wh_{\text{BSM}})$ scenario due to the lower $gg \rightarrow h_{\text{BSM}}$ production cross section. The $pp \rightarrow A/h_{\text{BSM}} \rightarrow \tau^+\tau^-$ search [202] excludes parts of the parameter region with $m_A \gtrsim 180$ GeV. The region excluded by $pp \rightarrow tbH^\pm, H^\pm \rightarrow \tau^\pm\nu_\tau$

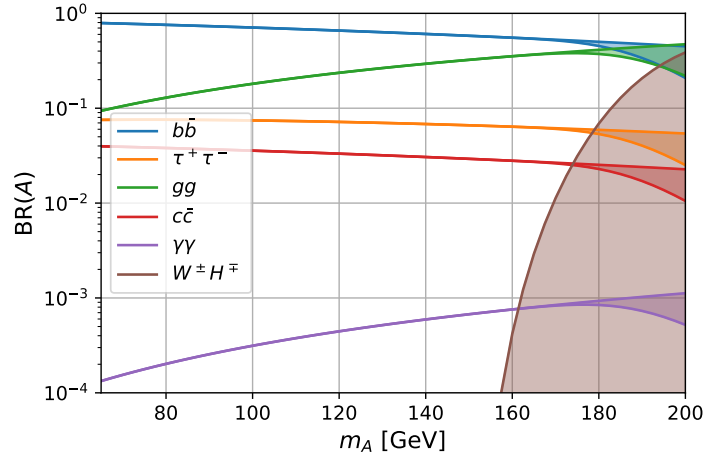


Figure 18.: Branching ratios of A in the $cH(WA)$ benchmark scenario as a function of m_A . The decays $A \rightarrow \gamma\gamma$ and $A \rightarrow W^\pm W^\mp$ additionally depend on m_{H^\pm} and induce a dependence in the remaining BRs through the total width. The bands for each BR indicate the impact of this dependence for $150 \text{ GeV} < m_{H^\pm} < 300 \text{ GeV}$.

searches [183] is identical to the corresponding region in the $cH(Wh_{\text{BSM}})$ scenario. As an additional constraint in the $cH(WA)$ scenario, charged Higgs boson masses above $\sim 270 \text{ GeV}$ are excluded by perturbative unitarity. As for the $cH(Wh_{\text{BSM}})$ scenario, the maximal $\text{BR}(H^\pm \rightarrow W^\pm A)$ reaches values above 99%. In the $cH(WA)$ scenario, however, larger parts of the parameter space with $\text{BR}(H^\pm \rightarrow W^\pm A) \gtrsim 65\%$ at large m_{H^\pm} values are still unconstrained making this scenario a very interesting target scenario for future $H^\pm \rightarrow W^\pm A$ searches. As in the $cH(Wh_{\text{BSM}})$ scenario, the existing searches all rely on fermionic production modes and quickly loose sensitivity for larger values of $\tan\beta$.

The future potential of this channel becomes even more apparent from the 13 TeV LHC signal cross section values, as shown in the remaining plots of Fig. 17. These are the same as in the $cH(Wh_{\text{BSM}})$ scenario under the exchange $A \leftrightarrow h_{\text{BSM}}$, however, the experimental and theoretical constraints differ. Large cross section are possible in particular in the mass region of $m_A \lesssim 120 \text{ GeV}$, which is now unexcluded compared to the $cH(Wh_{\text{BSM}})$ scenario. Through most of this region the cross section for tb -associated charged Higgs boson production, $\sigma(pp \rightarrow tbH^\pm, H^\pm \rightarrow W^\pm A)$ lies above $\sim 200 \text{ fb}$ and the cross section for charged Higgs boson production in association with an A (W) boson lies above 20 fb (1 fb).

Analogous to Fig. 16 for the previous scenario, we show the branching ratios of the A boson in the $cH(WA)$ scenario in Fig. 18. The overall behavior of the branching ratios is similar to those of the h_{BSM} boson in the previous scenario (see Fig. 16). As a consequence of the A boson being a \mathcal{CP} -odd scalar, the decays of the A boson into two gluons and two photons are enhanced in comparison to the decays of the h_{BSM} boson in the $cH(Wh_{\text{BSM}})$ scenario. For $m_A \sim 200 \text{ GeV}$, $\text{BR}(A \rightarrow gg)$ and $\text{BR}(A \rightarrow \gamma\gamma)$ reach

values of 47% and 0.1%, respectively.

In the $\text{cH}(WA)$ scenario, the charged Higgs boson contribution to the di-photon decay width (see Section 3.1) induces deviations of the h_{125} di-photon rate with respect to the SM of up to 9% (see Appendix A for more details).

5.3. $\text{cH}(Wh_{\text{BSM}}^{\text{fphob}})$ scenario with fermiophobic h_{BSM}

As a first benchmark model specialized on a rather exceptional parameter region with a very distinct collider phenomenology, we discuss the $\text{cH}(Wh_{\text{BSM}}^{\text{fphob}})$ scenario. We again choose $m_A = m_{H^\pm}$, and $m_{h_{\text{BSM}}}$ is allowed to vary. In this scenario we depart from the exact alignment limit by setting the coupling of h_{BSM} to the massive vector bosons to one fifth of the respective SM Higgs couplings. By choosing $\tan\beta$ according to Eq. (26) (taking a value of ~ 4.9), we realize the fermiophobic limit for h_{BSM} , which implies that h_{BSM} does not couple to fermions. Note that the realization of the fermiophobic limit very sensitively depends on the chosen $\tan\beta$ value. Already small deviations from Eq. (26) result in substantial couplings of h_{BSM} to fermions. This is discussed in more detail in Appendix B. In contrast, the choice of m_{12}^2 (see Table 5) only has a minor impact on the phenomenology of the $\text{cH}(Wh_{\text{BSM}}^{\text{fphob}})$ scenario but is important to satisfy the theoretical constraints. Earlier studies of scenarios with a fermiophobic Higgs boson can be found in Refs. [57, 157, 203–206]. This choice of parameters can be considered very fine-tuned from a theoretical perspective. Nevertheless, the collider signatures of this scenario are strikingly different from the scenarios discussed above and should not remain unexplored.

The branching ratio $\text{BR}(H^\pm \rightarrow W^\pm h_{\text{BSM}})$ for the $\text{cH}(Wh_{\text{BSM}}^{\text{fphob}})$ scenario is shown in the top-left panel of Fig. 19. As before, the results are displayed in the $(m_{H^\pm}, m_{h_{\text{BSM}}})$ parameter plane with current experimental and theoretical constraints shown as colored areas. Theoretical constraints in the $\text{cH}(Wh_{\text{BSM}}^{\text{fphob}})$ scenario are the boundedness from below (BfB) requirement on the Higgs potential (dark magenta) — excluding $m_{H^\pm} \lesssim 76 \text{ GeV}$ — and perturbative unitarity (gray) — excluding $m_{H^\pm} \gtrsim 160 \text{ GeV}$. Experimental constraints arise from searches for $pp \rightarrow h_{\text{BSM}} \rightarrow \gamma\gamma$ [207–209] (purple) — excluding $m_{h_{\text{BSM}}} \lesssim 95 \text{ GeV}$ except for a narrow region around the Z -boson mass —, searches for $pp \rightarrow A \rightarrow Zh_{\text{BSM}}$ [200] (orange) — excluding an otherwise unexcluded small patch around $m_{H^\pm} \sim 230 \text{ GeV}$ and $m_{h_{\text{BSM}}} \sim 155 \text{ GeV}$ —, as well as searches for $pp \rightarrow tbH^\pm, H^\pm \rightarrow \tau^\pm \nu_\tau$ [183] (blue) — excluding a small region around $m_{H^\pm} \sim 150 \text{ GeV}$ and $m_{h_{\text{BSM}}} \gtrsim 120 \text{ GeV}$. In the remaining allowed parameter region, $\text{BR}(H^\pm \rightarrow W^\pm h_{\text{BSM}})$ values of up to $\sim 90\%$ are possible. Especially the region of low $m_{h_{\text{BSM}}}$ and high m_{H^\pm} features large branching fractions.

The corresponding signal cross sections, shown in the remaining panels of Fig. 19, have a slightly different behavior. Since the production cross sections for a charged Higgs boson decrease with rising m_{H^\pm} , also the cross sections for charged Higgs boson production with the subsequent $H^\pm \rightarrow Wh_{\text{BSM}}$ decay tend to decrease for rising m_{H^\pm} . The cross section for $pp \rightarrow tbH^\pm, H^\pm \rightarrow W^\pm h_{\text{BSM}}$, shown in the top-right panel of Fig. 19, reaches values almost 5 pb. For $pp \rightarrow H^\pm h_{\text{BSM}} \rightarrow W^\pm h_{\text{BSM}} h_{\text{BSM}}$ production, shown in the bottom-left panel of Fig. 19, the maximal cross section is $\sim 200 \text{ fb}$. The

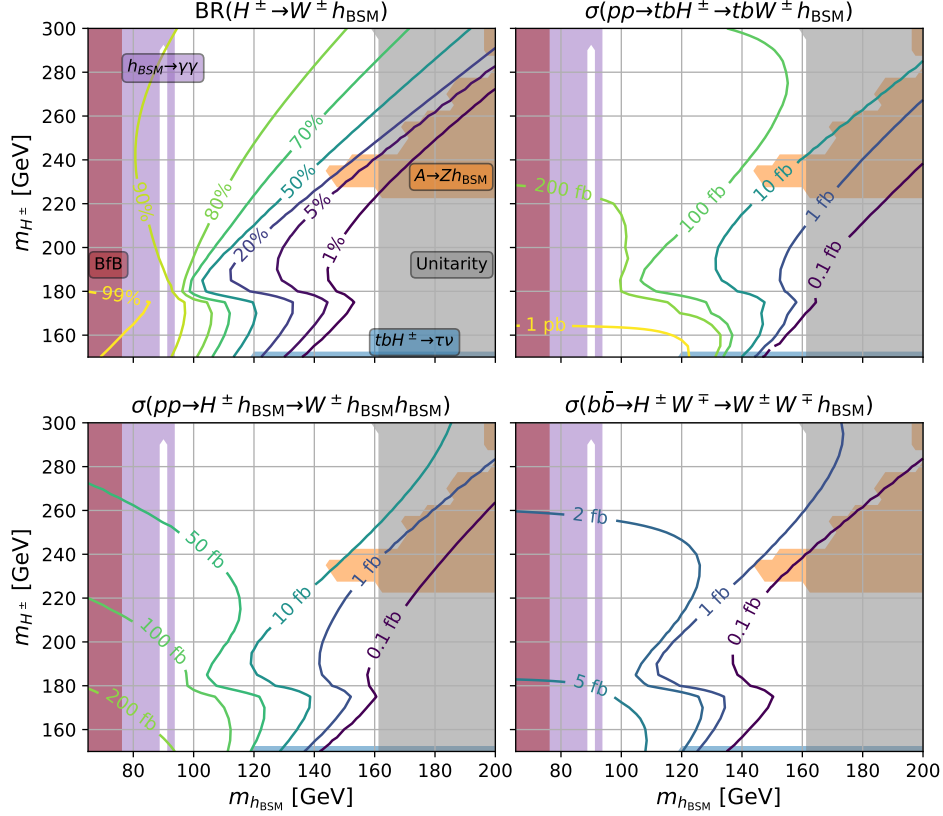


Figure 19.: Benchmark scenario $cH(W h_{\text{BSM}}^{\text{fphob}})$ in the $(m_{H^\pm}, m_{h_{\text{BSM}}})$ parameter plane. The *colored contour lines* indicate $\text{BR}(H^\pm \rightarrow W^\pm h_{\text{BSM}})$ in the *top-left* panel and the 13 TeV LHC signal cross sections in the $pp \rightarrow tbH^\pm \rightarrow tbW^\pm h_{\text{BSM}}$ (*top-right*), $pp \rightarrow H^\pm h_{\text{BSM}} \rightarrow W^\pm h_{\text{BSM}} h_{\text{BSM}}$ (*bottom-left*), and $pp \rightarrow W^\mp H^\pm \rightarrow W^\pm W^\mp h_{\text{BSM}}$ (*bottom-right*) channels in the remaining panels. The *colored regions* of parameter space are excluded by current constraints from searches in the $pp \rightarrow A \rightarrow Zh_{\text{BSM}}$ [200], $pp \rightarrow h_{\text{BSM}} \rightarrow \gamma\gamma$ [207–209] and $pp \rightarrow tbH^\pm, H^\pm \rightarrow \tau^\pm \nu_\tau$ [183] channels. Theoretical constraints from perturbative unitarity and boundedness from below (BfB) are also relevant.

$pp \rightarrow H^\pm W^\mp \rightarrow W^\pm W^\mp h_{\text{BSM}}$ production cross section, displayed in the bottom-right panel of Fig. 19, reaches values $\gtrsim 5$ fb.

Due to fermiophobic character of the h_{BSM} boson, its decays shown in Fig. 20 are very different from the ones in the $cH(W h_{\text{BSM}})$ scenario. For $m_{h_{\text{BSM}}} \lesssim 90$ GeV, the h_{BSM} boson decays dominantly to a pair of photons reaching a maximal branching ratio of $\sim 90\%$.¹⁸ For $m_{h_{\text{BSM}}} \gtrsim 90$ GeV, the (off-shell) decays into a pair of W or Z bosons become increasingly important with branching ratios of $\sim 90\%$ and $\sim 10\%$, respectively. Note that the decay modes into massive vector bosons are possible as the alignment of

¹⁸Due to h_{BSM} being fermiophobic its decay to a pair of photons is only mediated by the W boson and the charged Higgs boson in the loop (see also Ref. [210]).

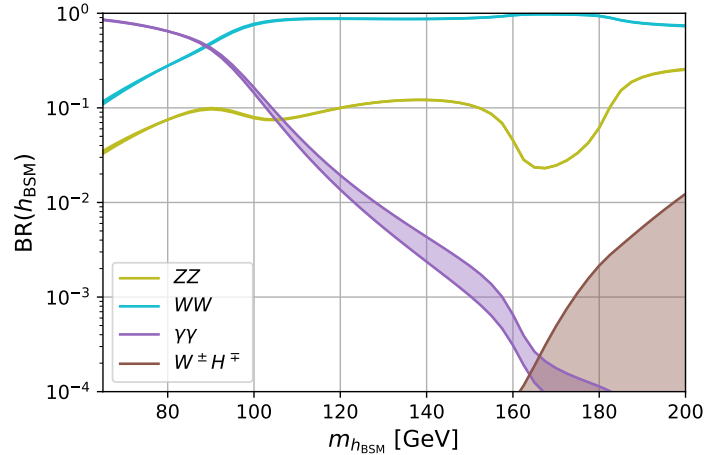


Figure 20.: Branching ratios of h_{BSM} in the $\text{cH}(Wh_{\text{BSM}}^{\text{fphob}})$ benchmark scenario as a function of $m_{h_{\text{BSM}}}$. The decays $h_{\text{BSM}} \rightarrow \gamma\gamma$ and $h_{\text{BSM}} \rightarrow W^\pm H^\mp$ additionally depend on m_{H^\pm} and induce a small dependence in the remaining BRs through the total width. The bands for each BR indicate the impact of this dependence for $150 \text{ GeV} < m_{H^\pm} < 300 \text{ GeV}$.

h_{125} is not exact in this scenario.

This departure from alignment, together with the charged Higgs boson effects, leads to deviations of the h_{125} di-photon decay rate from the SM by up to 14% (see Appendix A for more details) in the $\text{cH}(Wh_{\text{BSM}}^{\text{fphob}})$ scenario.

5.4. $\text{cH}(Wh_{\text{BSM}}^{\text{light}})$ scenario with light h_{BSM}

The second rather specialized benchmark model is the $\text{cH}(Wh_{\text{BSM}}^{\text{light}})$ scenario which features a light h_{BSM} with $m_{h_{\text{BSM}}} \leq 62.5 \text{ GeV}$. Similar to the other scenarios we choose again $m_A = m_{H^\pm}$. In order to suppress the $h_{125} \rightarrow h_{\text{BSM}}h_{\text{BSM}}$ decay channel we choose m_{12}^2 according to Eq. (33). As already mentioned in Section 3.2, unitarity and absolute vacuum stability requirements enforce a strong correlation between $c(h_{\text{BSM}}VV)$ and $\tan\beta$. For $\tan\beta$ values consistent with flavor constraints, $\tan\beta \gtrsim 3$, we need to slightly depart from the exact alignment limit. We therefore choose $c(h_{\text{BSM}}VV) = -0.062$ in this scenario, and we set $\tan\beta$ to 16.6 in order to fulfill the unitarity and vacuum stability requirements. See Appendix C for more details on these parameter choices showing that this kind of scenario in the 2HDM clearly requires significant tuning of the parameters. However, similar phenomenology may be far easier to achieve in more complex models, for which this scenario can serve as a simple benchmark.

Due to the low $m_{h_{\text{BSM}}}$ values and the relatively high $\tan\beta$, $\text{BR}(H^\pm \rightarrow W^\pm h_{\text{BSM}})$ is larger than 98% in the entire benchmark plane. The signal cross section for tb -associated charged Higgs boson production with a subsequent $H^\pm \rightarrow Wh_{\text{BSM}}$ decay is shown in the left panel of Fig. 21 in the $(m_{H^\pm}, m_{h_{\text{BSM}}})$ parameter plane. The colored areas are excluded by theoretical constraints: the region of $m_{H^\pm} \lesssim 21 \text{ GeV}$ is excluded

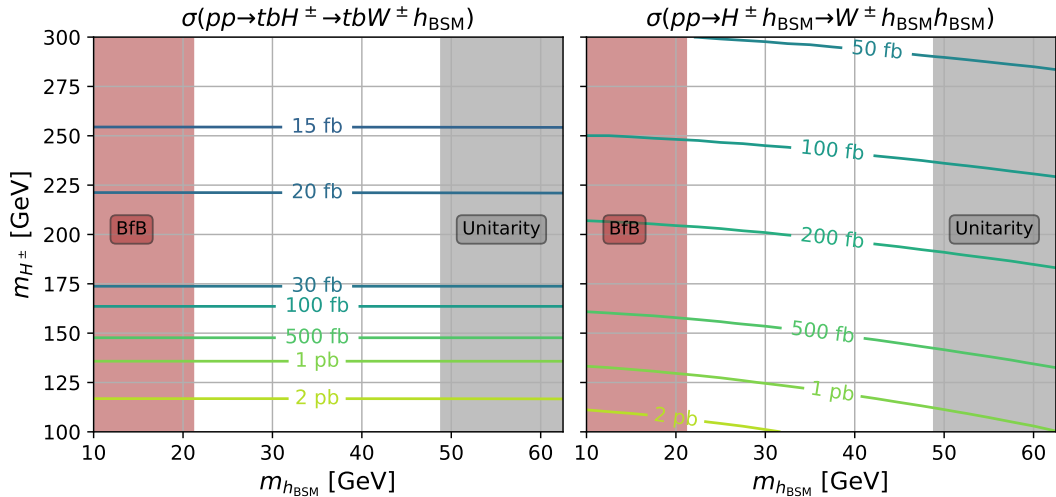


Figure 21.: Signal cross sections in the $(m_{H^\pm}, m_{h_{\text{BSM}}})$ parameter plane of benchmark scenario $\text{cH}(Wh_{\text{BSM}}^{\text{light}})$. The contour lines indicate the 13 TeV LHC cross sections for the processes $pp \rightarrow tbH^\pm, H^\pm \rightarrow W^\pm h_{\text{BSM}}$ (left) and $pp \rightarrow H^\pm h_{\text{BSM}} \rightarrow W^\pm h_{\text{BSM}} h_{\text{BSM}}$ (right). The shaded regions are excluded by perturbative unitarity and boundedness from below (BfB).

by requiring boundedness from below (BfB) of the scalar potential (red), and the region of $m_{H^\pm} \gtrsim 49$ GeV is excluded by perturbative unitarity (gray). The signal cross section $\sigma(p \rightarrow tbH^\pm, H^\pm \rightarrow W^\pm h_{\text{BSM}})$ strongly depends on m_{H^\pm} but it is nearly independent of $m_{h_{\text{BSM}}}$. It ranges from around 10 fb at $m_{H^\pm} = 300$ GeV to above 2 pb at $m_{H^\pm} \sim 100$ GeV. We find similar cross-section values for charged Higgs boson production in association with a h_{BSM} boson and the subsequent $H^\pm \rightarrow Wh_{\text{BSM}}$ decay, shown in the right panel of Fig. 21. Also for this production mode, cross-section values above 1 pb can be reached for $m_{H^\pm} \sim 100$ GeV. At H^\pm masses above ~ 150 GeV the cross section for the $pp \rightarrow H^\pm h_{\text{BSM}}$ channel even surpasses the one for the $pp \rightarrow tbH^\pm$ channel. The cross section for charged Higgs boson production in association with a W boson (not shown) is negligible in the $\text{cH}(Wh_{\text{BSM}}^{\text{light}})$ scenario, reaching values of only $\lesssim 0.1$ fb.

The branching ratios of the h_{BSM} decays are displayed in the left panel of Fig. 22. For very low masses, $m_{h_{\text{BSM}}} \sim 10$ GeV, h_{BSM} decays with almost equal probabilities to b quarks, c quarks, and τ leptons. For masses in the intermediate range, $10 \text{ GeV} < m_{h_{\text{BSM}}} \lesssim 40$ GeV, the $h_{\text{BSM}} \rightarrow b\bar{b}$ decay dominates with a branching ratio of $\sim 80 - 90\%$. For higher mass values, it is possible that h_{BSM} decays to two photons with a branching ratio of up to 25% in the allowed region. In the same region, the branching ratio of h_{BSM} decaying to two photons can, however, also be very close to zero.

This large variation originates from the varying charged Higgs mass. This dependence is shown in more detail in the right panel of Fig. 22, which displays $\text{BR}(h_{\text{BSM}} \rightarrow b\bar{b})$ (blue contours) and $\text{BR}(h_{\text{BSM}} \rightarrow \gamma\gamma)$ (purple contours) in the $(m_{h_{\text{BSM}}}, m_{H^\pm})$ parameter plane. While the decay of $h_{\text{BSM}} \rightarrow b\bar{b}$ dominates for low $m_{h_{\text{BSM}}}$ values irrespectively of the H^\pm mass, $\text{BR}(h_{\text{BSM}} \rightarrow \gamma\gamma)$ can reach values of up to $\sim 25\%$ in the allowed region for high

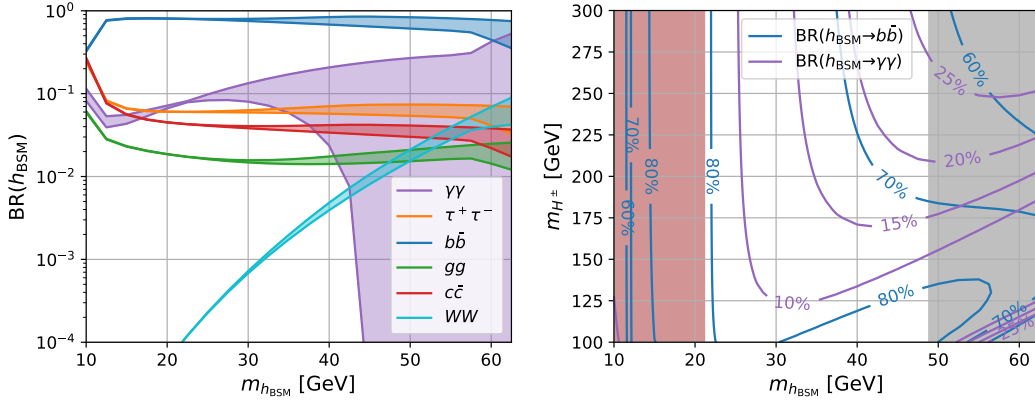


Figure 22.: Branching ratios of h_{BSM} in the $\text{cH}(Wh_{\text{BSM}}^{\text{light}})$ benchmark scenario. The *left panel* shows all important BRs as a function of $m_{h_{\text{BSM}}}$. The decay $h_{\text{BSM}} \rightarrow \gamma\gamma$ additionally depends on m_{H^\pm} and induces a dependence in the remaining BRs through the total width. The bands for each BR indicate the impact of this dependence within the parameter ranges of the scenario. The *right panel* shows the interplay of the two dominant BRs in the $(m_{H^\pm}, m_{h_{\text{BSM}}})$ parameter plane of $\text{cH}(Wh_{\text{BSM}}^{\text{light}})$.

values of $m_{h_{\text{BSM}}}$ and m_{H^\pm} . The dependence of $\text{BR}(h_{\text{BSM}} \rightarrow \gamma\gamma)$ on H^\pm is larger than in the other benchmark scenarios, since the top-quark and the W boson contribution to $h_{\text{BSM}} \rightarrow \gamma\gamma$ are suppressed by the high value of $\tan\beta$ and the approximately realized alignment limit, respectively.

In the $\text{cH}(Wh_{\text{BSM}}^{\text{light}})$ scenario, the h_{125} di-photon decay rate deviates from the SM by up to 14% (see Appendix A for more details).

5.5. $\text{cH}(Wh_{\text{BSM}}^{\text{phil}})$ scenario with light leptophilic h_{BSM}

As the last benchmark scenario we present the $\text{cH}(Wh_{\text{BSM}}^{\text{phil}})$ scenario. This scenario is defined with the same parameter values as the $\text{cH}(Wh_{\text{BSM}}^{\text{light}})$ scenario (see Table 5), however, instead of type-I, the $\text{cH}(Wh_{\text{BSM}}^{\text{phil}})$ scenario is defined in the lepton-specific 2HDM (see Section 2.2). As a direct consequence, h_{BSM} decays almost exclusively to tau leptons (with a branching ratio above 99%). Therefore, in contrast to the $\text{cH}(Wh_{\text{BSM}}^{\text{light}})$ scenario, LHC searches need to focus on the $h_{\text{BSM}} \rightarrow \tau^+\tau^-$ decay (following the charged Higgs boson decay $H^\pm \rightarrow W^\pm h_{\text{BSM}}$) in order to probe this scenario. The HL-LHC sensitivity to a phenomenologically similar scenario has previously been studied in Ref. [59].

As for the $\text{cH}(Wh_{\text{BSM}}^{\text{light}})$ scenario, $m_{h_{\text{BSM}}} \leq 62.5$ GeV is required. While it is in principle possible to define benchmark scenario within the lepton-specific 2HDM analogously to the $\text{cH}(Wh_{\text{BSM}})$ or $\text{cH}(WA)$ scenarios, we found that such scenarios are completely excluded experimentally by searches for a neutral Higgs decaying to tau leptons. These searches do, however, not cover the region $m_{h_{\text{BSM}}} \leq 62.5$ GeV.

The branching ratio $\text{BR}(H^\pm \rightarrow W^\pm h_{\text{BSM}})$ for the $\text{cH}(Wh_{\text{BSM}}^{\text{phil}})$ scenario is shown in the

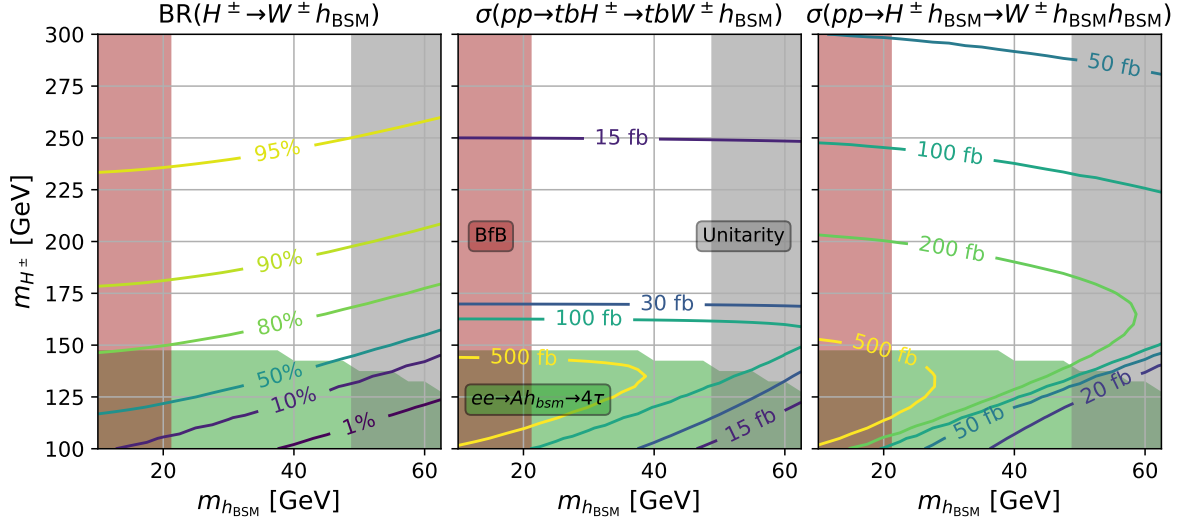


Figure 23.: Signal cross sections in the $(m_{H^\pm}, m_{h_{\text{BSM}}})$ parameter plane of benchmark scenario $\text{cH}(Wh_{\text{BSM}}^{\ell\text{phil}})$. All model parameters except for the Yukawa type are identical to the $\text{cH}(Wh_{\text{BSM}}^{\text{light}})$ scenario as given in Table 5. The *colored contours* indicate $\text{BR}(H^\pm \rightarrow W^\pm h_{\text{BSM}})$ in the *left* panel and the 13 TeV LHC cross sections for the search processes $pp \rightarrow tbH^\pm, H^\pm \rightarrow W^\pm h_{\text{BSM}}$ (*center*) and $pp \rightarrow H^\pm h_{\text{BSM}} \rightarrow W^\pm h_{\text{BSM}} h_{\text{BSM}}$ (*right*). The shaded regions are excluded by perturbative unitarity, boundedness from below, and LEP searches for di-Higgs production in the 4τ final state [211].

left panel of Fig. 23 in the $(m_{H^\pm}, m_{h_{\text{BSM}}})$ parameter plane. The colored areas are excluded by the following constraints: as for the $\text{cH}(Wh_{\text{BSM}}^{\text{light}})$ scenario, the region of $m_{h_{\text{BSM}}} \lesssim 21$ GeV is excluded by requiring boundedness from below (red) and the region of $m_{h_{\text{BSM}}} \gtrsim 50$ GeV by unitarity constraints (gray). While no experimental search constrains the $\text{cH}(Wh_{\text{BSM}}^{\text{light}})$ scenario, the region of $m_{H^\pm} \lesssim 140$ GeV is excluded in the $\text{cH}(Wh_{\text{BSM}}^{\ell\text{phil}})$ scenario by LEP searches for $e^+e^- \rightarrow Ah_{\text{BSM}} \rightarrow 4\tau$ (green). In the remaining unexcluded parameter space, $\text{BR}(H^\pm \rightarrow W^\pm h_{\text{BSM}})$ is always above 50%, and reaches almost 100% for $m_{H^\pm} \sim 300$ GeV. $\text{BR}(H^\pm \rightarrow W^\pm h_{\text{BSM}})$ is smaller than in the $\text{cH}(Wh_{\text{BSM}}^{\text{light}})$ scenario due to the fact that the competing $\text{BR}(H^\pm \rightarrow \tau^\pm \bar{\nu}_\tau)$ decay is enhanced by the large $\tan\beta$ value in the lepton-specific 2HDM.

The signal cross section for charged Higgs boson production in association with a top and a bottom quark and its subsequent decay to a W boson and a h_{BSM} boson is shown in the center panel of Fig. 23. In the allowed parameter space, $\sigma(p \rightarrow tbH^\pm, H^\pm \rightarrow W^\pm h_{\text{BSM}})$ can reach almost 500 fb for $m_{H^\pm} \sim 150$ GeV. For higher values of m_{H^\pm} the cross section quickly drops below 100 fb. In this region, $\sigma(p \rightarrow H^\pm h_{\text{BSM}}, H^\pm \rightarrow W^\pm h_{\text{BSM}} h_{\text{BSM}})$ — shown in the right panel of Fig. 23 — exceeds $\sigma(p \rightarrow tbH^\pm, H^\pm \rightarrow W^\pm h_{\text{BSM}})$, still reaching e.g. 200 fb for $m_{H^\pm} \sim 200$ GeV and $m_{h_{\text{BSM}}} \sim 30$ GeV. Note in particular, that — since $\text{BR}(h_{\text{BSM}} \rightarrow \tau^+\tau^-) \approx 1$ — the signal cross sections for the $tbW^\pm\tau^+\tau^-$ and $W^\pm\tau^+\tau^-\tau^+\tau^-$ final states are almost as large as the corresponding cross

sections without the h_{BSM} decays. Charged Higgs production in association with a W boson is negligible in the $\text{cH}(Wh_{\text{BSM}}^{\ell\text{phil}})$ scenario.

In the $\text{cH}(Wh_{\text{BSM}}^{\ell\text{phil}})$ scenario, the h_{125} di-photon decay rate deviates from the SM by up to 7% (see Appendix A for more details).

6. Conclusions

The presence of charged Higgs bosons is a generic prediction of multiplet extensions of the SM Higgs sector. Collider searches for charged Higgs bosons are, therefore, an important puzzle piece in the search for new physics in the Higgs sector. While many LHC searches for charged Higgs bosons decaying to SM fermions exist, the bosonic decay modes of charged Higgs bosons have so far received much less attention.

Focussing on the 2HDM, we discussed the charged Higgs boson phenomenology taking into account all applicable constraints of theoretical as well as experimental nature. We considered type I and lepton specific Yukawa sectors, where light charged Higgs bosons are not excluded by flavor observables. We revisited two genuine BSM effects on the discovered SM-like Higgs boson — the non-decoupling charged Higgs boson contribution to the SM-like Higgs boson decay into two photons, as well as the decay of the SM-like Higgs boson into two non-SM-like Higgs bosons — and their impact on the charged Higgs boson phenomenology. These effects even appear in the alignment limit, in which the SM-like Higgs boson has exactly SM-like couplings.

We then investigated in detail the production and decay modes of the charged Higgs bosons. We demonstrated that the charged Higgs boson decays predominantly to a W boson and a neutral non-SM-like Higgs state (which could be either \mathcal{CP} -even or \mathcal{CP} -odd) in large parts of the allowed parameter space. This decay mode is especially large close to the observationally-favored alignment limit, in which the charged Higgs boson coupling to a non-SM-like Higgs boson and a W boson is maximized.

We discussed current experimental searches for charged Higgs bosons at the LHC and pointed out the so-far unexplored decay signatures that arise from the above-mentioned decay to a W boson and a neutral non-SM-like Higgs state. In order to facilitate future searches for these signatures, and as the main result of this work, we introduced five benchmark scenarios, each featuring a distinct phenomenology: the $\text{cH}(Wh_{\text{BSM}})$ scenario, the $\text{cH}(WA)$ scenario, the $\text{cH}(Wh_{\text{BSM}}^{\text{phob}})$ scenario, the $\text{cH}(Wh_{\text{BSM}}^{\text{light}})$ scenario, and the $\text{cH}(Wh_{\text{BSM}}^{\ell\text{phil}})$ scenario. All scenarios exhibit a large decay rate of the charged Higgs boson to a W boson and a neutral non-SM-like Higgs boson. The scenarios are defined in a 2HDM of type I, except for $\text{cH}(Wh_{\text{BSM}}^{\ell\text{phil}})$ where the Yukawa sector is chosen to be lepton specific.

In the $\text{cH}(Wh_{\text{BSM}})$ scenario, the charged Higgs boson decays dominantly to a non-SM-like \mathcal{CP} -even Higgs boson and a W boson. The signal cross section for the production of the charged Higgs boson in association with a top and a bottom quark and its subsequent decay reaches up to 5 pb in significant parts of the yet-unconstrained parameter space. The experimentally most interesting decay modes of the non-SM-like Higgs boson in this scenario are the decay into bottom quarks and the decay into tau leptons.

In contrast to the $\text{cH}(Wh_{\text{BSM}})$ scenario, the charged Higgs boson decays dominantly to a \mathcal{CP} -odd A boson and a W boson in the $\text{cH}(WA)$ scenario, while the h_{BSM} boson has the same mass as the charged Higgs boson. Also in this scenario, signal cross sections of up to 5 pb can be reached in large parts of unconstrained parameter space. Due to the \mathcal{CP} -odd nature of the A boson, its decay width into two photons is enhanced with respect to the corresponding decay width of the h_{BSM} boson in the $\text{cH}(Wh_{\text{BSM}})$ scenario.

As in the $\text{cH}(Wh_{\text{BSM}})$ scenario, the charged Higgs boson decays dominantly to a non-SM-like \mathcal{CP} -even Higgs boson and a W boson in the $\text{cH}(Wh_{\text{BSM}}^{\text{fphob}})$ scenario reaching signal cross sections of up to 1 pb. In contrast to the previous scenarios, the non-SM-like \mathcal{CP} -even Higgs boson is fermiophobic in the $\text{cH}(Wh_{\text{BSM}}^{\text{fphob}})$ scenario, which results in large branching ratios of the h_{BSM} decays into massive vector bosons and photons.

In the $\text{cH}(Wh_{\text{BSM}}^{\text{light}})$ scenario the non-SM-like \mathcal{CP} -even Higgs boson is much lighter than the SM-like Higgs boson, allowing in principle for decays of the SM-like Higgs boson into two light non-SM-like \mathcal{CP} -even Higgs bosons. We, however, showed that this decay mode can be suppressed by suitable parameter choices. In that case, strong constraints on additional decay modes of the SM-like Higgs boson arising from precision rate measurements can be avoided. LHC searches for the charged Higgs boson decay into a light, non-SM-like \mathcal{CP} -even Higgs boson and a W boson therefore would provide an important complementary probe of such scenarios. In this scenario, the branching ratio of h_{BSM} to two photons can become quite large, i.e. up to 25 % within the allowed parameter region.

For the $\text{cH}(Wh_{\text{BSM}}^{\ell\text{phil}})$ scenario, we use the same parameters as in the $\text{cH}(Wh_{\text{BSM}}^{\text{light}})$ scenario. However, in contrast to all other benchmark scenarios, which are defined in the 2HDM type-I, the $\text{cH}(Wh_{\text{BSM}}^{\ell\text{phil}})$ scenario is defined in the lepton-specific 2HDM. Consequently, the h_{BSM} boson almost exclusively decays to tau leptons, while the remaining phenomenology is very similar to the $\text{cH}(Wh_{\text{BSM}}^{\text{light}})$ scenario.

We hope that the presented work and in particular the five benchmark scenarios serve as an encouragement as well as an useful set of tools for future experimental searches for bosonic charged Higgs boson decays at the LHC.

Acknowledgments

We are grateful to Liron Barak, David Brunner, Dirk Krücker and Isabell Melzer-Pellmann for useful discussions of experimental questions, and thank Hass AbouZeid and Mike Hance for collaboration at an initial stage of the project. We thank Stefan Liebler for discussions and assistance with `vh@nn10-2`. H.B. and T.S. acknowledge support by the Deutsche Forschungsgemeinschaft (DFG, German Research Foundation) under Germany’s Excellence Strategy — EXC 2121 “Quantum Universe” — 390833306. The work of J.W. is supported by the Swedish Research Council, contract number 2016-05996 and was in part funded by the European Research Council (ERC) under the European Union’s Horizon 2020 research and innovation programme, grant agreement No 668679.

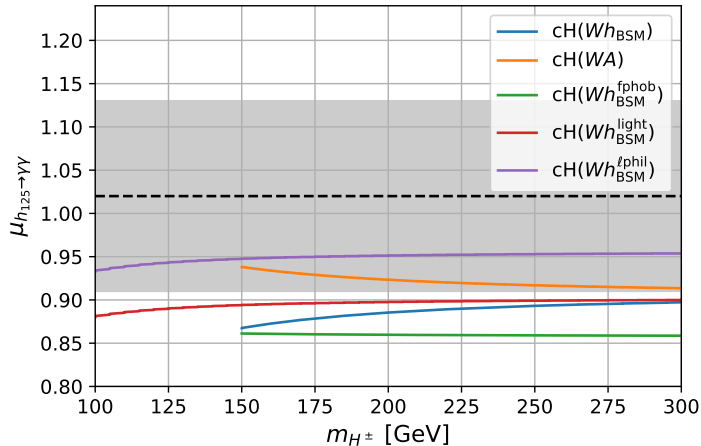


Figure 24.: Di-photon rate of h_{125} for the fermionic production modes (ggF+bbH) in dependence of m_{H^\pm} for the various benchmark scenarios defined in Section 5. The dashed line indicates the central value of the latest ATLAS measurement [117], the shaded region is the corresponding 1σ uncertainty and the displayed $\mu_{h_{125}\rightarrow\gamma\gamma}$ range corresponds to the 2σ uncertainty region (assuming a Gaussian uncertainty).

A. Benchmark scenarios: di-photon rate of h_{125}

As discussed in Section 3.1, the presence of the charged Higgs boson can result in deviations of the h_{125} di-photon rate even in the exact alignment limit. Fig. 24 shows these deviations for the various benchmark scenarios defined in Section 5: the $\text{cH}(Wh_{\text{BSM}})$ scenario (blue), the $\text{cH}(WA)$ scenario (orange), the $\text{cH}(Wh_{\text{BSM}}^{\text{fphob}})$ scenario (green), the $\text{cH}(Wh_{\text{BSM}}^{\text{light}})$ scenario (dark red), and the $\text{cH}(Wh_{\text{BSM}}^{\text{lphil}})$ scenario (purple). For all these scenarios the di-photon rate of h_{125} is suppressed with respect to the SM with the deviations ranging from $\sim 5\%$ (for the $\text{cH}(Wh_{\text{BSM}}^{\text{lphil}})$ scenario) to $\sim 14\%$ (for the $\text{cH}(Wh_{\text{BSM}}^{\text{fphob}})$ scenario). While the deviation is entirely caused by the charged Higgs effects in the $\text{cH}(Wh_{\text{BSM}})$ and $\text{cH}(WA)$ scenarios, which are defined in the exact alignment limit, the deviations in the other scenarios are also slightly affected by the departure from exact alignment. In the $\text{cH}(Wh_{\text{BSM}}^{\text{fphob}})$ scenario, $c(h_{125}t\bar{t}) \approx 1.02$ and $c(h_{125}VV) \approx 0.98$, while the misalignment is even smaller in the $\text{cH}(Wh_{\text{BSM}}^{\text{light}})$ and $\text{cH}(Wh_{\text{BSM}}^{\text{lphil}})$ scenarios with $c(h_{125}t\bar{t}) \approx 1.002$ and $c(h_{125}VV) \approx 0.998$.

This suggests that large parts of the considered parameter space can be probed by future Higgs precision measurements (e.g. at the HL-LHC [3]). The deviation of the di-photon rate, however, strongly depends on the value of m_{12}^2 . Correspondingly, it is possible to define phenomenologically similar benchmark scenarios with smaller (or even positive) deviations of the di-photon rate with respect to the SM.

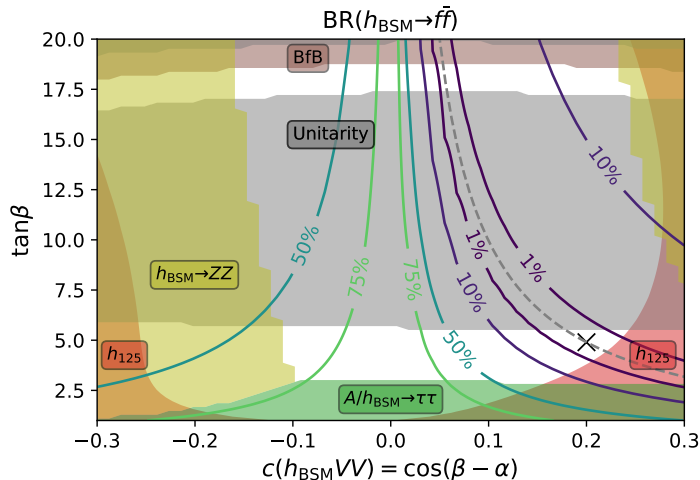


Figure 25.: The $(c(h_{\text{BSM}}VV), \tan\beta)$ parameter plane orthogonal to the $\text{cH}(Wh_{\text{BSM}}^{\text{fphob}})$ benchmark scenario. The masses are fixed to $m_{h_{\text{BSM}}} = 150$ GeV and $m_A = m_{H^\pm} = 200$ GeV and all remaining parameters are as given in Table 5. The contours indicate $\text{BR}(h_{\text{BSM}} \rightarrow f\bar{f})$ and the \times marks where this plane touches the mass plane of the $\text{cH}(Wh_{\text{BSM}}^{\text{fphob}})$ scenario. The dashed line denotes the fermiophobic limit. The shaded regions are excluded by existing theoretical constraints — boundedness from below and perturbative unitarity — experimental searches — $pp \rightarrow A/h_{\text{BSM}} \rightarrow \tau^+\tau^-$ [202, 212] and $pp \rightarrow h_{\text{BSM}} \rightarrow ZZ$ [213] — as well as h_{125} measurements.

B. Realizing the fermiophobic limit

The $\text{cH}(Wh_{\text{BSM}}^{\text{fphob}})$ scenario is defined as a $(m_{h_{\text{BSM}}}, m_{H^\pm})$ parameter plane with $\tan\beta \sim 4.9$ and $\cos(\beta - \alpha) = 0.2$ taking fixed values (see Section 5). In order to motivate the choice of $\tan\beta$ and $\cos(\beta - \alpha)$, we show $\text{BR}(h_{\text{BSM}} \rightarrow f\bar{f})$ as a function of $\tan\beta$ as well as $\cos(\beta - \alpha)$ for $m_{h_{\text{BSM}}} = 150$ GeV and $m_{H^\pm} = 200$ GeV in Fig. 25. All other parameters are chosen as in the $\text{cH}(Wh_{\text{BSM}}^{\text{fphob}})$ scenario. The shaded regions are excluded by boundedness from below (brown) — excluding the region of $\tan\beta \gtrsim 18$ —, perturbative unitarity (gray) — excluding the region of $6 \lesssim \tan\beta \lesssim 17$ —, searches for $pp \rightarrow A/h_{\text{BSM}} \rightarrow \tau^+\tau^-$ [202, 212] (green) — excluding the region of $\tan\beta \lesssim 2.5$ —, searches for $pp \rightarrow h_{\text{BSM}} \rightarrow ZZ$ [213] — excluding the region of $\cos(\beta - \alpha) \lesssim -0.15$ and $\cos(\beta - \alpha) \gtrsim 0.25$ — as well as h_{125} measurements — excluding the region of large $|\cos(\beta - \alpha)|$ and low $\tan\beta$.

In the still unconstrained parameter region, the fermiophobic limit (see Section 2.3) can be realized either for $\tan\beta \sim 5$ or $\tan\beta \sim 17.5$. While choosing $\tan\beta \sim 17.5$ would allow to approach the alignment more closely, the high $\tan\beta$ value would result in a relatively low charged Higgs production cross section (see Section 4.1). Therefore, we choose $\tan\beta \sim 4.9$ for the definition of the $\text{cH}(Wh_{\text{BSM}}^{\text{fphob}})$ scenario (as marked by the cross in Fig. 25).

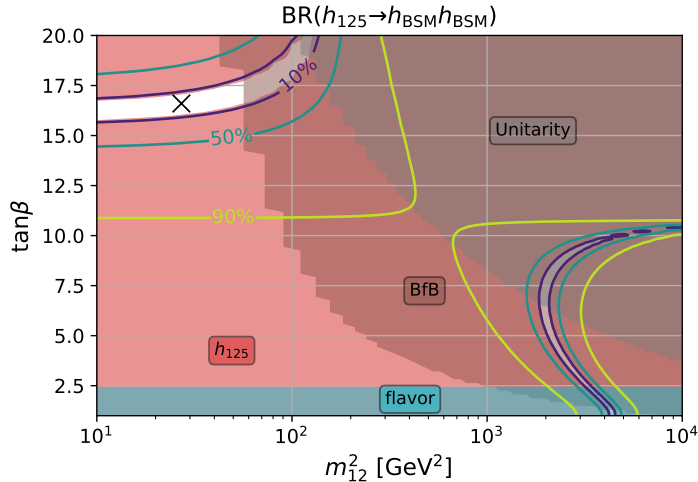


Figure 26.: The $(\tan \beta, m_{12}^2)$ parameter plane orthogonal to the $\text{cH}(Wh_{\text{BSM}}^{\text{light}})$ benchmark scenario. The masses are fixed to $m_{h_{\text{BSM}}} = 30 \text{ GeV}$ and $m_A = m_{H^\pm} = 200 \text{ GeV}$ and all remaining parameters are as given in Table 5. The contours indicate $\text{BR}(h_{125} \rightarrow h_{\text{BSM}}h_{\text{BSM}})$ and the \times marks where this plane touches the mass plane of the $\text{cH}(Wh_{\text{BSM}}^{\text{light}})$ scenario. The shaded regions are excluded by existing theoretical constraints — boundedness from below and perturbative unitarity — as well as h_{125} measurements and flavor constraints.

C. Suppressing $h_{125} \rightarrow h_{\text{BSM}}h_{\text{BSM}}$ in the $\text{cH}(Wh_{\text{BSM}}^{\text{light}})$ scenario

As discussed in Section 3.2, the $h_{125} \rightarrow h_{\text{BSM}}h_{\text{BSM}}$ decay can be suppressed by an appropriate choice of m_{12}^2 . This choice of m_{12}^2 for the $\text{cH}(Wh_{\text{BSM}}^{\text{light}})$ scenario is motivated in Fig. 26 showing $\text{BR}(h_{125} \rightarrow h_{\text{BSM}}h_{\text{BSM}})$. All parameters are chosen as for the $\text{cH}(Wh_{\text{BSM}}^{\text{light}})$ scenarios except of m_{12}^2 and $\tan \beta$ which are treated as free parameters while $m_{h_{\text{BSM}}} = 30 \text{ GeV}$ and $m_{H^\pm} = 200 \text{ GeV}$ are fixed. The shaded regions are excluded by boundedness from below (brown) and perturbative unitarity (gray) — excluding the region of high m_{12}^2 and $\tan \beta$ —, flavor constraints — excluding the region of $\tan \beta \lesssim 2.5$ —, as well as h_{125} measurements — excluding most of the remaining region, except for a band of $15.5 \lesssim \tan \beta \lesssim 17$.

While $\text{BR}(h_{125} \rightarrow h_{\text{BSM}}h_{\text{BSM}})$ can be close to zero in the region of $\tan \beta \lesssim 10$ and $m_{12}^2 > 1000 \text{ GeV}^2$, this region is completely excluded by existing constraints. The only still unconstrained region with $\text{BR}(h_{125} \rightarrow h_{\text{BSM}}h_{\text{BSM}}) \sim 0$ lies in the region of $15.5 \lesssim \tan \beta \lesssim 17$ and $m_{12}^2 \lesssim 60 \text{ GeV}^2$. The $\text{cH}(Wh_{\text{BSM}}^{\text{light}})$ scenario, marked by the cross, is chosen in the center of this region.

References

- [1] CMS, “Observation of a New Boson at a Mass of 125 GeV with the CMS Experiment at the LHC”, Phys. Lett. B **716** (2012) 30, 1207.7235.
- [2] ATLAS, “Observation of a new particle in the search for the Standard Model Higgs boson with the ATLAS detector at the LHC”, Phys. Lett. B **716** (2012) 1, 1207.7214.
- [3] M. Cepeda et al., “Report from Working Group 2: Higgs Physics at the HL-LHC and HE-LHC”, CERN Yellow Rep. Monogr. **7** (2019) 221, ed. by A. Dainese et al., 1902.00134.
- [4] ATLAS, CMS, “Measurements of the Higgs boson production and decay rates and constraints on its couplings from a combined ATLAS and CMS analysis of the LHC pp collision data at $\sqrt{s} = 7$ and 8 TeV”, JHEP **08** (2016) 045, 1606.02266.
- [5] ATLAS, “Combined measurements of Higgs boson production and decay using up to 80 fb⁻¹ of proton-proton collision data at $\sqrt{s} = 13$ TeV collected with the ATLAS experiment”, Phys. Rev. D **101** (2020) 012002, 1909.02845.
- [6] CMS, “Combined measurements of Higgs boson couplings in proton–proton collisions at $\sqrt{s} = 13$ TeV”, Eur. Phys. J. C **79** (2019) 421, 1809.10733.
- [7] CMS, “Combined Higgs boson production and decay measurements with up to 137 fb-1 of proton-proton collision data at sqrts = 13 TeV”, (2020), CMS-PAS-HIG-19-005.
- [8] G. Arcadi, A. Djouadi, and M. Raidal, “Dark Matter through the Higgs portal”, Phys. Rept. **842** (2020) 1, 1903.03616.
- [9] J. M. Cline, K. Kainulainen, and M. Trott, “Electroweak Baryogenesis in Two Higgs Doublet Models and B meson anomalies”, JHEP **11** (2011) 089, 1107.3559.
- [10] J. Shu and Y. Zhang, “Impact of a CP Violating Higgs Sector: From LHC to Baryogenesis”, Phys. Rev. Lett. **111** (2013) 091801, 1304.0773.
- [11] N. Blinov, S. Profumo, and T. Stefaniak, “The Electroweak Phase Transition in the Inert Doublet Model”, JCAP **07** (2015) 028, 1504.05949.
- [12] G. C. Dorsch et al., “A Second Higgs Doublet in the Early Universe: Baryogenesis and Gravitational Waves”, JCAP **05** (2017) 052, 1611.05874.
- [13] P. Basler, M. Mühlleitner, and J. Müller, “Electroweak Phase Transition in Non-Minimal Higgs Sectors”, JHEP **05** (2020) 016, 1912.10477.
- [14] S. Fabian, F. Goertz, and Y. Jiang, “Dark Matter and Nature of Electroweak Phase Transition with an Inert Doublet”, (2020), 2012.12847.
- [15] H. E. Haber and G. L. Kane, “The Search for Supersymmetry: Probing Physics Beyond the Standard Model”, Phys. Rept. **117** (1985) 75, UM-HE-TH-83-17, SCIPP-85-47.

- [16] J. F. Gunion and H. E. Haber, “Higgs Bosons in Supersymmetric Models. 1.”, Nucl. Phys. B **272** (1986) 1, SLAC-PUB-3404.
- [17] J. F. Gunion and H. E. Haber, “Higgs Bosons in Supersymmetric Models. 2. Implications for Phenomenology”, Nucl. Phys. B **278** (1986) 449, ed. by S. C. Loken, UCD-86-12.
- [18] J. R. Ellis et al., “Higgs Bosons in a Nonminimal Supersymmetric Model”, Phys. Rev. D **39** (1989) 844, SLAC-PUB-4565, UCD-88-07, LBL-25107, UCB/PTH/88/8, SCIPP-88/07.
- [19] J. F. Gunion and H. E. Haber, “The CP conserving two Higgs doublet model: The Approach to the decoupling limit”, Phys. Rev. D **67** (2003) 075019, hep-ph/0207010.
- [20] N. Craig, J. Galloway, and S. Thomas, “Searching for Signs of the Second Higgs Doublet”, (2013), 1305.2424.
- [21] J. Bernon et al., “Scrutinizing the alignment limit in two-Higgs-doublet models: $m_h=125$ GeV”, Phys. Rev. D **92** (2015) 075004, 1507.00933.
- [22] J. Bernon et al., “Scrutinizing the alignment limit in two-Higgs-doublet models. II. $m_H=125$ GeV”, Phys. Rev. D **93** (2016) 035027, 1511.03682.
- [23] M. Carena et al., “Impersonating the Standard Model Higgs Boson: Alignment without Decoupling”, JHEP **04** (2014) 015, 1310.2248.
- [24] M. Carena et al., “Complementarity between Nonstandard Higgs Boson Searches and Precision Higgs Boson Measurements in the MSSM”, Phys. Rev. D **91** (2015) 035003, 1410.4969.
- [25] P. Bechtle et al., “The Light and Heavy Higgs Interpretation of the MSSM”, Eur. Phys. J. C **77** (2017) 67, 1608.00638.
- [26] H. E. Haber, S. Heinemeyer, and T. Stefaniak, “The Impact of Two-Loop Effects on the Scenario of MSSM Higgs Alignment without Decoupling”, Eur. Phys. J. C **77** (2017) 742, 1708.04416.
- [27] E. Bagnaschi et al., “MSSM Higgs Boson Searches at the LHC: Benchmark Scenarios for Run 2 and Beyond”, Eur. Phys. J. C **79** (2019) 617, 1808.07542.
- [28] W. G. Hollik, G. Weiglein, and J. Wittbrodt, “Impact of Vacuum Stability Constraints on the Phenomenology of Supersymmetric Models”, JHEP **03** (2019) 109, 1812.04644.
- [29] M. Carena et al., “Alignment limit of the NMSSM Higgs sector”, Phys. Rev. D **93** (2016) 035013, 1510.09137.
- [30] N. M. Coyle and C. E. M. Wagner, “Dynamical Higgs field alignment in the NMSSM”, Phys. Rev. D **101** (2020) 055037, 1912.01036.
- [31] A. Djouadi et al., “Direct Detection of Higgs-Portal Dark Matter at the LHC”, Eur. Phys. J. C **73** (2013) 2455, 1205.3169.

- [32] ATLAS, CMS, “Combined Measurement of the Higgs Boson Mass in pp Collisions at $\sqrt{s} = 7$ and 8 TeV with the ATLAS and CMS Experiments”, Phys. Rev. Lett. **114** (2015) 191803, 1503.07589.
- [33] P. Baldi, P. Sadowski, and D. Whiteson, “Searching for Exotic Particles in High-Energy Physics with Deep Learning”, Nature Commun. **5** (2014) 4308, 1402.4735.
- [34] G. Kasieczka et al., “Deep-learning Top Taggers or The End of QCD?”, JHEP **05** (2017) 006, 1701.08784.
- [35] A. J. Larkoski, I. Mout, and B. Nachman, “Jet Substructure at the Large Hadron Collider: A Review of Recent Advances in Theory and Machine Learning”, Phys. Rept. **841** (2020) 1, 1709.04464.
- [36] G. Louppe et al., “QCD-Aware Recursive Neural Networks for Jet Physics”, JHEP **01** (2019) 057, 1702.00748.
- [37] S. Macaluso and D. Shih, “Pulling Out All the Tops with Computer Vision and Deep Learning”, JHEP **10** (2018) 121, 1803.00107.
- [38] G. Carleo et al., “Machine learning and the physical sciences”, Rev. Mod. Phys. **91** (2019) 045002, 1903.10563.
- [39] J. Y. Araz and M. Spannowsky, “Combine and Conquer: Event Reconstruction with Bayesian Ensemble Neural Networks”, (2021), 2102.01078.
- [40] C. Gao et al., “Searching for Additional Higgs Bosons via Higgs Cascades”, Phys. Rev. D **97** (2018) 075040, 1604.03108.
- [41] S. Gori, Z. Liu, and B. Shakya, “Heavy Higgs as a Portal to the Supersymmetric Electroweak Sector”, JHEP **04** (2019) 049, 1811.11918.
- [42] H. Bahl, S. Liebler, and T. Stefaniak, “MSSM Higgs benchmark scenarios for Run 2 and beyond: the low $\tan\beta$ region”, Eur. Phys. J. C **79** (2019) 279, 1901.05933.
- [43] T. Robens, T. Stefaniak, and J. Wittbrodt, “Two-real-scalar-singlet extension of the SM: LHC phenomenology and benchmark scenarios”, Eur. Phys. J. C **80** (2020) 151, 1908.08554.
- [44] A. Adhikary et al., “Searching for heavy Higgs in supersymmetric final states at the LHC”, (2020), 2002.07137.
- [45] J. Liu et al., “Searching for the Higgsino-Bino Sector at the LHC”, JHEP **09** (2020) 073, 2006.07389.
- [46] M. Aiko, S. Kanemura, and K. Mawatari, “Exploring the global symmetry structure of the Higgs potential via same-sign pair production of charged Higgs bosons”, Phys. Lett. B **797** (2019) 134854, 1906.09101.
- [47] K. Cheung et al., “Disentangling new physics effects on nonresonant Higgs boson pair production from gluon fusion”, Phys. Rev. D **103** (2021) 015019, 2003.11043.
- [48] E. Arganda et al., “Potential discovery of staus through heavy Higgs boson decays at the LHC”, JHEP **09** (2018) 056, 1804.10698.

- [49] E. Arganda et al., “Discovery and exclusion prospects for staus produced by heavy Higgs bosons decays at the LHC”, (2021), 2102.02290.
- [50] A. G. Akeroyd, “Three body decays of Higgs bosons at LEP-2 and application to a hidden fermiophobic Higgs”, Nucl. Phys. B **544** (1999) 557, hep-ph/9806337.
- [51] L. Basso et al., “Probing the charged Higgs boson at the LHC in the CP-violating type-II 2HDM”, JHEP **11** (2012) 011, 1205.6569.
- [52] B. Coleppa, F. Kling, and S. Su, “Charged Higgs search via AW^\pm/HW^\pm channel”, JHEP **12** (2014) 148, 1408.4119.
- [53] F. Kling, A. Pyarelal, and S. Su, “Light Charged Higgs Bosons to AW/HW via Top Decay”, JHEP **11** (2015) 051, 1504.06624.
- [54] H. E. Haber and O. Stål, “New LHC benchmarks for the CP -conserving two-Higgs-doublet model”, Eur. Phys. J. C **75** (2015) 491, 1507.04281.
- [55] A. G. Akeroyd et al., “Prospects for charged Higgs searches at the LHC”, Eur. Phys. J. C **77** (2017) 276, 1607.01320.
- [56] A. Arhrib, R. Benbrik, and S. Moretti, “Bosonic Decays of Charged Higgs Bosons in a 2HDM Type-I”, Eur. Phys. J. C **77** (2017) 621, 1607.02402.
- [57] A. Arhrib et al., “Identifying a light charged Higgs boson at the LHC Run II”, Phys. Lett. B **774** (2017) 591, 1706.01964.
- [58] D. S. M. Alves et al., “Charged Higgs Signals in $t\bar{t}H$ Searches”, Phys. Rev. D **96** (2017) 075032, 1703.06834.
- [59] E. J. Chun et al., “Reconstructing heavy Higgs boson masses in a type X two-Higgs-doublet model with a light pseudoscalar particle”, Phys. Rev. D **98** (2018) 075008, 1807.05379.
- [60] B. Coleppa, A. Sarkar, and S. K. Rai, “Charged Higgs boson discovery prospects”, Phys. Rev. D **101** (2020) 055030, 1909.11992.
- [61] J. F. Gunion et al., *The Higgs Hunter’s Guide*, vol. 80, 2000, SCIPP-89/13, UCD-89-4, BNL-41644.
- [62] M. Carena et al., “Effective Lagrangian for the $\bar{t}bH^+$ interaction in the MSSM and charged Higgs phenomenology”, Nucl. Phys. B **577** (2000) 88, hep-ph/9912516.
- [63] A. Djouadi, “The Anatomy of electro-weak symmetry breaking. II. The Higgs bosons in the minimal supersymmetric model”, Phys. Rept. **459** (2008) 1, hep-ph/0503173.
- [64] M. Carena et al., “MSSM Higgs boson searches at the Tevatron and the LHC: Impact of different benchmark scenarios”, Eur. Phys. J. C **45** (2006) 797, hep-ph/0511023.
- [65] CMS, “Search for a light charged Higgs boson decaying to a W boson and a CP-odd Higgs boson in final states with $e\mu\mu$ or $\mu\mu\mu$ in proton-proton collisions at $\sqrt{s} = 13$ TeV”, Phys. Rev. Lett. **123** (2019) 131802, 1905.07453.

- [66] I. P. Ivanov, “Building and testing models with extended Higgs sectors”, *Prog. Part. Nucl. Phys.* **95** (2017) 160, 1702.03776.
- [67] M. P. Bento et al., “Multi-Higgs doublet models: physical parametrization, sum rules and unitarity bounds”, *JHEP* **11** (2017) 095, 1708.09408.
- [68] G. C. Branco et al., “Theory and phenomenology of two-Higgs-doublet models”, *Phys. Rept.* **516** (2012) 1, 1106.0034.
- [69] M. Misiak and M. Steinhauser, “Weak radiative decays of the B meson and bounds on M_{H^\pm} in the Two-Higgs-Doublet Model”, *Eur. Phys. J. C* **77** (2017) 201, 1702.04571.
- [70] A. Arbey et al., “Status of the Charged Higgs Boson in Two Higgs Doublet Models”, *Eur. Phys. J. C* **78** (2018) 182, 1706.07414.
- [71] R. Coimbra, M. O. P. Sampaio, and R. Santos, “ScannerS: Constraining the phase diagram of a complex scalar singlet at the LHC”, *Eur. Phys. J. C* **73** (2013) 2428, 1301.2599.
- [72] P. M. Ferreira et al., “Wrong sign and symmetric limits and non-decoupling in 2HDMs”, *JHEP* **12** (2014) 067, 1409.6723.
- [73] R. Costa et al., “Singlet Extensions of the Standard Model at LHC Run 2: Benchmarks and Comparison with the NMSSM”, *JHEP* **06** (2016) 034, 1512.05355.
- [74] M. Muhlleitner et al., “The N2HDM under Theoretical and Experimental Scrutiny”, *JHEP* **03** (2017) 094, 1612.01309.
- [75] M. Muhlleitner et al., “ScannerS: Parameter Scans in Extended Scalar Sectors”, (2020), 2007.02985.
- [76] A. Barroso et al., “Metastability bounds on the two Higgs doublet model”, *JHEP* **06** (2013) 045, 1303.5098.
- [77] W. Grimus et al., “A Precision constraint on multi-Higgs-doublet models”, *J. Phys. G* **35** (2008) 075001, 0711.4022.
- [78] W. Grimus et al., “The Oblique parameters in multi-Higgs-doublet models”, *Nucl. Phys. B* **801** (2008) 81, 0802.4353.
- [79] J. Haller et al., “Update of the global electroweak fit and constraints on two-Higgs-doublet models”, *Eur. Phys. J. C* **78** (2018) 675, 1803.01853.
- [80] P. Bechtle et al., “HiggsBounds: Confronting Arbitrary Higgs Sectors with Exclusion Bounds from LEP and the Tevatron”, *Comput. Phys. Commun.* **181** (2010) 138, 0811.4169.
- [81] P. Bechtle et al., “HiggsBounds 2.0.0: Confronting Neutral and Charged Higgs Sector Predictions with Exclusion Bounds from LEP and the Tevatron”, *Comput. Phys. Commun.* **182** (2011) 2605, 1102.1898.
- [82] P. Bechtle et al., “Recent Developments in HiggsBounds and a Preview of HiggsSignals”, *PoS CHARGED2012* (2012) 024, ed. by R. Enberg and A. Ferrari, 1301.2345.

- [83] P. Bechtle et al., “HiggsBounds – 4: Improved Tests of Extended Higgs Sectors against Exclusion Bounds from LEP, the Tevatron and the LHC”, *Eur. Phys. J. C* **74** (2014) 2693, 1311.0055.
- [84] P. Bechtle et al., “Applying Exclusion Likelihoods from LHC Searches to Extended Higgs Sectors”, *Eur. Phys. J. C* **75** (2015) 421, 1507.06706.
- [85] P. Bechtle et al., “HiggsBounds-5: Testing Higgs Sectors in the LHC 13 TeV Era”, *Eur. Phys. J. C* **80** (2020) 1211, 2006.06007.
- [86] O. Stål and T. Stefaniak, “Constraining extended Higgs sectors with HiggsSignals”, *PoS EPS-HEP2013* (2013) 314, 1310.4039.
- [87] P. Bechtle et al., “*HiggsSignals*: Confronting arbitrary Higgs sectors with measurements at the Tevatron and the LHC”, *Eur. Phys. J. C* **74** (2014) 2711, 1305.1933.
- [88] P. Bechtle et al., “Probing the Standard Model with Higgs signal rates from the Tevatron, the LHC and a future ILC”, *JHEP* **11** (2014) 039, 1403.1582.
- [89] P. Bechtle et al., “HiggsSignals-2: Probing new physics with precision Higgs measurements in the LHC 13 TeV era”, (2020), 2012.09197.
- [90] ATLAS, “Search for Higgs bosons produced via vector-boson fusion and decaying into bottom quark pairs in $\sqrt{s} = 13$ TeV pp collisions with the ATLAS detector”, *Phys. Rev. D* **98** (2018) 052003, 1807.08639.
- [91] ATLAS, “Search for the standard model Higgs boson produced in association with top quarks and decaying into a $b\bar{b}$ pair in pp collisions at $\sqrt{s} = 13$ TeV with the ATLAS detector”, *Phys. Rev. D* **97** (2018) 072016, 1712.08895.
- [92] ATLAS, “Analysis of $t\bar{t}H$ and $t\bar{t}W$ production in multilepton final states with the ATLAS detector”, (2019), ATLAS-CONF-2019-045.
- [93] ATLAS, “Measurements of gluon-gluon fusion and vector-boson fusion Higgs boson production cross-sections in the $H \rightarrow WW^* \rightarrow e\nu\mu\nu$ decay channel in pp collisions at $\sqrt{s} = 13$ TeV with the ATLAS detector”, *Phys. Lett. B* **789** (2019) 508, 1808.09054.
- [94] ATLAS, “Higgs boson production cross-section measurements and their EFT interpretation in the 4ℓ decay channel at $\sqrt{s} = 13$ TeV with the ATLAS detector”, *Eur. Phys. J. C* **80** (2020) 957, 2004.03447.
- [95] ATLAS, “Measurements and interpretations of Higgs-boson fiducial cross sections in the diphoton decay channel using 139 fb^{-1} of pp collision data at $\sqrt{s} = 13$ TeV with the ATLAS detector”, (2019), ATLAS-CONF-2019-029.
- [96] ATLAS, “Cross-section measurements of the Higgs boson decaying into a pair of τ -leptons in proton-proton collisions at $\sqrt{s} = 13$ TeV with the ATLAS detector”, *Phys. Rev. D* **99** (2019) 072001, 1811.08856.

- [97] ATLAS, “Measurement of the production cross section for a Higgs boson in association with a vector boson in the $H \rightarrow WW^* \rightarrow \ell\nu\ell\nu$ channel in pp collisions at $\sqrt{s} = 13$ TeV with the ATLAS detector”, Phys. Lett. B **798** (2019) 134949, 1903.10052.
- [98] ATLAS, “Measurements of WH and ZH production in the $H \rightarrow b\bar{b}$ decay channel in pp collisions at 13 TeV with the ATLAS detector”, Eur. Phys. J. C **81** (2021) 178, 2007.02873.
- [99] CMS, “Search for the Higgs boson decaying to two muons in proton-proton collisions at $\sqrt{s} = 13$ TeV”, Phys. Rev. Lett. **122** (2019) 021801, 1807.06325.
- [100] CMS, “Evidence for the Higgs boson decay to a bottom quark–antiquark pair”, Phys. Lett. B **780** (2018) 501, 1709.07497.
- [101] CMS, “Inclusive search for a highly boosted Higgs boson decaying to a bottom quark-antiquark pair”, Phys. Rev. Lett. **120** (2018) 071802, 1709.05543.
- [102] CMS, “Search for $t\bar{t}H$ production in the $H \rightarrow b\bar{b}$ decay channel with leptonic $t\bar{t}$ decays in proton-proton collisions at $\sqrt{s} = 13$ TeV”, JHEP **03** (2019) 026, 1804.03682.
- [103] CMS, “Measurement of $t\bar{t}H$ production in the $H \rightarrow b\bar{b}$ decay channel in 41.5 fb^{-1} of proton-proton collision data at $\sqrt{s} = 13$ TeV”, (2019), CMS-PAS-HIG-18-030.
- [104] CMS, “Evidence for associated production of a Higgs boson with a top quark pair in final states with electrons, muons, and hadronically decaying τ leptons at $\sqrt{s} = 13$ TeV”, JHEP **08** (2018) 066, 1803.05485.
- [105] CMS, “Measurement of the associated production of a Higgs boson with a top quark pair in final states with electrons, muons and hadronically decaying τ leptons in data recorded in 2017 at $\sqrt{s} = 13$ TeV”, (2018), CMS-PAS-HIG-18-019.
- [106] CMS, “Measurement of the inclusive and differential Higgs boson production cross sections in the leptonic WW decay mode at $\sqrt{s} = 13$ TeV”, JHEP **03** (2021) 003, 2007.01984.
- [107] CMS, “Measurements of properties of the Higgs boson in the four-lepton final state in proton-proton collisions at $\sqrt{s} = 13$ TeV”, (2019), CMS-PAS-HIG-19-001.
- [108] CMS, “Measurements of Higgs boson production via gluon fusion and vector boson fusion in the diphoton decay channel at $\sqrt{s} = 13$ TeV”, (2019), CMS-PAS-HIG-18-029.
- [109] CMS, “Measurements of $t\bar{t}H$ Production and the CP Structure of the Yukawa Interaction between the Higgs Boson and Top Quark in the Diphoton Decay Channel”, Phys. Rev. Lett. **125** (2020) 061801, 2003.10866.
- [110] CMS, “Measurement of Higgs boson production and decay to the $\tau\tau$ final state”, (2019), CMS-PAS-HIG-18-032.

- [111] A. Djouadi, J. Kalinowski, and M. Spira, “HDECAY: A Program for Higgs boson decays in the standard model and its supersymmetric extension”, *Comput. Phys. Commun.* **108** (1998) 56, [hep-ph/9704448](#).
- [112] R. Harlander et al., “Interim recommendations for the evaluation of Higgs production cross sections and branching ratios at the LHC in the Two-Higgs-Doublet Model”, (2013), [1312.5571](#).
- [113] A. Djouadi et al., “HDECAY: Twenty₊₊ years after”, *Comput. Phys. Commun.* **238** (2019) 214, [1801.09506](#).
- [114] R. V. Harlander, S. Liebler, and H. Mantler, “SusHi: A program for the calculation of Higgs production in gluon fusion and bottom-quark annihilation in the Standard Model and the MSSM”, *Comput. Phys. Commun.* **184** (2013) 1605, [1212.3249](#).
- [115] R. V. Harlander, S. Liebler, and H. Mantler, “SusHi Bento: Beyond NNLO and the heavy-top limit”, *Comput. Phys. Commun.* **212** (2017) 239, [1605.03190](#).
- [116] H. E. Haber and D. O’Neil, “Basis-independent methods for the two-Higgs-doublet model III: The CP-conserving limit, custodial symmetry, and the oblique parameters S, T, U”, *Phys. Rev. D* **83** (2011) 055017, [1011.6188](#).
- [117] ATLAS, “Measurement of the properties of Higgs boson production at $\sqrt{s}=13$ TeV in the $H \rightarrow \gamma\gamma$ channel using 139 fb^{-1} of pp collision data with the ATLAS experiment”, (2020), [ATLAS-CONF-2020-026](#).
- [118] A. Arhrib et al., “Higgs decays in the two Higgs doublet model: Large quantum effects in the decoupling regime”, *Phys. Lett. B* **579** (2004) 361, [hep-ph/0307391](#).
- [119] G. Bhattacharyya et al., “Scalar sector properties of two-Higgs-doublet models with a global U(1) symmetry”, *JHEP* **10** (2013) 081, [1308.4297](#).
- [120] P. M. Ferreira et al., “Probing wrong-sign Yukawa couplings at the LHC and a future linear collider”, *Phys. Rev. D* **89** (2014) 115003, [1403.4736](#).
- [121] B. Dumont et al., “Constraints on and future prospects for Two-Higgs-Doublet Models in light of the LHC Higgs signal”, *Phys. Rev. D* **90** (2014) 035021, [1405.3584](#).
- [122] G. Bhattacharyya and D. Das, “Nondecoupling of charged scalars in Higgs decay to two photons and symmetries of the scalar potential”, *Phys. Rev. D* **91** (2015) 015005, [1408.6133](#).
- [123] CMS, “Search for an exotic decay of the Higgs boson to a pair of light pseudoscalars in the final state of two muons and two τ leptons in proton-proton collisions at $\sqrt{s} = 13$ TeV”, *JHEP* **11** (2018) 018, [1805.04865](#).
- [124] CMS, “Search for an exotic decay of the Higgs boson to a pair of light pseudoscalars in the final state with two b quarks and two τ leptons in proton-proton collisions at $\sqrt{s} = 13$ TeV”, *Phys. Lett. B* **785** (2018) 462, [1805.10191](#).

- [125] ATLAS, “Search for the Higgs boson produced in association with a vector boson and decaying into two spin-zero particles in the $H \rightarrow aa \rightarrow 4b$ channel in pp collisions at $\sqrt{s} = 13$ TeV with the ATLAS detector”, JHEP **10** (2018) 031, 1806.07355.
- [126] ATLAS, “Search for Higgs boson decays into pairs of light (pseudo)scalar particles in the $\gamma\gamma jj$ final state in pp collisions at $\sqrt{s} = 13$ TeV with the ATLAS detector”, Phys. Lett. B **782** (2018) 750, 1803.11145.
- [127] CMS, “Search for an exotic decay of the Higgs boson to a pair of light pseudoscalars in the final state with two muons and two b quarks in pp collisions at 13 TeV”, Phys. Lett. B **795** (2019) 398, 1812.06359.
- [128] ATLAS, “Search for Higgs boson decays into a pair of light bosons in the $bb\mu\mu$ final state in pp collision at $\sqrt{s} = 13$ TeV with the ATLAS detector”, Phys. Lett. B **790** (2019) 1, 1807.00539.
- [129] CMS, “Search for a light pseudoscalar Higgs boson in the boosted $\mu\mu\tau\tau$ final state in proton-proton collisions at $\sqrt{s} = 13$ TeV”, JHEP **08** (2020) 139, 2005.08694.
- [130] L. A. Harland-Lang et al., “Parton distributions in the LHC era: MMHT 2014 PDFs”, Eur. Phys. J. C **75** (2015) 204, 1412.3989.
- [131] J. Alwall and J. Rathsmann, “Improved description of charged Higgs boson production at hadron colliders”, JHEP **12** (2004) 050, hep-ph/0409094.
- [132] S. Moretti et al., “Implementation of supersymmetric processes in the HERWIG event generator”, JHEP **04** (2002) 028, hep-ph/0204123.
- [133] K. A. Assamagan, M. Guchait, and S. Moretti, “Charged Higgs bosons in the transition region $M(H^{\pm}) \sim m(t)$ at the LHC”, in: *3rd Les Houches Workshop on Physics at TeV Colliders*, 2004, hep-ph/0402057.
- [134] S.-h. Zhu, “Complete next-to-leading order QCD corrections to charged Higgs boson associated production with top quark at the CERN large hadron collider”, Phys. Rev. D **67** (2003) 075006, hep-ph/0112109.
- [135] G.-p. Gao et al., “Loop effects and nondecoupling property of SUSY QCD in $g b \rightarrow t H^-$ ”, Phys. Rev. D **66** (2002) 015007, hep-ph/0202016.
- [136] T. Plehn, “Charged Higgs boson production in bottom gluon fusion”, Phys. Rev. D **67** (2003) 014018, hep-ph/0206121.
- [137] E. L. Berger et al., “Associated production of a top quark and a charged Higgs boson”, Phys. Rev. D **71** (2005) 115012, hep-ph/0312286.
- [138] N. Kidonakis, “Charged Higgs production: Higher-order corrections”, PoS **HEP2005** (2006) 336, ed. by G. Barreira, hep-ph/0511235.
- [139] S. Dittmaier et al., “Charged-Higgs-boson production at the LHC: NLO supersymmetric QCD corrections”, Phys. Rev. D **83** (2011) 055005, 0906.2648.
- [140] C. Weydert et al., “Charged Higgs boson production in association with a top quark in MC@NLO”, Eur. Phys. J. C **67** (2010) 617, 0912.3430.

- [141] M. Klasen et al., “Associated production of charged Higgs bosons and top quarks with POWHEG”, *Eur. Phys. J. C* **72** (2012) 2088, 1203.1341.
- [142] C. Degrande et al., “Heavy charged Higgs boson production at the LHC”, *JHEP* **10** (2015) 145, 1507.02549.
- [143] M. Jezabek and J. H. Kuhn, “QCD Corrections to Semileptonic Decays of Heavy Quarks”, *Nucl. Phys. B* **314** (1989) 1, MPI-PAE/PTh-16/88.
- [144] C. S. Li, R. J. Oakes, and T. C. Yuan, “QCD corrections to $t \rightarrow W^+b$ ”, *Phys. Rev. D* **43** (1991) 3759, NUHEP-TH-90-27.
- [145] A. Czarnecki and S. Davidson, “QCD corrections to the charged Higgs decay of a heavy quark”, *Phys. Rev. D* **48** (1993) 4183, hep-ph/9301237.
- [146] J. M. Campbell, R. K. Ellis, and F. Tramontano, “Single top production and decay at next-to-leading order”, *Phys. Rev. D* **70** (2004) 094012, hep-ph/0408158.
- [147] A. Czarnecki and K. Melnikov, “Two loop QCD corrections to top quark width”, *Nucl. Phys. B* **544** (1999) 520, hep-ph/9806244.
- [148] K. G. Chetyrkin et al., “Second order QCD corrections to $\Gamma(t \rightarrow W b)$ ”, *Phys. Rev. D* **60** (1999) 114015, hep-ph/9906273.
- [149] I. R. Blokland et al., “Heavy to light decays with a two loop accuracy”, *Phys. Rev. Lett.* **93** (2004) 062001, hep-ph/0403221.
- [150] I. R. Blokland et al., “Next-to-next-to-leading order calculations for heavy-to-light decays”, *Phys. Rev. D* **71** (2005) 054004, hep-ph/0503039.
- [151] A. Czarnecki, J. G. Korner, and J. H. Piclum, “Helicity fractions of W bosons from top quark decays at NNLO in QCD”, *Phys. Rev. D* **81** (2010) 111503, 1005.2625.
- [152] J. Gao, C. S. Li, and H. X. Zhu, “Top Quark Decay at Next-to-Next-to Leading Order in QCD”, *Phys. Rev. Lett.* **110** (2013) 042001, 1210.2808.
- [153] M. Brucherseifer, F. Caola, and K. Melnikov, “ $\mathcal{O}(\alpha_s^2)$ corrections to fully-differential top quark decays”, *JHEP* **04** (2013) 059, 1301.7133.
- [154] C. Degrande et al., “Accurate predictions for charged Higgs production: Closing the $m_{H^\pm} \sim m_t$ window”, *Phys. Lett. B* **772** (2017) 87, 1607.05291.
- [155] Particle Data Group, “Review of Particle Physics”, *PTEP* **2020** (2020) 083C01.
- [156] S. Kanemura and C. P. Yuan, “Testing supersymmetry in the associated production of CP odd and charged Higgs bosons”, *Phys. Lett. B* **530** (2002) 188, hep-ph/0112165.
- [157] A. G. Akeroyd and M. A. Diaz, “Searching for a light fermiophobic Higgs boson at the Tevatron”, *Phys. Rev. D* **67** (2003) 095007, hep-ph/0301203.
- [158] A. G. Akeroyd, “Searching for a very light Higgs boson at the Tevatron”, *Phys. Rev. D* **68** (2003) 077701, hep-ph/0306045.

- [159] Q.-H. Cao, S. Kanemura, and C. P. Yuan, “Associated production of CP odd and charged Higgs bosons at hadron colliders”, Phys. Rev. D **69** (2004) 075008, hep-ph/0311083.
- [160] A. Belyaev et al., “Light MSSM Higgs boson scenario and its test at hadron colliders”, Phys. Rev. Lett. **100** (2008) 061801, hep-ph/0609079.
- [161] X. Miao, S. Su, and B. Thomas, “Trilepton Signals in the Inert Doublet Model”, Phys. Rev. D **82** (2010) 035009, 1005.0090.
- [162] O. Brein, R. V. Harlander, and T. J. E. Zirke, “vh@nnlo - Higgs Strahlung at hadron colliders”, Comput. Phys. Commun. **184** (2013) 998, 1210.5347.
- [163] R. V. Harlander et al., “vh@nnlo-v2: New physics in Higgs Strahlung”, JHEP **05** (2018) 089, 1802.04817.
- [164] J. Alwall et al., “The automated computation of tree-level and next-to-leading order differential cross sections, and their matching to parton shower simulations”, JHEP **07** (2014) 079, 1405.0301.
- [165] D. A. Dicus et al., “W[±] H[±] PRODUCTION AT HADRON COLLIDERS”, Phys. Rev. D **40** (1989) 787, MAD/PH/468.
- [166] A. A. Barrientos Bendezu and B. A. Kniehl, “W[±] H[±] associated production at the large hadron collider”, Phys. Rev. D **59** (1999) 015009, hep-ph/9807480.
- [167] A. A. Barrientos Bendezu and B. A. Kniehl, “Quark loop amplitudes for W[±] H[±] associated hadroproduction”, Phys. Rev. D **61** (2000) 097701, hep-ph/9909502.
- [168] O. Brein, W. Hollik, and S. Kanemura, “The MSSM prediction for W[±] H[±] production by gluon fusion”, Phys. Rev. D **63** (2001) 095001, hep-ph/0008308.
- [169] S.-S. Bao, Y. Tang, and Y.-L. Wu, “W[±]H[∓] associated production at LHC in the general 2HDM with Spontaneous CP Violation”, Phys. Rev. D **83** (2011) 075006, 1011.1409.
- [170] W. Hollik and S.-h. Zhu, “O(α_s) corrections to b anti-b → W[±] H[±] at the CERN large hadron collider”, Phys. Rev. D **65** (2002) 075015, hep-ph/0109103.
- [171] T. N. Dao, W. Hollik, and D. N. Le, “W⁻⁺ H⁺⁻ production and CP asymmetry at the LHC”, Phys. Rev. D **83** (2011) 075003, 1011.4820.
- [172] R. Enberg, R. Pasechnik, and O. Stal, “Enhancement of associated H[±]W[∓] production in the NMSSM”, Phys. Rev. D **85** (2012) 075016, 1112.4699.
- [173] N. Kidonakis, “Higher-order radiative corrections for $b\bar{b} \rightarrow H^-W^+$ ”, Phys. Rev. D **97** (2018) 034002, 1704.08549.
- [174] S. Moretti and K. Odagiri, “The Phenomenology of W[±] H[±] production at the large hadron collider”, Phys. Rev. D **59** (1999) 055008, hep-ph/9809244.
- [175] E. Asakawa, O. Brein, and S. Kanemura, “Enhancement of W[±] H[±] production at hadron colliders in the two Higgs doublet model”, Phys. Rev. D **72** (2005) 055017, hep-ph/0506249.

- [176] D. Eriksson, S. Hesselbach, and J. Rathsmann, “Associated charged Higgs and W boson production in the MSSM at the CERN Large Hadron Collider”, *Eur. Phys. J. C* **53** (2008) 267, [hep-ph/0612198](#).
- [177] M. Hashemi, “Possibility of observing MSSM charged Higgs in association with a W boson at LHC”, *Phys. Rev. D* **83** (2011) 055004, [1008.3785](#).
- [178] S.-S. Bao et al., “Identify Charged Higgs Boson in $W^\pm H^\mp$ Associated Production at LHC”, *Phys. Rev. D* **85** (2012) 075005, [1112.0086](#).
- [179] M. Aoki et al., “Light Charged Higgs bosons at the LHC in 2HDMs”, *Phys. Rev. D* **84** (2011) 055028, [1104.3178](#).
- [180] ATLAS, “Search for charged Higgs bosons decaying via $H^\pm \rightarrow \tau^\pm \nu$ in fully hadronic final states using pp collision data at $\sqrt{s} = 8$ TeV with the ATLAS detector”, *JHEP* **03** (2015) 088, [1412.6663](#).
- [181] CMS, “Search for a charged Higgs boson in pp collisions at $\sqrt{s} = 8$ TeV”, *JHEP* **11** (2015) 018, [1508.07774](#).
- [182] ATLAS, “Search for charged Higgs bosons produced in association with a top quark and decaying via $H^\pm \rightarrow \tau \nu$ using pp collision data recorded at $\sqrt{s} = 13$ TeV by the ATLAS detector”, *Phys. Lett. B* **759** (2016) 555, [1603.09203](#).
- [183] ATLAS, “Search for charged Higgs bosons decaying via $H^\pm \rightarrow \tau^\pm \nu_\tau$ in the τ +jets and τ +lepton final states with 36 fb^{-1} of pp collision data recorded at $\sqrt{s} = 13$ TeV with the ATLAS experiment”, *JHEP* **09** (2018) 139, [1807.07915](#).
- [184] CMS, “Search for charged Higgs bosons in the $H^\pm \rightarrow \tau^\pm \nu_\tau$ decay channel in proton-proton collisions at $\sqrt{s} = 13$ TeV”, *JHEP* **07** (2019) 142, [1903.04560](#).
- [185] ATLAS, “Search for charged Higgs bosons decaying into top and bottom quarks at $\sqrt{s} = 13$ TeV with the ATLAS detector”, *JHEP* **11** (2018) 085, [1808.03599](#).
- [186] ATLAS, “Search for charged Higgs bosons decaying into a top-quark and a bottom-quark at $\sqrt{s} = 13$ TeV with the ATLAS detector”, (2020), [ATLAS-CONF-2020-039](#).
- [187] ATLAS, “Search for charged Higgs bosons decaying into a top quark and a bottom quark at $\sqrt{s}=13$ TeV with the ATLAS detector”, (2021), [2102.10076](#).
- [188] CMS, “Search for a charged Higgs boson decaying to charm and bottom quarks in proton-proton collisions at $\sqrt{s} = 8$ TeV”, *JHEP* **11** (2018) 115, [1808.06575](#).
- [189] ATLAS, “Search for a light charged Higgs boson in the decay channel $H^+ \rightarrow c\bar{s}$ in $t\bar{t}$ events using pp collisions at $\sqrt{s} = 7$ TeV with the ATLAS detector”, *Eur. Phys. J. C* **73** (2013) 2465, [1302.3694](#).
- [190] CMS, “Search for a light charged Higgs boson decaying to $c\bar{s}$ in pp collisions at $\sqrt{s} = 8$ TeV”, *JHEP* **12** (2015) 178, [1510.04252](#).
- [191] CMS, “Search for Charged Higgs Bosons Produced via Vector Boson Fusion and Decaying into a Pair of W and Z Bosons Using pp Collisions at $\sqrt{s} = 13$ TeV”, *Phys. Rev. Lett.* **119** (2017) 141802, [1705.02942](#).

- [192] ATLAS, “Search for resonant WZ production in the fully leptonic final state in proton-proton collisions at $\sqrt{s} = 13$ TeV with the ATLAS detector”, Phys. Lett. B **787** (2018) 68, 1806.01532.
- [193] ATLAS, “Search for doubly and singly charged Higgs bosons decaying into vector bosons in multi-lepton final states with the ATLAS detector using proton-proton collisions at $\sqrt{s} = 13$ TeV”, (2021), 2101.11961.
- [194] ALEPH, DELPHI, L3, OPAL, LEP, “Search for Charged Higgs bosons: Combined Results Using LEP Data”, Eur. Phys. J. C **73** (2013) 2463, 1301.6065.
- [195] ATLAS, “Search for the Decay of the Higgs Boson to Charm Quarks with the ATLAS Experiment”, Phys. Rev. Lett. **120** (2018) 211802, 1802.04329.
- [196] CMS, “A search for the standard model Higgs boson decaying to charm quarks”, JHEP **03** (2020) 131, 1912.01662.
- [197] A. Alves and F. F. Freitas, “Towards recognizing the light facet of the Higgs Boson”, Mach. Learn. Sci. Tech. **1** (2020) 045025, 1912.12532.
- [198] ATLAS, “ CP Properties of Higgs Boson Interactions with Top Quarks in the $t\bar{t}H$ and tH Processes Using $H \rightarrow \gamma\gamma$ with the ATLAS Detector”, Phys. Rev. Lett. **125** (2020) 061802, 2004.04545.
- [199] ATLAS, “Search for a heavy Higgs boson decaying into a Z boson and another heavy Higgs boson in the $\ell\ell b\bar{b}$ final state in pp collisions at $\sqrt{s} = 13$ TeV with the ATLAS detector”, Phys. Lett. B **783** (2018) 392, 1804.01126.
- [200] CMS, “Search for a heavy pseudoscalar boson decaying to a Z and a Higgs boson at $\sqrt{s} = 13$ TeV”, Eur. Phys. J. C **79** (2019) 564, 1903.00941.
- [201] ATLAS, “Search for heavy resonances decaying into a W or Z boson and a Higgs boson in final states with leptons and b -jets in 36 fb^{-1} of $\sqrt{s} = 13$ TeV pp collisions with the ATLAS detector”, JHEP **03** (2018) 174, 1712.06518.
- [202] ATLAS, “Search for heavy Higgs bosons decaying into two tau leptons with the ATLAS detector using pp collisions at $\sqrt{s} = 13$ TeV”, Phys. Rev. Lett. **125** (2020) 051801, 2002.12223.
- [203] A. G. Akeroyd, “Fermiophobic and other nonminimal neutral Higgs bosons at the LHC”, J. Phys. G **24** (1998) 1983, hep-ph/9803324.
- [204] A. G. Akeroyd, M. A. Diaz, and F. J. Pacheco, “Double fermiophobic Higgs boson production at the CERN LHC and LC”, Phys. Rev. D **70** (2004) 075002, hep-ph/0312231.
- [205] A. G. Akeroyd et al., “Multi-photon signatures at the Fermilab Tevatron”, Eur. Phys. J. C **48** (2006) 147, hep-ph/0512077.
- [206] U. Haisch and A. Malinauskas, “Let there be light from a second light Higgs doublet”, JHEP **03** (2018) 135, 1712.06599.

- [207] ATLAS, “Search for Scalar Diphoton Resonances in the Mass Range 65 – 600 GeV with the ATLAS Detector in pp Collision Data at $\sqrt{s} = 8 \text{ TeV}$ ”, Phys. Rev. Lett. **113** (2014) 171801, 1407.6583.
- [208] CMS, “Search for new resonances in the diphoton final state in the mass range between 80 and 115 GeV in pp collisions at $\sqrt{s} = 8 \text{ TeV}$ ”, (2015), CMS-PAS-HIG-14-037.
- [209] ATLAS, “Search for resonances in the 65 to 110 GeV diphoton invariant mass range using 80 fb^{-1} of pp collisions collected at $\sqrt{s} = 13 \text{ TeV}$ with the ATLAS detector”, (2018), ATLAS-CONF-2018-025.
- [210] A. G. Akeroyd, M. A. Diaz, and M. A. Rivera, “Effect of Charged Scalar Loops on Photonic Decays of a Fermiophobic Higgs”, Phys. Rev. D **76** (2007) 115012, 0708.1939.
- [211] ALEPH, DELPHI, L3, OPAL, LEP Working Group for Higgs Boson Searches, “Search for neutral MSSM Higgs bosons at LEP”, Eur. Phys. J. C **47** (2006) 547, hep-ex/0602042.
- [212] CMS, “Search for additional neutral Higgs bosons decaying to a pair of tau leptons in pp collisions at $\sqrt{s} = 7$ and 8 TeV ”, (2015), CMS-PAS-HIG-14-029.
- [213] CMS, “Search for a new scalar resonance decaying to a pair of Z bosons in proton-proton collisions at $\sqrt{s} = 13 \text{ TeV}$ ”, JHEP **06** (2018) 127, 1804.01939.